

Electronic Spectra of Ytterbium Fluoride from Relativistic Electronic Structure Calculations

Johann V. Pototschnig,^{*,†} Kenneth G. Dyall,^{*,‡} Lucas Visscher,^{*,†} and André Severo Pereira Gomes^{*,¶}

[†]*Amsterdam Center for Multiscale Modeling, Department of Theoretical Chemistry, Faculty of Sciences, VU University Amsterdam, De Boelelaan 1083, NL-1081 HV Amsterdam, The Netherlands*

[‡]*Dirac Solutions, 10527 NW Lost Park Drive, Portland, OR 97229, U.S.A.*

[¶]*Université de Lille, CNRS, UMR 8523 – PhLAM – Physique des Lasers, Atomes et Molécules, F-59000 Lille, France*

E-mail: j.v.pototschnig@vu.nl; diracsolutions@gmail.com; visscher@chem.vu.nl; andre.gomes@univ-lille.fr

Abstract

We report an investigation of the low-lying excited states of the YbF molecule—a candidate molecule for experimental measurements of the electron electric dipole moment—with 2-component based multi-reference configuration interaction (MRCI), equation of motion coupled cluster (EOM-CCSD) and the extrapolated intermediate Hamiltonian Fock-space coupled cluster (XIHFS-CCSD). Specifically, we address the question of the nature of these low-lying states in terms of configurations containing filled or partially-filled Yb $4f$ shells. We show that while it does not appear possible to carry out calculations with both kinds of configurations contained in the same active space, reliable information can be extracted from different sectors of Fock space—that is, by performing electron attachment and detachment IHFS-CCSD and EOM-CCSD calculation on the closed-shell YbF⁺ and YbF[−] species, respectively. From these we observe $\Omega = 1/2, 3/2$ states that arise from the $4f^{13}\sigma_{6s}^2$, $4f^{14}5d/6p$, and $4f^{13}5d\sigma_{6s}$ configurations appear in the same energy range around the ground-state equilibrium geometry and they are therefore able to interact. As these states are gener-

ated from different sectors of Fock space, they are almost orthogonal and provide complementary descriptions of parts of the excited state manifold. To obtain a comprehensive picture, we introduce a simple adiabaticization model to extract energies of interacting $\Omega = 1/2, 3/2$ states that can be compared to experimental observations.

1 Introduction

In a previous paper,¹ we introduced all-electron relativistic basis sets for the lanthanides (La – Lu) and discussed their performance for the determination of spectroscopic constants for the ground state of ytterbium fluoride (YbF), an open-shell molecule with a $^2\Sigma^+$ ground state. This molecule has received a fair amount of experimental and theoretical attention because of its potential application in the observation of parity-violating interactions^{2–4} via determination of the electric dipole moment of the electron (eEDM)—see, for instance refs. 4–11 and references therein). There is also some interest in the Yb atom, cation and dimer in connection to ultracold physics.^{12–14} An example¹⁵ is the parity violation observed in the Yb atom.

A noteworthy finding in our previous work was the sensitivity of coupled cluster calculations to the basis set in use and, indirectly, to the amount of electron correlation recovered in the calculations. We observed a spike in the values of the T_1 diagnostic around the ground state equilibrium geometry, so it appears that the perturbative treatment of triple excitations in the CCSD(T) calculations breaks down in this region of the potential energy curves unless there is enough flexibility in the correlation treatment. The same was recently observed by Pasteka et al.¹⁶ for the nuclear quadruple coupling constant. This suggests the existence of a low lying perturbing state, which we want to investigate further in the current work.

Experimental^{17,18} and previous theoretical¹⁹⁻²¹ investigations suggest that in the ground state the unpaired electron is located in a σ_s orbital with dominant contributions from the 6s orbital of Yb, corresponding to a $\text{Yb}(4f^{14}\sigma_{6s})\text{F}$ configuration. This ${}^2\Sigma_{1/2}$ state ground state was studied in greater detail by combining microwave and optical spectroscopy for the odd ${}^{171}\text{Yb}$ isotope.²²

Experimentally,¹⁸ the lowest excited state observed is assigned as ${}^2\Pi_{1/2}$, with an energy of 18106 cm^{-1} , while the ${}^2\Pi_{3/2}$ component is found at 19471 cm^{-1} , yielding a spin-orbit splitting of 1365 cm^{-1} of this spin-orbit split ${}^2\Pi$ state. The lower component will be denoted $3_{1/2}$ in the current work. Experiments indicate a perturbation of its vibrational levels,^{18,23-25} which was attributed to the presence of a perturbing state (denoted by $4_{1/2}$ here) found at 18705 cm^{-1} .¹⁸ This perturbing $4_{1/2}$ state is sometimes referred to as $[18.6]_{1/2}$ by experimentalists^{18,23} (energy in cm^{-1} divided by 10^3 in the square brackets, and Ω -value as subscript). The mixing of these two $\Omega = 1/2$ states gives rise to states designated as $[557]$ and $[561]$ (the values in square brackets referring to transition energies in Thz from the vibronic ground state) with transition energies of 18574 and 18699 cm^{-1} , respectively.^{24,25} These two states are of importance for laser cooling schemes that have been investigated²⁶ and tested²⁵ with the purpose of realizing high-accuracy measurements of YbF at very low temperatures.

Besides these first excited states, Smallman²⁶ investigated also two not yet fully characterized mixed states, $[574](\approx 19150\text{ cm}^{-1})$ and $[578](\approx 19280\text{ cm}^{-1})$ at higher energies. These can be compared with the $\Omega = 3/2$ state at 19471 cm^{-1} found earlier by Dunfield,¹⁸ which will be denoted $2_{3/2}$ in the current work. Uttam *et al.* furthermore measured additional unidentified higher bands at about 23035 , 23256 and 26015 cm^{-1} .^{27,28}

Theoretically, excited states arising from the $\text{Yb}(4f^{14}6p)\text{F}$ and $\text{Yb}(4f^{14}5d)\text{F}$ configurations were considered by Nayak and Chaudhuri⁶ with RAS-CI based on 4-component spinors, yielding the $A^2\Pi_{1/2}(3_{1/2})$, $A^2\Pi_{3/2}(2_{3/2})$, and a ${}^2\Sigma_{1/2}$ state. Earlier multireference CI calculations by Dolg et al.¹⁹ furthermore indicate the possibility of low-lying $\Omega = 1/2$ states arising from the $\text{Yb}(4f^{13}[F_{7/2}^\circ]\sigma_{6s}^2)\text{F}$ or $\text{Yb}(4f^{13}[F_{7/2}^\circ]5d\sigma_{6s})\text{F}$ configurations, to be lying below or close to the $\text{Yb}(4f^{14}6p)\text{F}$ states. This was also found in the DFT calculations of Liu et al.²⁰ who place excited states arising from the $\text{Yb}(4f^{13}[F_{7/2}^\circ]\sigma_{6s}^2)\text{F}$ configuration in the range from 9000 to 15000 cm^{-1} relative to the $\text{Yb}(4f^{14}\sigma_{6s})\text{F}$ ground state. These findings make it of interest to explicitly consider the configuration interaction between the f^{13} and f^{14} configurations in the Yb atom.²⁹

The vibronic states are additionally split due to hyperfine interactions. In atomic experiments they were measured for the ground and excited states^{9,22,30-33} also using Zeeman spectroscopy.³⁴ The hyperfine interaction of the atom³⁵⁻³⁷ and molecule³⁸ were studied theoretically, and should have similar uncertainties to the contribution of the eEDM to the spectrum due to the similarity of the matrix elements. Recently, uncertainties of the hyperfine constants arising in relativistic coupled cluster computations have been studied.³⁹

It is clear from the above that a proper description of the Yb atom and the YbF molecule requires an accurate treatment of both spin-orbit coupling and electron correlation, for ground as well as excited states. A popular approach is the so-called two-step approach to spin-orbit coupling (SOC), in which electron

correlation methods based on non-relativistic or scalar relativistic Hamiltonians are used to obtain excited state energies, that are in turn used to dress a spin-orbit configuration interaction (SOC) matrix. This approach can yield quite accurate spin-orbit coupled states, but results are particularly sensitive to the the number of spin-free states serving as a basis for the SOC step.^{40–46} An alternative is to include SOC already at the mean-field level, and use fully SO-coupled molecular spinors to construct the correlated wave functions.⁴⁷ This can be done with four-component Hamiltonians, as done for the ground¹ and excited states^{6,37,48,49} of YbF, or with more computationally efficient two-component Hamiltonians based on the eXact 2-Component (X2C) approach,^{50–57} in which a transformation to decouple the positive and negative energy states of the Dirac Hamiltonian can be carried out in matrix form, yielding the same positive energy spectrum as the original 4-component Hamiltonian. More details can be found in the recent review by Liu.⁴⁷ Among the different X2C flavors, we can distinguish two main strategies for the decoupling, which is performed based on : (i) the one-electron Dirac Hamiltonian prior to the mean-field step,^{54,57} and for which two-electron spin-orbit contributions due to the untransformed two-electron potential are included via atomic mean-field contributions calculated with the AMFI code^{41,58,59} (X2C-AMFI); (ii) after a converged 4-component mean-field calculation on atoms^{52,53,56} or molecules⁵⁵ (²DC^M). Recent benchmarks show that ²DC^M calculations closely reproduce equivalent 4-component ones for valence⁶⁰ or core⁶¹ states.

Moreover, the aforementioned calculations for the excited states of YbF have mostly employed multireference CI (MRCI) approaches. While these can provide great flexibility in capturing static correlation, it remains the case that dynamical correlation is better accounted for with coupled cluster approaches. Among the coupled cluster singles and doubles (CCSD) approaches for excited states, we have the equation of motion (EOM-CCSD) method as well as Fock-space (IHFS-CCSD) methods,⁶² of which the single electron attachment, detachment, and

singly excited states variants are the most commonly used. The two approaches have been found to yield very accurate results in general and in particular for calculations with relativistic Hamiltonians as discussed elsewhere (see ref. 60 and references therein).

The first goal of this work is therefore to go beyond the investigations performed to date in the literature, and apply the relativistic EOM-CCSD and IHFS-CCSD approaches to describe the low-lying excited states of YbF. For such states, where the most important excited state configurations appear have a single open-shell character ($4f^{14}\sigma_{6s}$, $4f^{13}[F_{7/2}^{\circ}]\sigma_{6s}^2$, $4f^{14}5d$, $4f^{13}[F_{7/2}^{\circ}]5d\sigma_{6s}$, $4f^{14}6p$), these coupled cluster approaches are in principle applicable, provided one starts from closed shell configurations such as Yb($4f^{14}\sigma_{6s}^2$)F⁻ or Yb($4f^{14}$)F⁺. Additionally, we assess the performance of relativistic MRCI with respect to the coupled cluster methods. Our second goal is to confirm whether any low-lying state is close enough to the ground state to perturb the latter, and explain the anomalous behavior observed in the open-shell ground-state calculations in the literature.

2 Computational Details

All relativistic electronic structure calculations were performed with a development version of the DIRAC program suite⁶³ (revision 6e10c5d3), employing for Yb the valence double-zeta (24s19p13d9f2g), triple-zeta (30s24p18d14f4g2h) and quadruple-zeta (35s30p19d16f6g4h2i) basis sets from the previous work,¹ along with the matching augmented correlation-consistent (aug-cc-pVnZ, $n = 2, 3, 4$) basis sets of Dunning⁶⁴ for F. All basis sets were kept uncontracted, with the small component basis generated by restricted kinetic balance. In addition to these individual basis sets, we have used the calculations with triple- and quadruple-zeta sets to construct extrapolations to the complete basis set limit (E_{∞}) for the underlying potential energy

curves, using the relation⁶⁵

$$E_\infty(\mathbf{R}) = \frac{4^3 E_4(\mathbf{R}) - 3^3 E_3(\mathbf{R})}{4^3 - 3^3} \quad (1)$$

where the subscripts denote the cardinal numbers for the basis sets and $E_n(\mathbf{R})$ the energy for a given geometry and electronic structure method for a basis of cardinal number n ($= 2, 3, 4$).

In the coupled cluster computations the $^2\text{DC}^M$ Hamiltonian^{54,55} was applied, all two-electron integrals over small component (S) basis sets (i.e. the so-called (SS|SS)-type integrals) appearing in the SCF step have been replaced by a simple correction.⁶⁶ In order to account for spin-orbit coupling and other relativistic effects the X2C-AMFI Hamiltonian was employed for the Kramers-restricted configuration interaction (KRCI) method.

Spectroscopic constants (r_e , D_e , ω_e and $\omega_e x_e$) were determined from a Morse potential fit in the vicinity of the potential energy minima. The potential energy curves were determined for bond lengths between 1.6 Å and 2.3 Å spaced by 0.02 Å and additional points with larger spacing up to 3.5 Å. In the calculation of D_e the asymptotic dissociation limit is calculated from the energies of the isolated neutral atoms, F in the $^2P_{3/2}$ state and Yb in the 1S_0 state.

The dataset associated with this manuscript (outputs from calculations, codes to extract and process information from these, and code to obtain the spectroscopic constants) is provided in ref. 67.

2.1 Kramers-restricted configuration interaction

For YbF we first consider Kramers-restricted configuration interaction (KRCI) based on an average-of-configuration Hartree-Fock approach (AOC-SCF).⁶⁸ This method was employed in order to treat the open shells, where one or two valence electrons were distributed over the s- and d-orbitals and the f-shell was either completely filled or contained one hole, depending on the states of interest. The AOC-

SCF reference wave function in the KRCI computation is occupied according to a definition given by a generalized active space (GAS).⁶⁹ In this approach the Hamiltonian is computed for all allowed configurations and then diagonalized. The GAS space was defined by a f-shell which was completely filled or contained one hole and one or two electrons distributed over 29 orbitals.

2.2 Equation-of-motion coupled cluster

The first approach we use to describe the dynamical correlation that is largely missing in KRCI is EOM-CCSD, which can give access to electronic states of different kinds, depending on the single determinant wave function that is chosen as the starting point. In it, the CCSD amplitudes are determined for the chosen ground state in the first step, and subsequently the similarity transformed Hamiltonian is constructed using these amplitudes and the desired states are generated by an operator that either removes or adds an electron.

The first set of states was obtained by electron attachment on Yb($4f^{14}$)F⁺ ion, where the HOMO ($\sigma_{6s,1/2}$) of YbF was initially empty. This computation on the (0h,1p) sector of Fock space yielded states with $4f^{14}$ and a valence electron in the σ_{6s} , d or p orbital. This means that, in the process of obtaining the potentials for the ground and excited states of YbF, we immediately obtain energies of CCSD quality for YbF⁺, and therefore vertical ionization potentials (IP) at each geometry.

Another set of states was obtained by ionizing the Yb($4f^{14}\sigma_{6s}^2$)F⁻ anion, where the HOMO ($\sigma_{6s,1/2}$) of YbF was initially doubly occupied. States arising from the Yb($4f^{14}\sigma_{6s}$)F, Yb($4f^{13}[F_{7/2}^\circ]\sigma_{6s}^2$)F, and Yb($4f^{13}[F_{5/2}^\circ]\sigma_{6s}^2$)F configurations were obtained by considering the (1h,0p) sector of Fock space. This means that, in the process of obtaining the potentials for the ground and excited states of YbF, we immediately obtain energies of CCSD quality for YbF⁻, and therefore vertical electron affinities (EA) at each geometry. We note that states arising from the (2h,1p) and (1h,2p) manifolds

are also accessible from EOM-IP and EOM-EA calculations, though the energy of electronic states determined by such configurations will be less accurate than states dominated by single detachment or attachment configurations.

The EOM-CCSD electronic states are obtained by an iterative diagonalization (Davidson) procedure in which only the energies of a certain number of the lowest states are determined. For the IP-EOM-CCSD we obtained 16 $\Omega = 1/2$, 8 $\Omega = 3/2$, 6 $\Omega = 5/2$ and 2 $\Omega = 7/2$ states, whereas for EA-EOM-CCSD we obtained 8 $\Omega = 1/2$, 6 $\Omega = 3/2$, 4 $\Omega = 5/2$ and 2 $\Omega = 7/2$ states.

As transition moments are not yet available for the EOM-CCSD implementation in DIRAC, we have only obtained the potential energy curves. These are nevertheless useful since, by not requiring the definition of model spaces or the use of an extrapolation procedure, they serve as a cross validation of the IHFS-CCSD calculations below.

2.3 Fock-space coupled cluster

Fock-space coupled cluster⁷⁰ (FS-CCSD) is our second approach to include dynamical correlation in the electronically excited states. Here it was employed in a similar fashion to EOM-CCSD, starting from YbF^+ or YbF^- and proceeding to the (0h,1p) and (1h,0p) sectors of Fock space, respectively. For FS-CCSD a model space is defined by selecting a number of occupied and virtual orbitals and how many electrons are added and removed. The matrix for this subspace is constructed and subsequently diagonalized, thus yielding all states within the chosen model space, in this case states arising from single electron attachment (EA) or single electron detachment (IP). This method requires solving first for the underlying sectors, starting with (0h,0p), which corresponds to CCSD. Due to computational constraints, we have truncated the virtual space so that 117, 230 and 296 orbitals were used in the double-, triple- and quadruple-zeta CCSD calculations, respectively.

The separation into a model and external space leads to the appearance of the so-called

intruder states, a well-known difficulty with Fock-space coupled cluster and other effective Hamiltonian approaches, that can be dealt with in many cases by the intermediate Hamiltonian (IH) Fock-space coupled cluster (IHFS-CCSD) method.^{71,72}

The IH approach was employed to compute $\text{Yb}(4f^{14}\{\sigma_{6s}, 6p, 5d \dots\}^1)\text{F}$ states starting from YbF^+ . The active P space in such calculations contained about 50 spinors varying slightly with bond distance and basis set. Of these 26 spinors are always present in the model (P_m) space, whereas the remaining active spinors are placed in the intermediate (P_I) space. Due to using the (0h,1p) sector for the cation, states arising from configurations where the Yb 4f shell is partially filled (such as $\text{Yb}(4f^{13}[F_{7/2}^\circ]\sigma_{6s}^2)\text{F}$, $\text{Yb}(4f^{13}[F_{7/2}^\circ]5d\sigma_{6s})\text{F}$ or $\text{Yb}(4f^{13}[F_{7/2}^\circ]\sigma_{6s}6p)\text{F}$) are not accessible in this calculation.

The approach outlined above was, however, not enough to avoid divergence in the computation of the (1h,0p) sector using the anion as a reference. Therefore, the extrapolated intermediate Hamiltonian (XIH) Fock-space coupled-cluster approach⁷³ (XIHFSC-CCSD) was applied using the same shifts as in reference 73. Values of 0.1 and 0.2 Hartree were selected if one of the holes is not in the model space. These shifts were doubled for two holes outside the model space. Using the determined energies an extrapolation to the system without shifts was performed. The model (P_m) space in these computations contained 22 spinors, the intermediate (P_I) space about 24 spinors depending on the bond distance and basis set. Since we start out from the anion and only allow holes, only $\text{Yb}(4f^{13}[F_{7/2}^\circ]\sigma_{6s}^2)\text{F}$, $\text{Yb}(4f^{14}\sigma_{6s})\text{F}$, and $\text{Yb}(4f^{14}\sigma_{6s}^2)\text{F}(2p^5)$ configurations are accessible in this computation.

Combining the two sectors allows us to get different excited states of YbF , although there are limitations. Firstly, the interactions between configurations with open f-shell and the ones with an electron in the p- or d-shell are not included, since they will be obtained for different sectors of Fock space. This interaction will nevertheless be treated with a simple adiabatic approach, described in sections 2.4

and 3.6. Secondly, configurations such as $\text{Yb}(4f^{13}[F_{7/2}^{\circ}]\sigma_{6s}6p)\text{F}$ or $\text{Yb}(4f^{13}[F_{7/2}^{\circ}]5d\sigma_{6s})\text{F}$ are not included in the current treatment. This limitation is not as significant because these states have higher energies than the ones we are interested in. Both of these problems could be dealt with by using the (1h,1p) sector, but this goes beyond the current work as convergence is very unstable for this sector and it requires the use of an open-shell reference.

2.4 Adiabaticization of electronic states

As we separated the computations of states with $4f^{13}$ and $4f^{14}$ character, these states cannot interact with each other, and states with the same Ω value cross although they should have an avoided crossing. In order to correct this deficiency we considered a simple adiabaticization model, in which we set up and diagonalize the following matrix for each Ω value:

$$M = \begin{pmatrix} E(f^{13}) & \mathbf{C} \\ \mathbf{C} & E(f^{14}) \end{pmatrix} \quad (2)$$

where \mathbf{C} is a matrix where every entry is a coupling constant (whose value is kept constant for all states and geometries considered; we have investigated values of 0.01, 0.001 and 0.0001 a.u.), E are matrices with the eigenvalues of the different electronic states on the diagonal. The potential curves were computed for different coupling constants and the results are shown in section 3.6. We note that since the ground state energy, associated with the $\text{Yb}(4f^{14}\sigma_{6s})\text{F}$ configuration, appears in both coupled cluster approaches for the coupled cluster methods, we have only considered one such energy. As we shall see in the discussion, this is valid in the region between 1.8 Å and 2.5 Å, since for these distances the ground-state energies from IP and EA calculations are nearly identical.

3 Results and Discussion

We start our discussion with the electronic transitions of the atomic Yb^+ cation, before moving

on to the YbF molecule. This is because because the atom's electronic structure is similar to the Yb in YbF since, due to the large electronegativity of fluorine, one electron is almost completely removed from the Yb atom.

Subsequently, the potential energy curves for Kramers-restricted configuration interaction are presented. A discussion of the coupled cluster approaches follows, with a focus on the comparison of the coupled cluster results for the Fock space and equation-of-motion approach. This section is followed by a presentation of the spectroscopic data for the ground and excited states. In the last part we take a closer look at the mixing of states at around 18000 cm^{-1} and apply the adiabaticization procedure.

3.1 Ytterbium cation

As discussed in the introduction, states from both the $4f^{13}$ and the $4f^{14}$ configurations are of importance. This is difficult to realize in a balanced manner when using one set of orbitals to describe all states. Any change in the occupation of the $4f$ -shell will alter the screening of the $5s$ and $5p$ orbitals of Yb, resulting in differences between orbital sets optimized for a $4f^{13}$ or a $4f^{14}$ configuration. Additionally, the $4f$ orbitals are very compact and since they are the first f -shell there are no orthogonality conditions limiting the radial expansion or contraction of the orbital. Depictions of the orbitals for both configurations can be found in the supporting information.

These observations help to understand why it turned out to be very difficult to treat both sets of states in the same calculation, which we attempted to do from AOC-SCF on the Yb^+ . We started out by performing AOC-SCF computations on the atom, based on the $4f$ closed shell configuration. While we obtained the correct ground state configuration, the ${}^2F_{7/2}^{\circ}$ has an energy of about 46000 cm^{-1} (over two times higher than the experimental value), and the wrong order for the hole states is observed. If the wave function is optimized for a $4f^{13}$ configuration, one obtains the ${}^2F_{7/2}^{\circ}$ as the lowest state and finds the true ground state more than 20000 cm^{-1} higher. Because of these difficul-

ties, the KRCI calculations discussed below all follow the strategy of different orbital sets that is also employed in the subsequent coupled cluster calculations.

Table 1 contains KRCI values of electronic transitions for the cation. The transition energies show deviations of about 10 % and the spin-orbit splitting is underestimated for states with a $4f^{14}$ configuration. The transition dipole moment (TDM) of the ${}^2P_{1/2}^{\circ}$ state is underestimated by about 13 %, the one for the ${}^2P_{3/2}^{\circ}$ state overestimated by about 47 %. The second set of states with a hole in the f-shell and different distributions of the 2 valence electrons are given in the lower part of table 1, the energies are relative to the ${}^2F_{7/2}^{\circ}$ state. In this case the two valence electrons are distributed over the *s*- and *d*-shell. The lowest state with a $4f^{13}[F_{7/2}^{\circ}]6s6p$ configuration has a transition energy of 47912.31 cm^{-1} and was not included in the current treatment.

The excited states of the Yb atom for the $4f^{14}$ configuration have already been investigated by relativistic Fock-space coupled cluster^{36,37,74,75} as well as for the cation,⁷⁴ including the transition moment of magnetic transitions.⁷⁵ With our current calculations we can go beyond these studies and investigate the f^{13} configurations as well. Before discussing our IHFS-CCSD calculations for Yb^+ , we focus on the EOM-CCSD excitation energies, shown in table 2. The EOM-IP-CCSD energies of $4f^{13}$ states obtained from the extrapolation to the complete basis set limit underestimate the experimental transition energies by around 3000 cm^{-1} , whereas the values for $4f^{14}$ states, obtained with EOM-EA-CCSD are within 1000 cm^{-1} of the experimental values, which yields a quantitative improvement over the KRCI ones for both configurations, even though qualitatively the two methods provide a similar picture. From that and the preceding discussion, we attribute the relatively lower accuracy for the $4f^{13}$ to arise from the incomplete account of the relaxation of the wave function upon the creation of the hole in the f shell. Beyond the states presented in table 2, which are dominated by single electron attachment and detachment, we are

able to access states with significant (1h,2p) and (2h,1p) character with EOM-CCSD. These states, available in the supplementary information, are about 10000 cm^{-1} higher in energy than the experimental ones.

Finally, our IHFS-CCSD results are presented in table 3. The transition energies for $4f^{14}$ configuration reproduce well the experimental ones, with errors below 6 %, and only show a small dependence on the basis set. The states arising from the $4f^{13}$ configuration ($4f^{13}[F_{7/2}^{\circ}]s^2$ etc.), in contrast, show a significant dependence on the basis and a rather slow convergence and underestimate the value by about 30 %, which makes them less accurate than the EOM-CCSD ones. This lower accuracy is a consequence of the reduced flexibility in the model spaces, due to the need of adding the $5p$ -shell just below the $4f$ -shell to the intermediate space, in order to achieve convergence. These results are in line with the observations of Shee et al.,⁶⁰ in that the formal equivalence between EOM-CCSD and IHFS-CCSD for the sectors of Fock space considered depends, in fact, on the flexibility of the main model space.

Furthermore, the removal of the $5p$ spinors from the main model space underscores the importance of the $5p$ for the energetics of the states with a hole in the $4f$ shell, since by doing so, we undress the contributions from the $5p$ configurations, and thus prevent them from interacting effectively with $4f^{13}$ determinants.

3.2 Kramers-restricted configuration interaction potential energy curves

The configuration interaction results for excited states of YbF were obtained by an approach corresponding to the one used for Yb^+ , the results for a closed f-shell are depicted in figure 1. The lowest two excited states in the upper part of the figure belong to the $\text{Yb}(4f^{14}6p)\text{F}$ configuration, but approach asymptotically the ${}^2D_{3/2}$ state. The asymptote of the next three states is ${}^2D_{5/2}$ corresponding to the $\text{Yb}(4f^{14}5d)\text{F}$ configuration for smaller internuclear separations. For $\Omega = 5/2$ the transition dipole moment with

Table 1: Kramers-restricted configuration interaction transition energies (in cm^{-1}), transition dipole moments (TDM), and line strength (S) for the Yb^+ cation, the later two are in atomic units($e^2a_0^2$). Reference values and notation have been taken from the NIST database.¹⁷ For the $4f^{13}$ configurations, energies relative to the ${}^2F_{7/2}^\circ$ state are also given. 2z,3z, 4z, and extr. indicate double, triple, quadruple zeta and extrapolated results, respectively.

| | | NIST ¹⁷ | | 2z | | 3z | | 4z | | extr. |
|---------------------------|---------------|--------------------|------------|------------|------|------------|------|------------|------|------------|
| state | conf | E | S | E | TDM | E | TDM | E | TDM | E |
| ${}^2S_{1/2}$ | $4f^{14}6s$ | 0 | | 0 | | 0 | | 0 | | 0 |
| ${}^2D_{3/2}$ | $4f^{14}5d$ | 22961 | | 23322 | 0.0 | 22802 | 0.0 | 23606 | 0.0 | 24192 |
| ${}^2D_{5/2}$ | $4f^{14}5d$ | 24333 | | 23882 | 0.0 | 23321 | 0.0 | 24117 | 0.0 | 24698 |
| ${}^2P_{1/2}^\circ$ | $4f^{14}6p$ | 27062 | 6.1 | 25210 | 3.5 | 24533 | 3.8 | 25331 | 3.6 | 25914 |
| ${}^2P_{3/2}^\circ$ | $4f^{14}6p$ | 30392 | 11.4 | 28104 | 16.9 | 27385 | 18.9 | 28153 | 17.4 | 28712 |
| state | conf | E | ΔE | ΔE | | ΔE | | ΔE | | ΔE |
| ${}^2F_{7/2}^\circ$ | $4f^{13}6s^2$ | 21419 | 0 | 0 | | 0 | | 0 | | 0 |
| ${}^3[3/2]_{5/2}^\circ$ | $4f^{13}5d6s$ | 26759 | 5340 | 4260 | | 5538 | | 4618 | | 3946 |
| ${}^3[3/2]_{3/2}^\circ$ | $4f^{13}5d6s$ | 28758 | 7339 | 6387 | | 7822 | | 7123 | | 6613 |
| ${}^3[11/2]_{9/2}^\circ$ | $4f^{13}5d6s$ | 30224 | 8806 | 8214 | | 9325 | | 8314 | | 7576 |
| ${}^3[11/2]_{11/2}^\circ$ | $4f^{13}5d6s$ | 30563 | 9144 | 8320 | | 9431 | | 8447 | | 7729 |

Table 2: Transition energies (in cm^{-1}) for the Yb^+ cation, obtained for different basis set with EOM-IP-CCSD ($4f^{13}$) and EOM-EA-CCSD ($4f^{14}$), except for the ground state, for which both methods yield the same configuration and total energy. 2z,3z, 4z, and extr. indicate double, triple, quadruple zeta and extrapolated results, respectively. Reference values were obtained from the NIST database.⁷⁶

| state | conf | NIST ¹⁷ | 2z | 3z | 4z | extr. |
|---------------------|---------------|--------------------|-------|-------|-------|-------|
| ${}^2S_{1/2}$ | $4f^{14}6s$ | 0 | 0 | 0 | 0 | 0 |
| ${}^2F_{7/2}^\circ$ | $4f^{13}6s^2$ | 21419 | 12054 | 13524 | 16092 | 17966 |
| ${}^2F_{5/2}^\circ$ | $4f^{13}6s^2$ | 31568 | 22629 | 24139 | 26655 | 28491 |
| ${}^2D_{3/2}$ | $4f^{14}5d$ | 22961 | 24073 | 24209 | 24060 | 23951 |
| ${}^2D_{5/2}$ | $4f^{14}5d$ | 24333 | 25351 | 25457 | 25341 | 25257 |
| ${}^2P_{1/2}^\circ$ | $4f^{14}6p$ | 27062 | 27539 | 27780 | 27857 | 27913 |
| ${}^2P_{3/2}^\circ$ | $4f^{14}6p$ | 30392 | 30954 | 31246 | 31323 | 31380 |

Table 3: Transition energies for the Yb^+ cation. Reference values have been obtained from the NIST database,¹⁷ the computed values were obtained for different basis set with Fock-space coupled cluster.

| state | conf | NIST ¹⁷ | 2z | 3z | 4z | extr. | DCB ⁷⁴ |
|---------------------|---------------|--------------------|-------|-------|-------|-------|-------------------|
| ${}^2S_{1/2}$ | $4f^{14}6s$ | 0 | 0 | 0 | 0 | 0 | 0 |
| ${}^2F_{7/2}^\circ$ | $4f^{13}6s^2$ | 21419 | 11087 | 12390 | 13618 | 14514 | |
| ${}^2F_{5/2}^\circ$ | $4f^{13}6s^2$ | 31568 | 21631 | 22976 | 24170 | 25042 | |
| ${}^2D_{3/2}$ | $4f^{14}5d$ | 22961 | 24058 | 24223 | 24059 | 23938 | 23720 |
| ${}^2D_{5/2}$ | $4f^{14}5d$ | 24333 | 25336 | 25469 | 25340 | 25246 | 24998 |
| ${}^2P_{1/2}^\circ$ | $4f^{14}6p$ | 27062 | 27518 | 27774 | 27851 | 27907 | 27870 |
| ${}^2P_{3/2}^\circ$ | $4f^{14}6p$ | 30392 | 30934 | 31241 | 31316 | 31371 | 31312 |

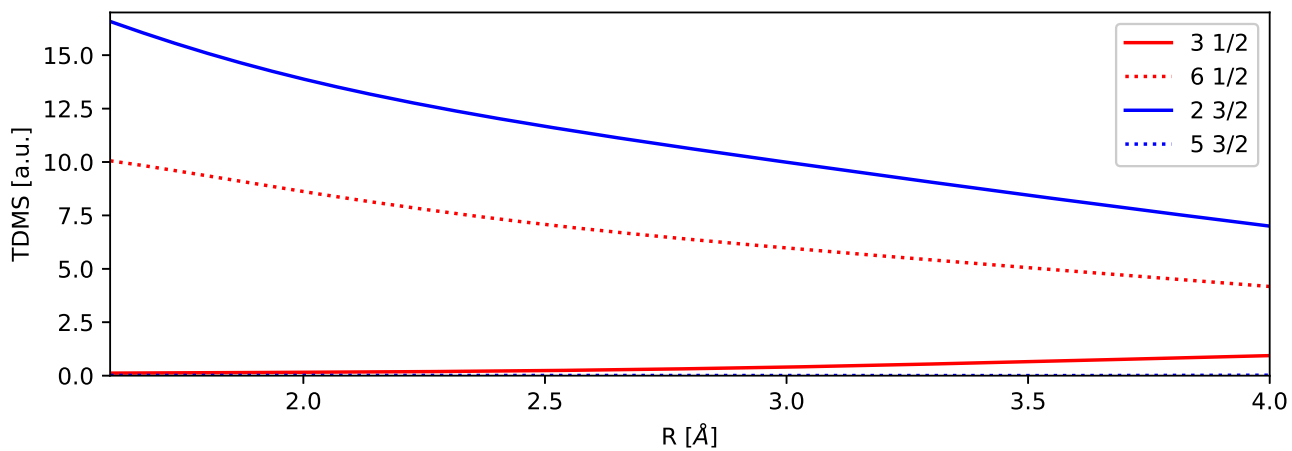
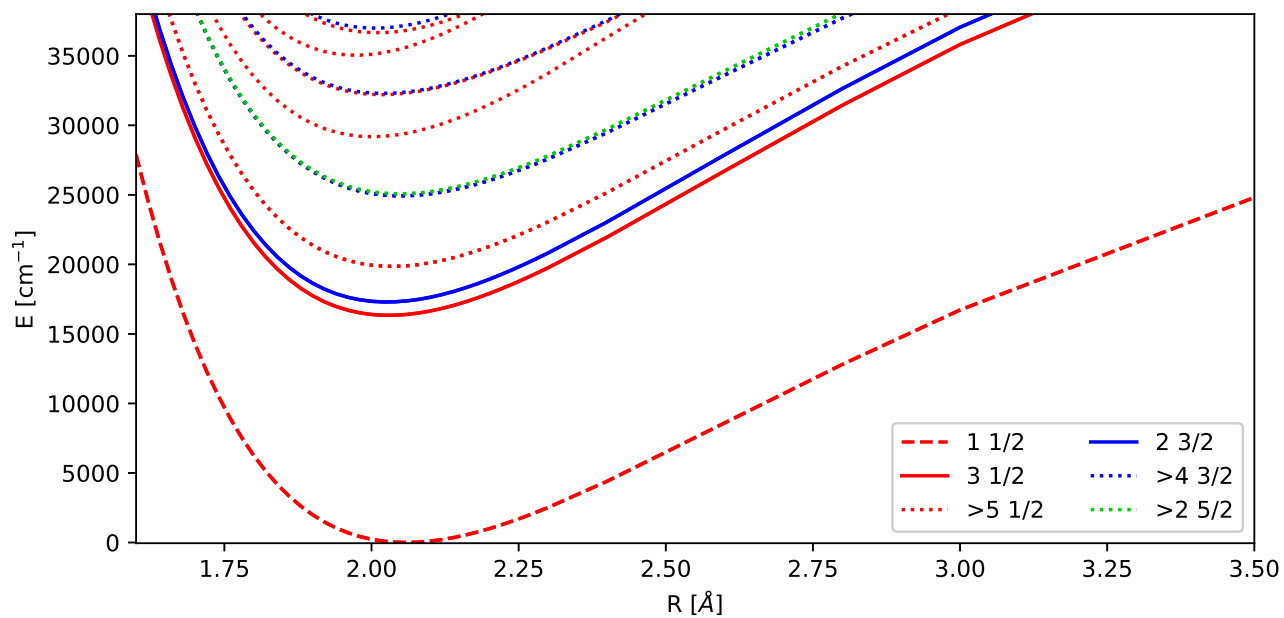


Figure 1: Kramers-restricted configuration interaction potential energy curves (PECs) and transition dipole moments (TDMs) for states with $4f^{14}$ for a quadruple zeta basis set.

the ground state is zero, for the other four the values are shown in the lower part of figure 1. The first $\Omega = 3/2$ and the third $\Omega = 1/2$ state have a larger transition dipole moment close to equilibrium, but get close to each other at the largest internuclear separations.

The states of the $4f^{13}$ manifold are depicted in figure 2. The lowest four states belonging to the $\text{Yb}(4f^{13}[F_{7/2}^{\circ}]\sigma_{6s}^2)\text{F}$ configuration are well separated from a dense region with a lot of states about 12000 cm^{-1} higher. Most of these states are of the $\text{Yb}(4f^{13}[F_{7/2}^{\circ}]5d\sigma_{6s})\text{F}$ configuration, with the $\text{Yb}(4f^{13}[F_{5/2}^{\circ}]\sigma_{6s}^2)\text{F}$ state slightly higher in energy asymptotically and more strongly bound, resulting in several avoided crossings. For each of the four $\text{Yb}(4f^{13}[F_{7/2}^{\circ}]\sigma_{6s}^2)\text{F}$ states the transition dipole moments with higher excited states of varying Ω are plotted in the lower part of figure 2. The transition dipole moments are substantially smaller than the ones for the closed $4f$ -shells but some of them are non-zero.

The two separate sets of potential energy curves can now be combined and figure 3 is obtained. The potential energy curves have been determined up to 11 \AA and for the closed-shell case they were shifted so that the lowest state is at 0 cm^{-1} at the largest distance. Accordingly, the PECs for the hole states were shifted to 21418.75 cm^{-1} at this distance. There is still some interaction between ytterbium and fluorine at this distance, but the long range behaviour can be expected to be similar for the two configurations (this assumption was checked, see supplementary information for further details). Taking into account the position of the minima, the curvatures, spin-orbit splitting, the avoided crossings and asymptotes the states can be assigned to a dominant configuration, shown in figure 3.

An alternative to AOC-SCF for obtaining orbitals for several configurations is multiconfigurational SCF, but similar difficulties as for AOC-SCF in obtaining a balanced description of the $4f^{14}$ and $4f^{13}$ states are observed: either the wrong ground state is obtained (if only the hole states optimized in MCSCF), or the hole states are too high in energy by about 20000 cm^{-1} (if the ground state is optimized). We also

made attempts using state-averaged MCSCF in a non-relativistic quantum chemistry code and observed the same difficulties (see dataset⁶⁷). If the $4f^{13}$ configurations are excluded one obtains meaningful results, but at the expense of obtaining a $\text{Yb}(4f^{13}[F_{7/2}^{\circ}]\sigma_{6s}^2)\text{F}$ states too high in energy. If all the states are included, the wrong ground state is obtained.

3.3 Coupled cluster potential energy curves

The potential energy curves of excited states obtained by the equation-of-motion and Fock space methods are displayed in figure 4, the values for the complete basis set limit are shown. The basis set dependence in the molecule is similar to the one observed for Yb^+ : energies for $4f^{14}$ states depend only weakly on the basis set, while the gap between the ground state and the excited states corresponding to the $\text{Yb}(4f^{13}[F_{7/2}^{\circ}]\sigma_{6s}^2)\text{F}$ configuration increases upon improving the basis sets.

While the EOM-CCSD excitations energies of Yb^+ are closer to the experimental ones, the $\text{Yb}(4f^{13}[F_{5/2}^{\circ}]\sigma_{6s}^2)\text{F}$ states are too high to perturb the $\text{Yb}(4f^{14}5d_{[3/2]})\text{F}$ PECs. From the extended potential energy curves provided in the supporting information, we can observe that the ground state of the non-interacting system ($\text{Yb}(4f^{14}\sigma_{6s}^2)\text{F}(2p^5)$) is repulsive and has a high energy at the equilibrium distance. This results in several avoided crossings being observed at 3, 3.5, and 5 \AA .

Since the $\text{Yb}(4f^{14}\sigma_{6s})\text{F}$ ground state is accessible for both sectors employed in the coupled cluster calculations (Fock space as well as EOM), we can assess the compatibility of the two separate sets of calculations (in the sense of having comparable accuracies) by looking more closely at the differences between the ground states in figure 4. From that, we can see that the EOM-CCSD and IHFS-CCSD approaches the curves are on top of each other from the smallest considered internuclear separation up to about 2.8 \AA . This assures us that there should not be artifacts in putting together and comparing the calculations on the two sec-

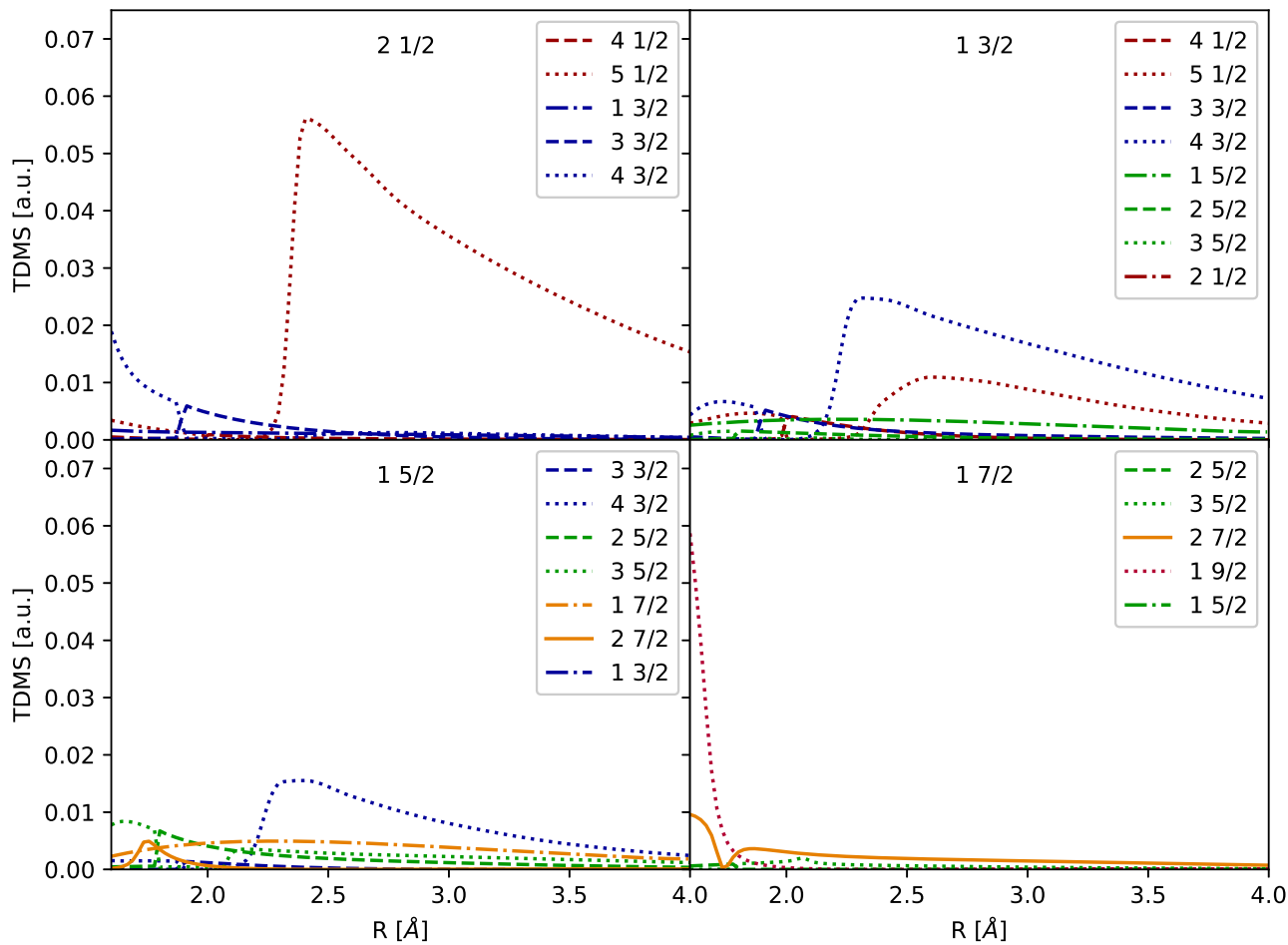
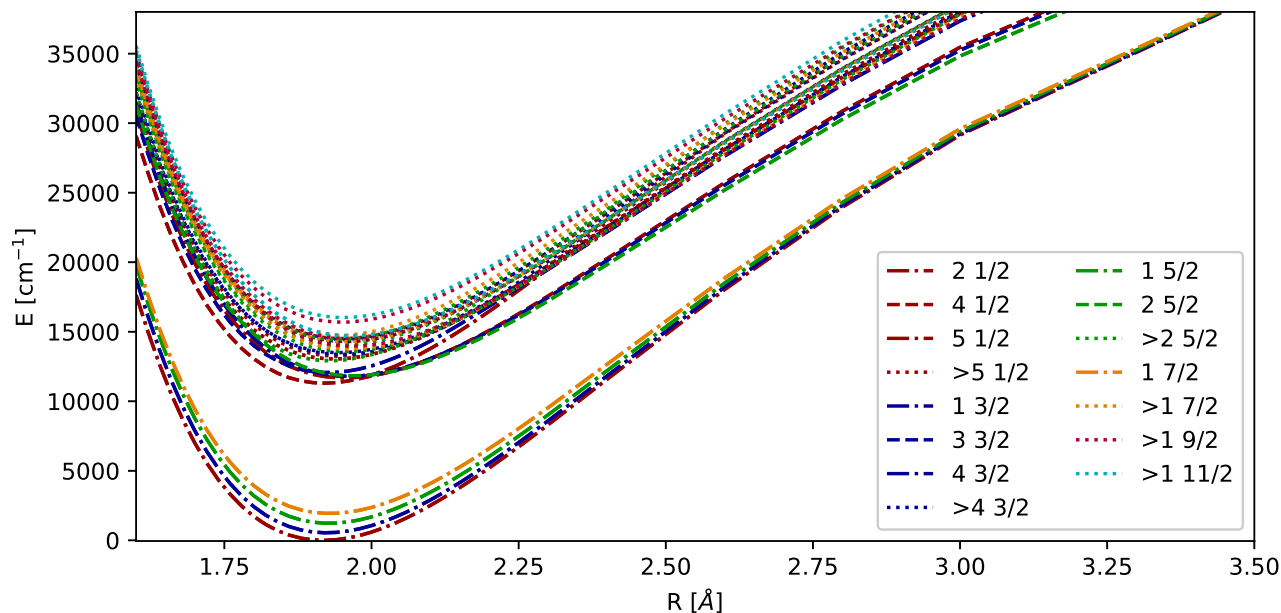


Figure 2: Kramers-restricted configuration interaction PECs and TDMs for states with $4f^{13}$ for a quadruple zeta basis set. The TDMs are provided for the different lowest states with $\Omega = 1/2, 3/2, 5/2,$ and $7/2$.

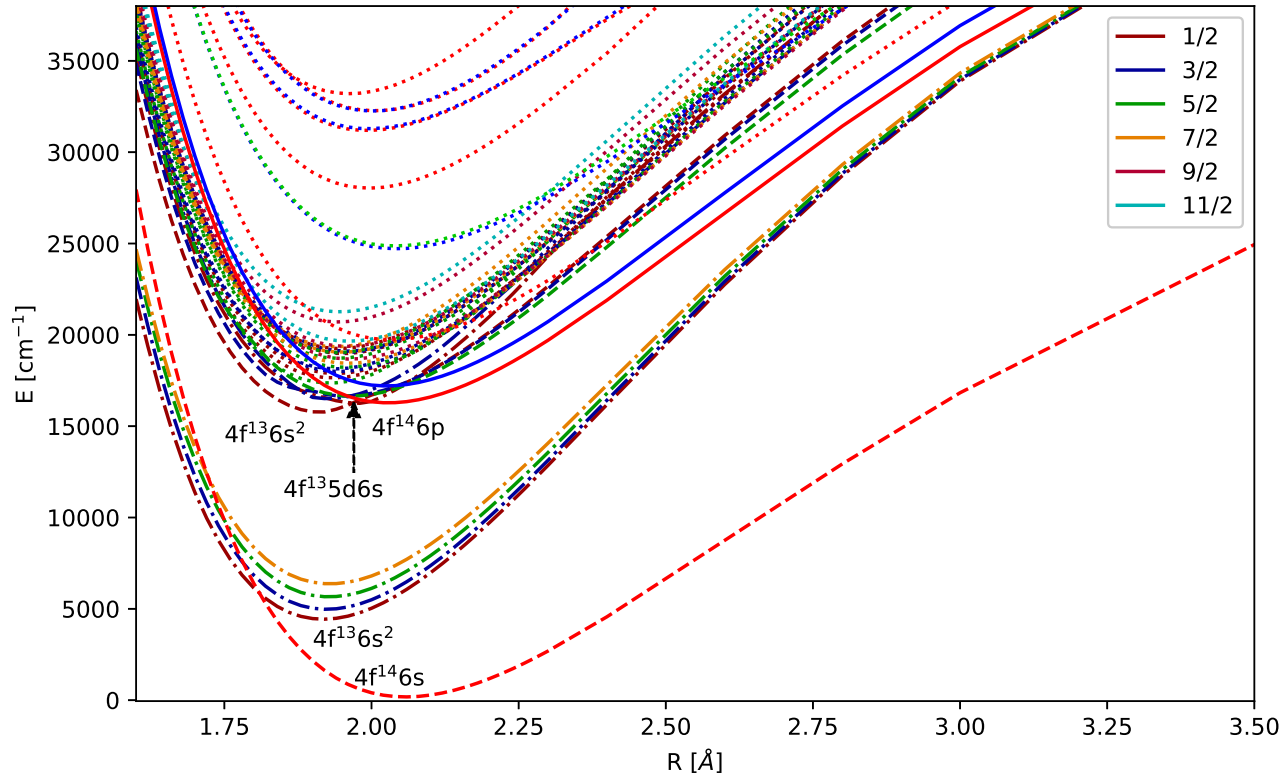


Figure 3: Combination of the sets of KRCI potentials for the CBS limit. The lowest $\Omega = 1/2$ are denoted by their dominant configuration.

tors.

3.4 Dissociation and ionization energies

Since the (1h,0p) and (0h,1p) sectors have been considered in our EOM-CCSD and IHFS-CCSD calculations, we have as a by-product of our calculations the ionization potentials (IP) and electron affinities (EA) for YbF for all computed distances. Therefore these quantities are presented first in table 4, before proceeding to the spectroscopic constants.

Unlike coupled cluster calculations, for KRCI a consistent definition of active spaces is difficult, and its lack of size-consistency results in large deviations from experiment and from the coupled cluster values. For adiabatic electron affinities, for which to the best of our knowledge there are no experimental values, the extrapolated values are 8393 and 8197 cm^{-1} for EOM-CCSD and IHFS-CCSD, respectively. For a distance of 6.5 Å a value of 28651 cm^{-1} was ob-

tained, which is reasonably close to the electron affinity of fluorine (27432 cm^{-1}).⁷⁷ Corresponding results for the atoms are listed in the table, which allow to calculate the dissociation energies (D_e). They deviate from the experimental values of $43600 \pm 800 \text{ cm}^{-1}$ by Kaledin et al.⁷⁸ and $43260 \pm 800 \text{ cm}^{-1}$ by Yokozeki and Menzinger.⁷⁹ The ionization potentials in table 4 show acceptable agreement with experimental values.

3.5 Spectroscopic constants

The spectroscopic constants for the ground state are now considered. In table 5 our results are summarized, along those from the literature. We observe that the extrapolated KRCI bond distances, at about 2.058 Å, are significantly longer (by around 0.04 Å) than experiment,³⁰ whereas the coupled cluster calculations show differences from experiment smaller than 0.01 Å, with EOM-CCSD showing slightly larger discrepancies than IHFS-

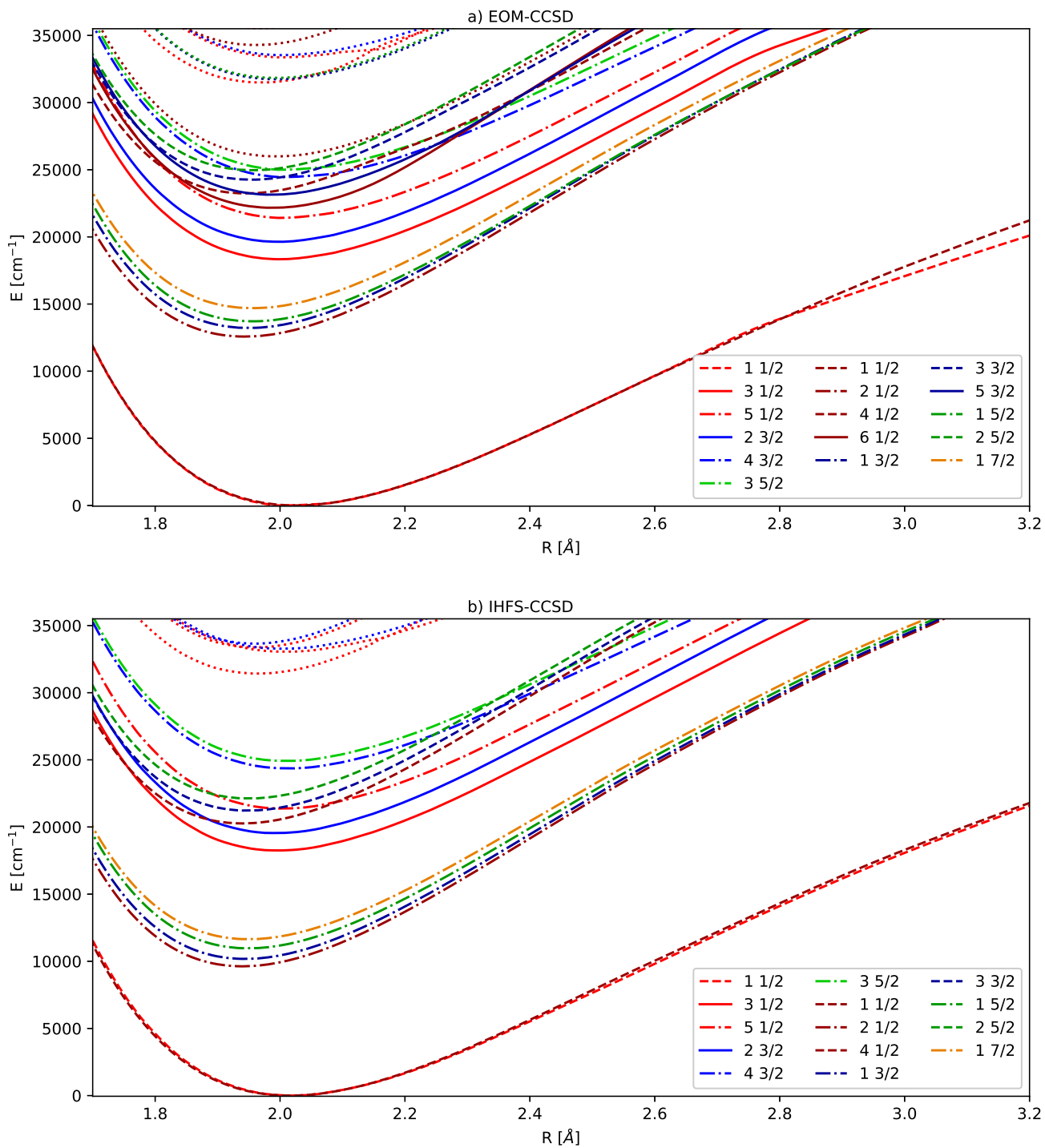


Figure 4: Potential energy curves obtained by extrapolating triple and quadruple zeta basis sets. EOM-CCSD results in the upper part, IHFS-CCSD in the lower part. The Ω values of $1/2$, $3/2$, $5/2$ and $7/2$ are indicated by the colors red, blue, green and orange. The light colors are used for the $(0h,1p)$ sector, dark ones for $(1h,0p)$. For the states below 30000 cm^{-1} we employ the same color coding and state notation as in figure 3.

Table 4: Ionization potential (IP), electron affinity (EA) and dissociation energy (D_e) of Yb, F, and YbF. All values in cm^{-1} . They are listed for a quadrupole zeta basis set and a basis set extrapolation. The minimum of the potentials were determined using a Morse fit and used to compute the adiabatic values listed here.

| quant. | system | KRCI | | EOM-CCSD | | IHFS-CCSD | | experiment |
|------------|--------|--------|--------|----------|--------|-----------|--------|----------------------|
| | | 4z | extr. | 4z | extr. | 4z | extr. | |
| IP | Yb | 38406 | 39128 | 50735 | 50822 | 50740 | 50837 | 50443 ⁷⁶ |
| IP2 | Yb | 90581 | 90926 | 97919 | 98035 | 97918 | 98040 | 98232 ⁷⁶ |
| IP | F | 127131 | 126617 | 144153 | 143321 | 144076 | 144703 | 140525 ⁷⁶ |
| EA | F | 13326 | 11978 | 27279 | 27740 | 27246 | 27759 | 27432 ⁷⁷ |
| IP | YbF | 58478 | 56884 | 48471 | 48578 | 48426 | 49901 | 47700 ⁷⁸ |
| EA | YbF | 7423 | 7326 | 9713 | 9876 | 9579 | 8197 | |
| D_e (IP) | YbF | 26059 | 25887 | 43824 | 47782 | 40591 | 40931 | 43260 ⁷⁹ |
| D_e (EA) | YbF | 40394 | 39660 | 45534 | 49629 | 40430 | 49053 | 43260 ⁷⁹ |

Table 5: Spectroscopic constants for ground state parameters for different approaches. Dissociation energies (D_e), harmonic frequencies (ω_e) and anharmonicity constants ($\omega_e\chi_e$) are given in cm^{-1} , the equilibrium bond distances (r_e) in Å. For the theoretical results we listed the CBS values.

| method | ref. | r_e | ω_e | $\omega_e\chi_e$ | D_e |
|-----------------------|------------------|----------|------------|------------------|-------|
| KRCI | YbF | 2.0829 | 465 | 2.40 | 0 |
| EOM-CCSD | YbF ⁺ | 2.0230 | 511 | 2.80 | 49629 |
| | YbF ⁻ | 2.0250 | 508 | 2.53 | 47782 |
| IHFS-CCSD | YbF ⁺ | 2.0176 | 515 | 2.82 | 49053 |
| | YbF ⁻ | 2.0159 | 513 | 2.42 | 40931 |
| CCSD ¹ | YbF | 2.0174 | 507.6 | 2.357 | 40904 |
| CCSD(T) ¹ | YbF | 2.0289 | 528.2 | 1.939 | 41156 |
| CCSD ²¹ | | 2.0127 | 566.8 | 3.7885 | 55650 |
| RASCI ⁶ | | 2.051 | 529 | | |
| CCSD(T) ⁸⁰ | | 2.03 | | | 38900 |
| CISD ⁸¹ | | 2.034 | 502 | | 42100 |
| DFT ²⁰ | | 1.987 | 532 | | 45000 |
| exp. ⁷⁹ | | | | | 43260 |
| exp. ¹⁸ | | 2.0158 | 506.6674 | 2.2452 | |
| exp. ²⁷ | | | 505.5 | 1.9 | |
| exp. ⁷⁸ | | | | | 43600 |
| exp. ³⁰ | | 2.016514 | | | |
| exp. ²⁴ | | 2.0195 | 506.616 | 2.235 | |

CCSD. Between the extrapolated EOM-CCSD and IHFS-CCSD, we also see small differences between the $4f^{14}$ and $4f^{13}$: for EOM-CCSD these differ by around 0.001\AA whereas for IHFS-CCSD the difference is slightly under 0.002\AA , with the $4f^{13}$ configuration yielding a slightly underestimated value, compared to experiment, something that can be traced back to the differences in model spaces for this configuration.

Our results for harmonic frequencies further indicate that KRCI seems to underestimate the bonding strength in YbF, as the harmonic vibrational frequency is smaller (491 cm^{-1}) than experiment (between 505.5 and 506.7 cm^{-1} depending on the experiment). The coupled cluster results, on the other hand, show the typical $5\text{-}6\text{ cm}^{-1}$ overestimation of the harmonic frequencies with respect to experiment (something also seen for the anharmonic constants), which can be attributed to lack of triples in the EOM or FS treatment, that would introduce further orbital relaxation. This can be seen in comparison to the unrestricted coupled cluster calculations of Gomes et al.,¹ which in spite of the large value of the T_1 diagnostic, reproduce well the experimental bond lengths, harmonic frequencies and anharmonic constants.

Taken together, our 2-component CCSD-based calculations and the 4-component ones of Gomes et al.¹ compare consistently better to experiment than the other theoretical works for bond lengths, vibrational frequencies and anharmonic constants. For the dissociation energies, on the other hand, the extrapolated calculations presented here do not provide a significant improvement over the results of prior theoretical investigations (quadruple zeta values are closer to the experimental ones for this quantity, see table 4). Especially, electron attachment values are off, which might be related to the absence of the configuration with a hole in the p orbitals of fluorine.

Moving now to excited states, we start by considering the four lowest excited states, which belong to the $\text{Yb}(4f^{13}[F_{7/2}^{\circ}]\sigma_{6s}^2)\text{F}$ configuration. These states are well separated from the ground state (the lowest excited state is about 10000 cm^{-1} above the ground state) and higher excited states. That such states are quite well

separated from the ground state would, in our view, tend to exclude the interaction with a low-lying excited state as an explanation for the appearance of the large T_1 diagnostic values observed by Gomes et al.¹ From their spectroscopic constants, presented in table 6, we see that with the exception of DFT all methods yield similar level splittings of about 500 , 1200 , and 2000 cm^{-1} . To the best of the authors knowledge there is no experimental data available for these states, due to their negligible transition dipole moments for dipole excitations (see for instance figure 2) and small Franck-Condon factors due to the difference in bond distances between these states and the ground state.

The smallest equilibrium distance was obtained for the $2_{1/2}$ state with 1.94 \AA for the coupled cluster methods and 0.02 \AA less for KRCI. The vibrational frequencies are between 570 and 600 cm^{-1} for the coupled cluster methods and about 30 cm^{-1} higher for KRCI.

For higher excited states, as apparent from the figures in the previous section, the identification and assignment of states gets more difficult and there are differences between the methods. We have nevertheless provided in table 7 the spectroscopic constants for excited with Ω values of $1/2$, $3/2$, and $5/2$, respectively.

Table 6: Spectroscopic constants for the lowest excited states $\text{Yb}(4f^{13}[F_{7/2}^{\circ}]\sigma_{6s}^2)\text{F}$ for different wave function methods using the potential energy curves extrapolated to the basis set limit. In the case of KRCI and MRCI¹⁹ the ground state is not included in the computation and absolute transition energies are not available. The transition energy (T_e), level splitting (T_{rel} , energy relative to $2_{1/2}$), harmonic frequencies (ω_e) and anharmonicity constants ($\omega_e\chi_e$) are given in cm^{-1} , the equilibrium bond distances (r_e) in Å.

| state | method | T_e | r_e | ω_e | $\omega_e\chi_e$ | T_{rel} |
|-----------|--------------------|-------|---------|------------|------------------|-----------|
| $2_{1/2}$ | KRCI | | 1.9200 | 631 | 2.51 | |
| | EOM-CCSD | 12568 | 1.9432 | 591 | 2.59 | |
| | IHFS-CCSD | 9627 | 1.9396 | 599 | 2.79 | |
| | DFT ²⁰ | 3790 | 1.9570 | 561 | | |
| | MRCI ¹⁹ | | 1.9480 | 600 | | |
| $1_{3/2}$ | KRCI | | 1.9253 | 628 | 2.50 | 540 |
| | EOM-CCSD | 13211 | 1.9494 | 588 | 2.61 | 643 |
| | IHFS-CCSD | 10180 | 1.9438 | 595 | 2.79 | 553 |
| | DFT ²⁰ | 9520 | 1.9440 | 597 | | 5730 |
| | MRCI ¹⁹ | | 1.951 0 | 598 | | 428 |
| $1_{5/2}$ | KRCI | | 1.9296 | 622 | 2.45 | 1223 |
| | EOM-CCSD | 13703 | 1.9553 | 582 | 2.61 | 1135 |
| | IHFS-CCSD | 10968 | 1.9493 | 589 | 2.78 | 1341 |
| | DFT ²⁰ | 10970 | 1.9360 | 598 | | 7180 |
| | MRCI ¹⁹ | | 1.9540 | 594 | | 1021 |
| $1_{7/2}$ | KRCI | | 1.9315 | 616 | 2.43 | 1933 |
| | EOM-CCSD | 14685 | 1.9556 | 577 | 2.62 | 2117 |
| | IHFS-CCSD | 11645 | 1.9496 | 583 | 2.77 | 2018 |
| | DFT ²⁰ | 16530 | 1.936 | 592 | | 12740 |
| | MRCI ¹⁹ | | 1.954 | 589 | | 1709 |

Table 7: Spectroscopic constants for excited states with $\Omega = 1/2, 3/2, 5/2$, starting from 18000 cm^{-1} for different methods using the values after extrapolation to the basis set limit. Transition energy (T_e), vibrational constant (ω_e), and anharmonicity constant ($\omega_e\chi_e$) are given in cm^{-1} , the equilibrium bond distance (r_e) in Å. Experimental transitions that were not assigned(n.a.) are also listed.

| Ω | method | state | configuration | T_e | r_e | ω_e | $\omega_e\chi_e$ | |
|--------------------|----------------------|------------------------|------------------------|------------------------|--------|------------|------------------|------|
| 1/2 | KRCI ^a | 3 | $4f^{13}\sigma_{6s}^2$ | 15572 | 1.9038 | 655 | 13.57 | |
| | | 4 | $4f^{13}5d\sigma_{6s}$ | 16020 | 1.9603 | 620 | 0.08 | |
| | | 5 | $4f^{14}6p$ | 16189 | 2.0504 | 496 | 2.38 | |
| | | 6 | $4f^{13}5d\sigma_{6s}$ | 17350 | 1.9360 | 598 | 2.50 | |
| | | 7 | $4f^{13}5d\sigma_{6s}$ | 17587 | 1.9417 | 592 | 2.56 | |
| | | 8 | $4f^{13}5d\sigma_{6s}$ | 18675 | 1.9539 | 582 | 2.71 | |
| | | 9 | $4f^{13}5d\sigma_{6s}$ | 18952 | 1.9479 | 578 | 2.71 | |
| | | 10 | $4f^{14}5d$ | 19631 | 2.0552 | 490 | 2.49 | |
| | | EOM-CCSD | 3 | $4f^{14}6p$ | 18373 | 2.0004 | 536 | 2.72 |
| | | | 4 | $4f^{14}5d$ | 21448 | 2.0079 | 532 | 2.78 |
| | 5 | | $4f^{14}6p$ | 22147 | 1.9886 | 573 | 1.18 | |
| | 6 | | $4f^{13}\sigma_{6s}^2$ | 23241 | 1.9432 | 582 | 4.06 | |
| | IHFS-CCSD | 3 | $4f^{14}6p$ | 18249 | 1.9953 | 539 | 2.63 | |
| | | 4 | $4f^{13}\sigma_{6s}^2$ | 20267 | 1.9397 | 597 | 2.78 | |
| | | 5 | $4f^{14}5d$ | 21375 | 2.0032 | 533 | 2.73 | |
| | MRCI ¹⁹ | | $4f^{13}\sigma_{6s}^2$ | | 1.948 | 600 | | |
| | exp. ^{18 a} | 3 | | 18106.20 | | 537 | 3 | |
| | exp. ¹⁸ | 4 | [18.6] _{1/2} | 18705.06 | | | | |
| | exp. ²⁴ | | [557] | 18574 | 1.9656 | 502.15 | | |
| | exp. ²⁴ | | [561] | 18699 | 1.9571 | | | |
| 3/2 | KRCI ^a | 2 | $4f^{13}\sigma_{6s}^2$ | 16206 | 1.9331 | 711 | 8.45 | |
| | | 3 | $4f^{13}5d\sigma_{6s}$ | 16346 | 1.9505 | 516 | 0.80 | |
| | | 4 | $4f^{14}6p$ | 17123 | 2.0473 | 499 | 2.37 | |
| | | 5 | $4f^{13}5d\sigma_{6s}$ | 17693 | 1.9473 | 585 | 2.47 | |
| | | 6 | $4f^{13}5d\sigma_{6s}$ | 17843 | 1.9408 | 584 | 3.30 | |
| | | EOM-CCSD | 2 | $4f^{14}6p$ | 19672 | 1.9971 | 540 | 2.72 |
| | 3 | | $4f^{14}6p$ | 23137 | 1.9857 | 557 | 2.28 | |
| | 4 | | $4f^{13}\sigma_{6s}^2$ | 24251 | 1.9537 | 584 | 2.64 | |
| | 5 | | $4f^{14}5d$ | 24468 | 2.0177 | 509 | 2.78 | |
| | IHFS-CCSD | 2 | $4f^{14}6p$ | 19543 | 1.9920 | 542 | 2.63 | |
| | | 3 | $4f^{13}\sigma_{6s}^2$ | 21222 | 1.9480 | 591 | 2.80 | |
| | | 4 | $4f^{14}5d$ | 24363 | 2.0120 | 512 | 2.73 | |
| MRCI ¹⁹ | | $4f^{13}\sigma_{6s}^2$ | | 1.953 | 596 | | | |
| exp. ¹⁸ | 2 | | 19471.49 | | | | | |
| 5/2 | KRCI ^a | 2 | $4f^{13}5d\sigma_{6s}$ | 16340 | 1.9677 | 564 | 2.42 | |
| | | 3 | $4f^{13}\sigma_{6s}^2$ | 17063 | 1.9302 | 635 | 1.41 | |
| | | 4 | $4f^{13}5d\sigma_{6s}$ | 17700 | 1.9627 | 571 | 0.93 | |
| | | 5 | $4f^{13}5d\sigma_{6s}$ | 18422 | 1.9451 | 584 | 3.07 | |
| | | EOM-CCSD | 2 | $4f^{13}\sigma_{6s}^2$ | 24957 | 1.95359 | 577 | 2.62 |

Continued on next page

Table 7 – *Continued from previous page*

| Ω | method | state | configuration | T_e | r_e | ω_e | $\omega_e \chi_e$ |
|----------|--------------------|-------|------------------------|---------|--------|------------|-------------------|
| | | 3 | $4f^{14}5d$ | 25023 | 2.0146 | 513 | 2.80 |
| | IHFS-CCSD | 2 | $4f^{13}\sigma_{6s}^2$ | 22127 | 1.9499 | 584 | 2.77 |
| | | 3 | $4f^{14}5d$ | 24919 | 2.0089 | 515 | 2.77 |
| | MRCI ¹⁹ | | $4f^{13}\sigma_{6s}^2$ | | 1.954 | 590 | |
| n.a. | exp. ²⁶ | | [574] | 19150 | | | |
| | exp. ²⁶ | | [578] | 19280 | | | |
| | exp. ²⁷ | | Q | 23035.3 | | 523 | 2 |
| | exp. ²⁷ | | Q | 23256.0 | | 507 | 2 |
| | exp. ²⁷ | | P | 26014.8 | | 574.6 | 2.8 |

^a KRCI transition energies for the $4f^{13}$ sector were obtained by adding 4144 cm^{-1} , an estimate for the energy of the lowest state in this manifold.

The comparison with experimental results allows assignment of the lowest excited state reported in experiments and give some indications for higher states. The lowest $\Omega = 1/2$ state observed in experiment can be identified as the $3_{1/2}$ state. Spectroscopic parameters agree well with the ones obtained by fitting to the $A^2\Pi_{1/2}$ in experiments. A bond distance of 1.9935 Å obtained by fitting to the same states in ref. 34 agrees well with the coupled cluster values for the $3_{1/2}$ state, the vibrational constant of about 540 cm^{-1} is close to the experimental value of ref. 18. Similarly, the lowest $\Omega = 3/2$ state reported by Dunfield et al.¹⁸ can be identified as the $2_{3/2}$ state, see table 7.

The lowest states with $\Omega = 1/2$ and $\Omega = 3/2$ for this energy range approach asymptotically a state with a $\text{Yb}(4f^{14}5d)\text{F}$ configuration, but if one analyses the EOM-CCSD and IHFS-CCSD orbital composition, significant contributions of the atomic $6p$ are identified. The $\Omega = 3/2$ state is dominated (97%) by a single configuration, corresponding to a $\text{HOMO}(\sigma_{6s,1/2}) \rightarrow \text{LUMO}+1$ where the latter is made up of a mixture of $6p_\pi$ and $5d_\pi$ orbitals (the $6p_\pi$ contributions being the dominant – $\simeq 80\%$ – in the reference YbF^+ orbitals). The few other significant configurations arise from excitations to higher-lying orbitals with increasingly large ($\geq 50\%$ $5d_\pi$) contributions. The $\Pi_{1/2}$ state is also dominated by a single configuration, now corresponding to a $\text{HOMO}(\sigma_{1/2}) \rightarrow \text{LUMO}$ transition, and shows a rather similar picture in terms of the relative weights of the $6p_\pi$ and $5d_\pi$ orbitals, with very small contributions from the ground-state mixing due to spin-orbit coupling. The splitting in Yb^+ of $^2\text{D}_{3/2}$ and $^2\text{D}_{5/2}$ is 1372 cm^{-1} , for $^2\text{P}_{1/2}$ and $^2\text{P}_{3/2}$ it is 3330 cm^{-1} . The separation between the lowest excited $\Omega = 1/2$ states in the closed shell computation is 3779 and 3126 cm^{-1} for EOM-CCSD and IHFS-CCSD, respectively. This is an indication that the two states must be regarded as a fairly strong admixture of $6p$ and $5d$ orbitals of $j=1/2$ or $3/2$, as one can expect a much smaller spin-orbit splitting in the axial field of the molecule (about 1/3 of the atomic spin-orbit splitting for the P state). This picture also finds experimental support in recent measurements of hyperfine constants (d

and eQ_0q) for the ground and $\Pi_{1/2}$ excited state of YbF ,⁹ where a simple ligand-field model disregarding the contributions from $5d_\pi$ orbitals predicted values of d a factor of 2 larger than the measurements. For bond distances much larger than the equilibrium one the system gets closer to the configurations in Yb^+ with a dominating $5d$ contribution.

As already mentioned this energy range above 18000 cm^{-1} is dense with a large number of excited states that can mix with each other and result in new mixed states, like the [557] and [561] ones.²⁴ These will be addressed in section 3.6.

Uttam *et al.*²⁷ reported three unidentified states with energies above 22000 cm^{-1} which are listed in table 7 and cannot uniquely be identified with the current results. The one at 26014.8 cm^{-1} has a larger vibrational constant indicating a more strongly bound state, possibly of the $4f^{13}\sigma_{6s}^2$ configuration. The vibrational spacing of the two states at 23000 cm^{-1} rather points to states with a closed f shell.

3.6 Perturbation of the $3_{1/2}$ excited state

Due to the use of different sectors of Fock space to obtain the $4f^{14}$ and $4f^{13}$ configurations, the excited states with the same Ω values cannot interact among themselves, as is the case within each sector. However, from the discussion above, it is clear that dealing with states which are artificially prevented from interaction makes it difficult to establish a comparison to experiment, for states from about 18000 cm^{-1} to about 26000 cm^{-1} , which is where these configurations should be the most entangled. In order to remedy that, in the following we introduce a simple adiabaticization model (equation 2) that allows us to investigate how coupling such states would affect the overall spectra in the aforementioned energy region.

In the following we only consider the IHFS-CCSD potential energy curves, as the spectroscopic parameters are more reliable for CCSD than for KRCI. The coupled cluster results for the two methods are quite similar, and FS-CCSD was selected (because it does not in-

clude the (2h,1p) and (1h,2p) transitions with rather large uncertainties). Figure 5 contains the original FS-CCSD curves as well as the ones obtained after adiabaticization with three different coupling constants. Looking at the potential energy curves for this energetic region, there are two $\Omega = 1/2$ and two $\Omega = 3/2$ states of $\text{Yb}(4f^{14}6p)\text{F}$ and $\text{Yb}(4f^{14}5d)\text{F}$ configurations originating from the (0h,1p) sector. For both Ω values there is an additional state with a $\text{Yb}(4f^{13}[F_{5/2}^{\circ}]\sigma_{6s}^2)\text{F}$ configuration stemming from the (1h,0p) sector. By looking at the KRCI results one expects additional states belonging to the $\text{Yb}(4f^{13}[F_{7/2}^{\circ}]5d\sigma_{6s})\text{F}$ configuration for this energy range, which will not be included in the current considerations.

As already mentioned earlier the lowest $\Omega = 1/2$ and $\Omega = 3/2$ states can be identified clearly and assigned to experimental observations. There are several experimental states in this energy region attributed to the mixing of states. The [557] and [561] ones²⁴ are assumed to arise from a mixing of the $3_{1/2}$ and $4_{1/2}$. The vibrational constant of the perturbing state ($4_{1/2}$) was estimated to be 605 cm^{-1} in ref. 18. This agrees with the $4_{1/2}$ state in figure 5 with a $\text{Yb}(4f^{13}[F_{5/2}^{\circ}]\sigma_{6s}^2)\text{F}$ configuration, see also table 7. [574] and [578]²⁶ have not been identified and since their Ω value is unknown, we were not able to assign them to a configuration.

Next we take a look at the changes introduced by adiabaticization. For small and intermediate coupling strengths there are no major differences in the potential energy curves, although close to the crossing points the potentials are deformed. Intermediate coupling strengths with slightly deformed potentials close to the avoided crossings will be the most realistic description. For very large coupling strengths one obtains parallel potential energy curves due to the strong repulsion. This also results in a major change of the spectra above 19000 cm^{-1} . One of the differences between the adiabatic spectrum and the uppermost one in figure 5 is that the Frank-Condon factors of the $4_{1/2}$ state, which is of the $\text{Yb}(4f^{13}\sigma_{6s}^2)\text{F}$ configuration, are now noticeable and the spacing of the energy levels of the $5 \ 1/2$ is changed. Similarly, tran-

sitions belonging to the $5 \ 1/2$ appear.

The influence of adiabaticization on spectroscopic parameters can be investigated by comparing spectroscopic constants calculated for the IHFS-CCSD curves without and with a coupling of 100 cm^{-1} (table 8). We observe that for this coupling strength, there are small but non-negligible changes for the excitation energies, harmonic frequencies and anharmonicity constants, for all but the fourth and fifth $\Omega = 1/2$ states; there, the coupling does seem to significantly change the anharmonicity constants. Equilibrium distances, on the other hand, are largely unperturbed in all cases. Furthermore, as expected from the preceding discussion, no changes are observed for the ground-state, since it is too separated in energy from the other electronic states.

4 Conclusion

In this manuscript we have presented a study of the ground and excited states of the YbF molecule, with 2-component multireference CI, equation of motion and Fock space coupled cluster approaches (in all cases, performing extrapolations to the complete basis set limit). In particular, we have focused on obtaining electronic states up to around 24000 cm^{-1} arising from configurations which differ in the occupation of the $4f$ shell ($4f^{14}$ and $4f^{13}$), which are very difficult to treat on the same footing due to a number of subtle correlation and relaxation effects.

In order to achieve such a balanced description, our strategy consisted of starting from YbF^+ and YbF^- , in order to arrive at the wavefunctions for YbF through the (1h,0p) and (0h,1p) sectors of Fock space. Once obtained, electronic states with same Ω values coming from these different sectors are further coupled through a simple adiabaticization model in which the coupling strength is taken as a constant.

As a general rule we find that the CI calculations do capture the essential physics of the system, though they are not as reliable as the coupled cluster approaches for excitation energies, bond lengths, harmonic vibrational fre-

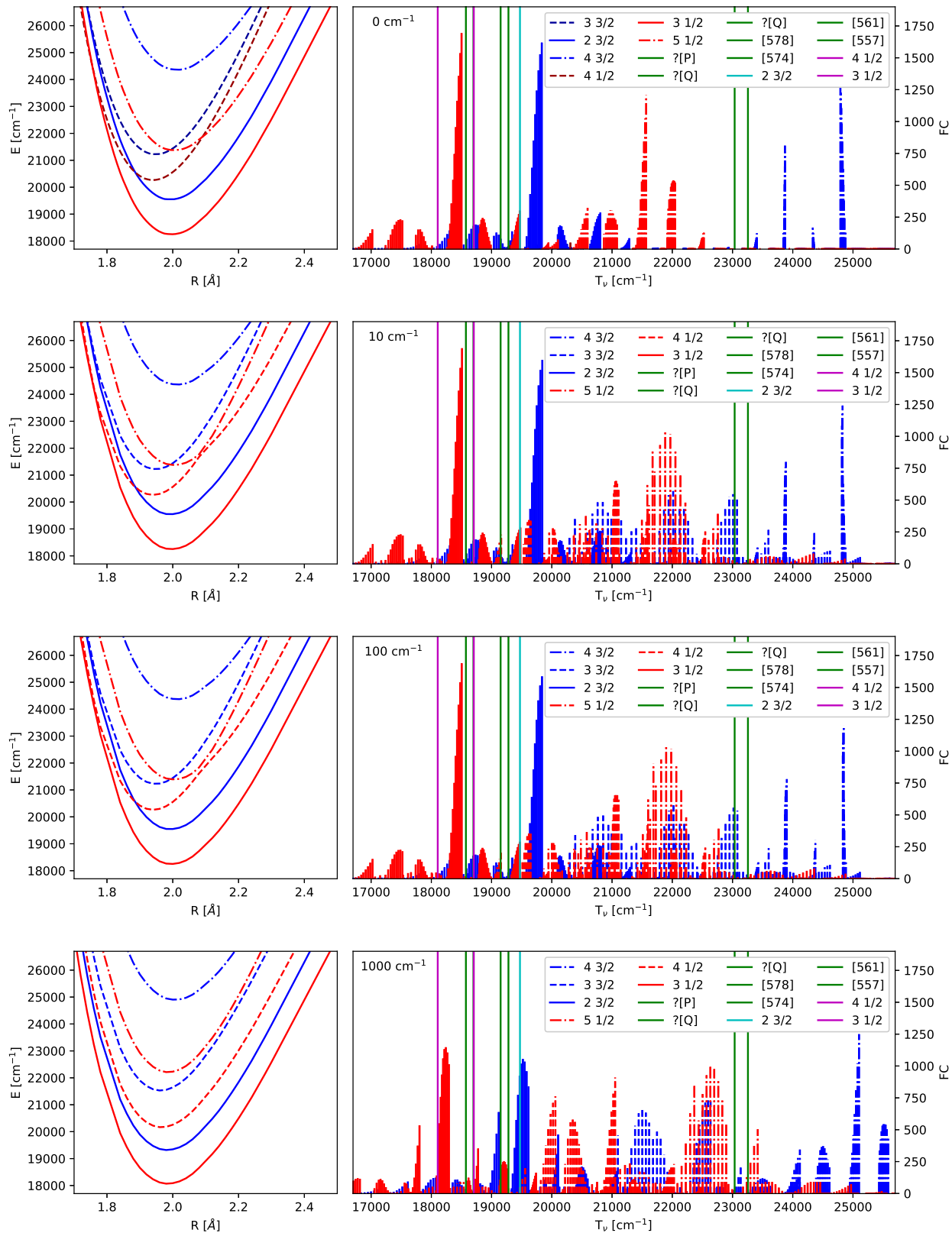


Figure 5: Frank-Condon factors before and after adiabaticization for the IHFS-CCSD potential energy curves. C is the coupling strength in Hartree. The lowest 10 vibrational levels of the ground state were used as well as the lowest 60 vibrational levels of the excited state. The experimental values have been added as straight lines.^{18,24,26}

Table 8: Spectroscopic data obtained by fitting Morse potentials to the lowest points of the potential energy curves obtained with FSCC for the extrapolated basis set(CBS). This table combines results from both sectors starting either with a closed (f^{14}) or open (f^{13}) f-shell. Additionally, the table contains spectroscopic parameters after adiabaticization with a specific coupling constant (C). The transition energy (T_e), vibrational constant (ω_e), and anharmonicity constant ($\omega_e x_e$) are given in cm^{-1} , the equilibrium bond distance (r_e) in Å.

| Ω | CBS | | | | | C = 100 cm^{-1} | | | | |
|----------|--------------|-------|------------|----------------|-------|--------------------------|-------|------------|----------------|-------|
| | state | r_e | ω_e | $\omega_e x_e$ | T_e | state | r_e | ω_e | $\omega_e x_e$ | T_e |
| 1/2 | $f^{14} - 1$ | 2.018 | 515 | 2.9 | 0 | 1 | 2.018 | 515 | 2.8 | 0 |
| | $f^{13} - 2$ | 1.940 | 599 | 2.8 | 9627 | 2 | 1.940 | 599 | 2.8 | 9617 |
| | $f^{14} - 2$ | 1.995 | 539 | 2.6 | 18249 | 3 | 1.995 | 538 | 2.6 | 18247 |
| | $f^{13} - 3$ | 1.940 | 597 | 2.8 | 20267 | 4 | 1.935 | 603 | 8.6 | 20258 |
| | $f^{14} - 3$ | 2.003 | 533 | 2.7 | 21375 | 5 | 2.002 | 586 | 0.4 | 21359 |
| | $f^{14} - 4$ | 1.964 | 581 | 1.8 | 31416 | 6 | 1.964 | 581 | 1.8 | 31419 |
| 3/2 | $f^{13} - 1$ | 1.944 | 595 | 2.8 | 10180 | 1 | 1.944 | 594 | 2.8 | 10170 |
| | $f^{14} - 1$ | 1.992 | 542 | 2.6 | 19543 | 2 | 1.992 | 542 | 2.6 | 19540 |
| | $f^{13} - 2$ | 1.948 | 591 | 2.8 | 21222 | 3 | 1.948 | 591 | 2.8 | 21217 |
| | $f^{14} - 2$ | 2.012 | 512 | 2.7 | 24363 | 4 | 2.012 | 512 | 2.7 | 24369 |
| 5/2 | $f^{13} - 1$ | 1.949 | 589 | 2.8 | 10967 | 1 | 1.949 | 589 | 2.8 | 10960 |
| | $f^{13} - 2$ | 1.950 | 584 | 2.8 | 22127 | 2 | 1.950 | 583 | 2.8 | 22117 |
| | $f^{14} - 1$ | 2.009 | 515 | 2.8 | 24919 | 3 | 2.009 | 516 | 2.7 | 24926 |

quencies and anharmonic constants. In effect, the coupled cluster calculations for the (1h,0p) and (0h,1p) sectors yield the same potential energy curves for the ground state, for internuclear distances up to around 2.8\AA , which is sufficient to capture the bound regions of all states under consideration,

We have determined that the lowest lying excited states arise from the $\text{Yb}(4f^{13}[F_{7/2}^{\circ}]\sigma_{6s}^2)\text{F}$ configuration, with transition energies of around 10000 cm^{-1} , and a splitting about 2000 cm^{-1} . These states are, however, not generally accessible in experiment due to their low dipolar intensity and significantly shifted minima of the potential energy curve resulting in small Frank-Condon factors.

The next set of states, coming above 18000 cm^{-1} , arise from the $\text{Yb}(4f^{14}6p)\text{F}$, $\text{Yb}(4f^{14}5d)\text{F}$, $\text{Yb}(4f^{13}[F_{5/2}^{\circ}]\sigma_{6s}^2)\text{F}$, and $\text{Yb}(4f^{13}[F_{7/2}^{\circ}]5d\sigma_{6s})\text{F}$ configurations. Among these, the $\text{Yb}(4f^{13}[F_{7/2}^{\circ}]\sigma_{6s}^2)\text{F}$ configurations generally display the shortest equilibrium distances and deepest potential well, while the $\text{Yb}(4f^{14}5d)\text{F}$ and $\text{Yb}(4f^{14}6p)\text{F}$ configurations exhibits the largest bond distances and smallest

harmonic frequencies, with the other configurations falling somewhere in between. The lowest $\Omega = 1/2$ and $\Omega = 3/2$ states of this group show a $\text{Yb}(4f^{14}6p)\text{F}$ orbital composition around the ground-state equilibrium structure, though for longer bond lengths they asymptotically approach the $\text{Yb}(4f^{14}5d)\text{F}$ configuration.

We note that configurations with three unpaired electrons, such as $\text{Yb}(4f^{13}[F_{7/2}^{\circ}]5d\sigma_{6s})\text{F}$, were only considered with the KRCI method, which has larger uncertainties. This only allows us to make some qualitative statements, e.g. that their bond distances and vibrational constant should be between the values for the other configurations and that they should be higher in energy than the lowest excited $\text{Yb}(4f^{14}6p)\text{F}$ and $\text{Yb}(4f^{13}[F_{5/2}^{\circ}]\sigma_{6s}^2)\text{F}$ states.

A simple method was applied in order to adiabaticize the curves obtained for different sectors and reference wave functions. It was applied to potential energy curves between 18000 and 26000 cm^{-1} and small changes of the Franck-Condon factors were observed. The influence on spectroscopic constant was minor, with the exception of the asymmetry constant for two states. However, the approximation introduced

(same coupling strength for all states and all geometries) is perhaps not flexible enough, and more sophisticated models should be investigated.

5 Acknowledgements

LV and JVP wish to thank The Netherlands Organization for Scientific Research (NWO) for financial support via the ECHO and computer time. JVP acknowledges funding by the Austrian Science Fund(FWF):J 4177-N36. ASPG acknowledges support from PIA ANR project CaPPA (ANR-11-LABX-0005-01), the Franco-German project CompRIXS (Agence nationale de la recherche ANR-19-CE29-0019, Deutsche Forschungsgemeinschaft JA 2329/6-1), I-SITE ULNE projects OVER-SEE, the French Ministry of Higher Education and Research, region Hauts de France council and European Regional Development Fund (ERDF) project CPER CLIMIBIO, and the French national supercomputing facilities (grants DARI A0070801859 and A0090801859). ASPG, LH, JP and LV acknowledge support from MESONM International Associated Laboratory (LAI) (ANR-16-IDEX-0004).

References

- (1) Gomes, A. S. P.; Dyllal, K. G.; Visscher, L. Relativistic double-zeta, triple-zeta, and quadruple-zeta basis sets for the lanthanides La-Lu. *Theoretical Chemistry Accounts* **2010**, *127*, 369–381.
- (2) Sapirstein, J. In *Theoretical and Computational Chemistry*; Schwerdtfeger, P., Ed.; Elsevier, 2002; Vol. 11; pp 468–522.
- (3) Berger, R. In *Theoretical and Computational Chemistry*; Schwerdtfeger, P., Ed.; Elsevier, 2004; Vol. 14; pp 188–288.
- (4) Sunaga, A.; Abe, M.; Hada, M.; Das, B. P. Relativistic coupled-cluster calculation of the electron-nucleus scalar-pseudoscalar interaction constant W_s in YbF. *Phys. Rev. A* **2016**, *93*, 042507.
- (5) Parpia, F. A. Ab initio calculation of the enhancement of the electric dipole moment of an electron in the YbF molecule. *Journal of Physics B: Atomic, Molecular and Optical Physics* **1998**, *31*, 1409–1430.
- (6) Nayak, M. K.; Chaudhuri, R. K. Ab initio calculation of P,T-odd effects in YbF molecule. *Chemical Physics Letters* **2006**, *419*, 191–194.
- (7) Titov, A. V.; Mosyagin, N. S.; Petrov, A. N.; Isaev, T. A. Two-step method for precise calculation of core properties in molecules. *Int. J. Quantum Chem.* **2005**, *104*, 223–239.
- (8) Hudson, J. J.; Sauer, B. E.; Tarbutt, M. R.; Hinds, E. A. Measurement of the Electron Electric Dipole Moment Using YbF Molecules. *Phys. Rev. Lett.* **2002**, *89*, 023003.
- (9) Steimle, T. C.; Ma, T. M.; Linton, C. The hyperfine interaction in the A(2)Pi(1/2) and X(2)Sigma(+) states of ytterbium monofluoride. *Journal of Chemical Physics* **2007**, *127*, 234316.
- (10) Fukuda, M.; Soga, K.; Senami, M.; Tachibana, A. Local spin dynamics with the electron electric dipole moment. *Phys. Rev. A* **2016**, *93*, 012518.
- (11) Fitch, N. J.; Lim, J.; Hinds, E. A.; Sauer, B. E.; Tarbutt, M. R. Methods for measuring the electron’s electric dipole moment using ultracold YbF molecules. *Quantum Science and Technology* **2020**, *6*, 014006.
- (12) Takasu, Y.; Maki, K.; Komori, K.; Takano, T.; Honda, K.; Kumakura, M.; Yabuzaki, T.; Takahashi, Y. Spin-Singlet Bose-Einstein Condensation of Two-Electron Atoms. *PRL* **2003**, *91*, 040404.
- (13) Fukuhara, T.; Sugawa, S.; Takasu, Y.; Takahashi, Y. All-optical formation of quantum degenerate mixtures. *PRA* **2009**, *79*, 021601.

- (14) Tecmer, P.; Boguslawski, K.; Borkowski, M.; Zuchowski, P. S.; Kedziera, D. Modeling the electronic structures of the ground and excited states of the ytterbium atom and the ytterbium dimer: A modern quantum chemistry perspective. *International Journal of Quantum Chemistry* **2019**, *119*, e25983.
- (15) Tsigutkin, K.; Dounas-Frazer, D.; Family, A.; Stalnaker, J. E.; Yashchuk, V. V.; Budker, D. Observation of a Large Atomic Parity Violation Effect in Ytterbium. *PRL* **2009**, *103*, 071601.
- (16) Pasteka, L. F.; Mawhorter, R. J.; Schwerdtfeger, P. Relativistic coupled-cluster calculations of the ^{173}Yb nuclear quadrupole coupling constant for the YbF molecule. *Molecular Physics* **2016**, *114*, 1110–1117.
- (17) Huber, K.; Herzberg, G. Constants of Diatomic Molecules. National Institute of Standards and Technology, Gaithersburg MD, 20899, 2005; (data prepared by J.W. Gallagher and R.D. Johnson, III) in NIST Chemistry WebBook, NIST Standard Reference Database Number 69, Eds. P.J. Linstrom and W.G. Mallard.
- (18) Dunfield, K. L.; Linton, C.; Clarke, T. E.; McBride, J.; Adam, A. G.; Peers, J. R. D. Laser spectroscopy of the lanthanide monofluorides: Analysis of the $A(2)\Pi-X(2)\Sigma(+)$ transition of ytterbium monofluoride. *Journal of Molecular Spectroscopy* **1995**, *174*, 433–445.
- (19) Dolg, M.; Stoll, H.; Preuss, H. Abinitio Pseudopotential Study of Ybh and Ybf. *Chemical Physics* **1992**, *165*, 21–30.
- (20) Liu, W.; Dolg, M.; Li, L. Fully relativistic density functional calculations of the ground and excited states of Yb, YbH, YbF, and YbO. *J. Chem. Phys.* **1998**, *108*, 2886–2895.
- (21) Su, T.; Yang, C. L.; Wang, X. Q.; Bai, F. J.; Wang, M. S. Theoretical characters of the ground states of YbX (X = F, Cl, Br, I, At). *Chemical Physics Letters* **2009**, *467*, 265–269.
- (22) Glassman, Z.; Mawhorter, R.; Grabow, J. U.; Le, A.; Steimle, T. C. The hyperfine interaction in the odd isotope of ytterbium fluoride, (YbF)-Yb-171. *Journal of Molecular Spectroscopy* **2014**, *300*, 7–11.
- (23) Sauer, B. E.; Cahn, S. B.; Kozlov, M. G.; Redgrave, G. D.; Hinds, E. A. Perturbed hyperfine doubling in the $A\ 2\Pi_{1/2}$ and $[18.6]0.5$ states of YbF. *J. Chem. Phys.* **1999**, *110*, 8424–8428.
- (24) Lim, J.; Almond, J. R.; Tarbutt, M. R.; Nguyen, D. T.; Steimle, T. C. The $[557]-X-2\ \Sigma(+)$ and $[561]-X-2\ \Sigma(+)$ bands of ytterbium fluoride, (YbF)-Yb-174. *Journal of Molecular Spectroscopy* **2017**, *338*, 81–90.
- (25) Lim, J.; Almond, J. R.; Trigatzis, M. A.; Devlin, J. A.; Fitch, N. J.; Sauer, B. E.; Tarbutt, M. R.; Hinds, E. A. Laser Cooled YbF Molecules for Measuring the Electron's Electric Dipole Moment. *Phys. Rev. Lett.* **2018**, *120*, 123201.
- (26) Smallman, I. J.; Wang, F.; Steimle, T. C.; Tarbutt, M. R.; Hinds, E. A. Radiative branching ratios for excited states of ^{174}YbF : Application to laser cooling. *Spectroscopic Tests of Fundamental Physics* **2014**, *300*, 3–6.
- (27) Uttam, K. N.; Joshi, M. M. A New Band System of the YbF Molecule. *Journal of Molecular Spectroscopy* **1995**, *174*, 290–296.
- (28) Lee, H. U.; Zare, R. N. Chemiluminescent spectra of YbF and YbCl. *Journal of Molecular Spectroscopy* **1977**, *64*, 233–243.
- (29) Dzuba, V. A.; Derevianko, A. Dynamic polarizabilities and related properties of

- clock states of the ytterbium atom. *Journal of Physics B: Atomic, Molecular and Optical Physics* **2010**, *43*, 074011.
- (30) Dickinson, C. S.; Coxon, J. A.; Walker, N. R.; Gerry, M. C. L. Fourier transform microwave spectroscopy of the (2)Sigma(+) ground states of YbX (X=F, Cl, Br): Characterization of hyperfine effects and determination of the molecular geometries. *Journal of Chemical Physics* **2001**, *115*, 6979–6989.
- (31) Steimle, T. C.; Ma, T. M.; Linton, C. The hyperfine interaction in the A(2)Pi(1/2) and X(2)Sigma(+) states of ytterbium monofluoride (vol 127, art no 234316, 2007). *Journal of Chemical Physics* **2008**, *128*, 209903.
- (32) Steimle, T. C.; Ma, T. M.; Linton, C. The hyperfine interaction in the A(2)Pi(1/2) and X-2 Sigma(+) states of ytterbium monofluoride (vol 127, 234316, 2007). *Journal of Chemical Physics* **2012**, *137*, 109901.
- (33) Wang, H.; Le, A. T.; Steimle, T. C.; Koskelo, E. A. C.; Aufderheide, G.; Mawhorter, R.; Grabow, J.-U. Fine and hyperfine interaction in ^{173}YbF . *Phys. Rev. A* **2019**, *100*, 022516.
- (34) Ma, T.; Butler, C.; Brown, J. M.; Linton, C.; Steimle, T. C. Optical Zeeman Spectroscopy of Ytterbium Monofluoride, YbF. *J. Phys. Chem. A* **2009**, *113*, 8038–8044.
- (35) Porsev, S. G.; Rakhlina, Y. G.; Kozlov, M. G. Calculation of hyperfine structure constants for ytterbium. *Journal of Physics B: Atomic, Molecular and Optical Physics* **1999**, *32*, 1113–1120.
- (36) Mani, B. K.; Angom, D. Fock-space relativistic coupled-cluster calculations of two-valence atoms. *PRA* **2011**, *83*, 012501.
- (37) Nayak, M. K.; Chaudhuri, R. K. Relativistic coupled cluster method. *European Physical Journal D* **2006**, *37*, 171–176.
- (38) Naik, D.; Sikarwar, M.; Nayak, M. K.; Ghosh, S. K. Re-appraisal of the hyperfine-structure constants in YbF: relativistic configuration interaction approach. *Journal of Physics B: Atomic, Molecular and Optical Physics* **2014**, *47*, 225103.
- (39) Haase, P. A. B.; Eliav, E.; Iliáš, M.; Borschevsky, A. Hyperfine Structure Constants on the Relativistic Coupled Cluster Level with Associated Uncertainties. *J. Phys. Chem. A* **2020**, *124*, 3157–3169.
- (40) Vallet, V.; Maron, L.; Teichteil, C.; Flament, J.-P. A two-step uncontracted determinantal effective Hamiltonian-based SO-CI method. *J. Chem. Phys.* **2000**, *113*, 1391–1402.
- (41) Marian, C. M. *Reviews in Computational Chemistry*; John Wiley & Sons, Ltd, 2001; Chapter 3, pp 99–204.
- (42) Danilo, C.; Vallet, V.; Flament, J.-P.; Wahlgren, U. Effects of the first hydration sphere and the bulk solvent on the spectra of the f2 isoelectronic actinide compounds: U4+, NpO2+, and PuO22+. *Phys. Chem. Chem. Phys.* **2010**, *12*, 1116–1130.
- (43) Farhat, A.; Abdul-Al, S. N. Ab initio calculations of the ground and excited states of the ZrN molecule including spin-orbit effects. *Journal of Computational Chemistry* **2015**, *36*, 1252–1258.
- (44) Chmaisani, W.; Korek, M. Ab initio study of the low-lying electronic states of YbCl molecule including spin-orbit effects. *Journal of Quantitative Spectroscopy & Radiative Transfer* **2018**, *217*, 63–72.
- (45) Chmaisani, W.; El-Kork, N.; Elmoussaoui, S.; Korek, M. Electronic Structure Calculations with the Spin Orbit Effect of the Low-Lying Electronic States of the

- YbBr Molecule. *ACS Omega* **2019**, *4*, 14987–14995.
- (46) Kervazo, S.; Réal, F.; Virost, F.; Severo Pereira Gomes, A.; Vallet, V. Accurate Predictions of Volatile Plutonium Thermodynamic Properties. *Inorg. Chem.* **2019**, *58*, 14507–14521.
- (47) Liu, W. Essentials of relativistic quantum chemistry. *J. Chem. Phys.* **2020**, *152*, 180901.
- (48) Nayak, M. K.; Chaudhuri, R. K. Reappraisal of the P,T-odd interaction constant W-d in YbF: Relativistic configuration interaction approach. *Pramana-journal of Physics* **2009**, *73*, 581–586.
- (49) Nayak, M. K.; Chaudhuri, R. K. Determination of molecular hyperfine-structure constant using the second-order relativistic many-body perturbation theory. *Physical Review A* **2011**, *83*, 022504.
- (50) Jensen, H. J. Aa. 2005; *Douglas–Kroll the Easy Way*, Talk at Conference on Relativistic Effects in Heavy Elements - REHE, Mülheim, Germany, April, 2005. Available at <https://doi.org/10.6084/m9.figshare.12046158>.
- (51) Kutzelnigg, W.; Liu, W. Quasirelativistic theory equivalent to fully relativistic theory. *J. Chem. Phys.* **2005**, *123*, 241102.
- (52) Liu, W.; Peng, D. Infinite-order quasirelativistic density functional method based on the exact matrix quasirelativistic theory. *J. Chem. Phys.* **2006**, *125*, 044102.
- (53) Peng, D.; Liu, W.; Xiao, Y.; Cheng, L. Making four- and two-component relativistic density functional methods fully equivalent based on the idea of “from atoms to molecule”. *J. Chem. Phys.* **2007**, *127*, 104106.
- (54) Ilias, M.; Saue, T. An infinite-order two-component relativistic Hamiltonian by a simple one-step transformation. *J. Chem. Phys.* **2007**, *126*, 064102.
- (55) Sikkema, J.; Visscher, L.; Saue, T.; Iliáš, M. The molecular mean-field approach for correlated relativistic calculations. *J. Chem. Phys.* **2009**, *131*, 124116.
- (56) Liu, W.; Peng, D. Exact two-component Hamiltonians revisited. *J. Chem. Phys.* **2009**, *131*, 031104.
- (57) Konecny, L.; Kadec, M.; Komarovskiy, S.; Malkina, O. L.; Ruud, K.; Repisky, M. Acceleration of Relativistic Electron Dynamics by Means of X2C Transformation: Application to the Calculation of Nonlinear Optical Properties. *J. Chem. Theory Comput.* **2016**, *12*, 5823–5833.
- (58) Hess, B. A.; Marian, C. M.; Wahlgren, U.; Gropen, O. A mean-field spin-orbit method applicable to correlated wavefunctions. *Chem. Phys. Lett.* **1996**, *251*, 365–371.
- (59) Schimmelpfennig, B. *AMFI, an atomic mean-field spin-orbit integral program*. University of Stockholm, Stockholm, Sweden; 1999.
- (60) Shee, A.; Saue, T.; Visscher, L.; Severo Pereira Gomes, A. Equation-of-motion coupled-cluster theory based on the 4-component Dirac-Coulomb(-Gaunt) Hamiltonian. Energies for single electron detachment, attachment, and electronically excited states. *J. Chem. Phys.* **2018**, *149*, 174113.
- (61) Halbert, L.; Lopez Vidal, M.; Shee, A.; Coriani, S.; Gomes, A. S. P. Relativistic EOM-CCSD for core-excited and core-ionized state energies based on the 4-component Dirac-Coulomb(-Gaunt) Hamiltonian. *J. Chem. Theory Comput.* **2021**, *xxx*, xxx.
- (62) Bartlett, R. J.; Musiał, M. Coupled-cluster theory in quantum chemistry. *Rev. Mod. Phys.* **2007**, *79*, 291–352.
- (63) Saue, T.; Visscher, L.; Jensen, H. J. Aa.; Bast, R.; Gomes, A. S. P. DIRAC, a relativistic ab initio electronic structure pro-

- gram. 2019; with new contributions from R. Bast, S. Dubillard, K. G. Dyall, U. Ekström, E. Eliav, T. Fleig, A. S. P. Gomes, T. U. Helgaker, J. Henriksson, M. Iliáš, Ch. R. Jacob, S. Knecht, P. Norman, J. Olsen, M. Pernpointner, K. Ruud, P. Sałek, and J. Sikkema; see <http://www.diracprogram.org>.
- (64) Dunning, T. H. Gaussian basis sets for use in correlated molecular calculations. I. The atoms boron through neon and hydrogen. *J. Chem. Phys.* **1989**, *90*, 1007–1023.
- (65) Helgaker, T.; Joergensen, P.; Olsen, J. *Molecular Electronic-Structure Theory*; John Wiley & Sons, 2000.
- (66) Visscher, L. Approximate molecular relativistic Dirac-Coulomb calculations using a simple Coulombic correction. *Theoretical Chemistry Accounts* **1997**, *98*, 68–70.
- (67) Pototschnig, J. V.; Dyall, K. G.; Visscher, L.; André Severo Pereira Gomes, Dataset: Electronic Spectra of Ytterbium Fluoride from Relativistic Electronic Structure Calculations. 2021; <https://doi.org/10.5281/zenodo.5121372>.
- (68) Thyssen, J. Development and Applications of Methods for Correlated Relativistic Calculations of Molecular Properties. Ph.D. thesis, University of Southern Denmark, 2001.
- (69) Fleig, T.; Jensen, H. J. A.; Olsen, J.; Visscher, L. The generalized active space concept for the relativistic treatment of electron correlation. III. Large-scale configuration interaction and multiconfiguration self-consistent-field four-component methods with application to UO₂. *J. Chem. Phys.* **2006**, *124*, 104106.
- (70) Visscher, L.; Eliav, E.; Kaldor, U. Formulation and implementation of the relativistic Fock-space coupled cluster method for molecules. *J. Chem. Phys.* **2001**, *115*, 9720–9726.
- (71) Landau, A.; Eliav, E.; Ishikawa, Y.; Kaldor, U. Intermediate Hamiltonian Fock-space coupled-cluster method: Excitation energies of barium and radium. *J. Chem. Phys.* **2000**, *113*, 9905–9910.
- (72) Landau, A.; Eliav, E.; Ishikawa, Y.; Kaldor, U. Intermediate Hamiltonian Fock-space coupled cluster method in the one-hole one-particle sector: Excitation energies of xenon and radon. *J. Chem. Phys.* **2001**, *115*, 6862–6865.
- (73) Eliav, E.; Vilkas, M. J.; Ishikawa, Y.; Kaldor, U. Extrapolated intermediate Hamiltonian coupled-cluster approach: Theory and pilot application to electron affinities of alkali atoms. *J. Chem. Phys.* **2005**, *122*, 224113.
- (74) Eliav, E.; Kaldor, U.; Ishikawa, Y. Transition energies of ytterbium, lutetium, and lawrencium by the relativistic coupled-cluster method. *PRA* **1995**, *52*, 291–296.
- (75) Sur, C.; Chaudhuri, R. K. Relativistic multireference Fock-space coupled-cluster calculation of the forbidden $6s^2\ ^1S_0 \rightarrow 6s5d\ ^3D_1$ magnetic-dipole transition in ytterbium. *PRA* **2007**, *76*, 012509.
- (76) Kramida, A.; Yu. Ralchenko,; Reader, J.; and NIST ASD Team, NIST Atomic Spectra Database (ver. 5.8), [Online]. Available: <https://physics.nist.gov/asd> [2017, April 9]. National Institute of Standards and Technology, Gaithersburg, MD., 2020.
- (77) Blondel, C.; Delsart, C.; Goldfarb, F. Electron spectrometry at the mueV level and the electron affinities of Si and F. *Journal of Physics B: Atomic, Molecular and Optical Physics* **2001**, *34*, L281–L288.
- (78) Kaledin, L. A.; Heaven, M. C.; Field, R. W. Thermochemical properties (D-o(o) and IP) of the lanthanide monohalides. *Journal of Molecular Spectroscopy* **1999**, *193*, 285–292.

- (79) Yokozeki, A.; Menzinger, M. Molecular beam chemiluminescence. VIII: Pressure dependence and kinetics of Sm + (N₂O, O₃, F₂, Cl₂) and Yb + (O₃, F₂, Cl₂) reaction. Dissociation energies of the diatomic reaction products. *Chemical Physics* **1976**, *14*, 427–439.
- (80) Heiberg, H.; Gropen, O.; Laerdahl, J. K.; Swang, O.; Wahlgren, U. The performance of density functional theory for LnF (Ln = Nd, Eu, Gd, Yb) and YbH. *Theoretical Chemistry Accounts* **2003**, *110*, 118–125.
- (81) Cao, X. Y.; Liu, W. J.; Dolg, M. Molecular structure of diatomic lanthanide compounds. *Science in China Series B-chemistry* **2002**, *45*, 91–96.

Supplementary Information: Electronic Spectra of Ytterbium Fluoride from Relativistic Electronic Structure Calculations

Johann V. Pototschnig,^{*,†} Kenneth G. Dyall,^{*,‡} Lucas Visscher,^{*,†} and André
Severo Pereira Gomes^{*,¶}

[†]*Amsterdam Center for Multiscale Modeling, Department of Theoretical Chemistry, Faculty
of Sciences, VU University Amsterdam, De Boelelaan 1083, NL-1081 HV Amsterdam, The
Netherlands*

[‡]*Dirac Solutions, 10527 NW Lost Park Drive, Portland, OR 97229, U.S.A.*

[¶]*Université de Lille, CNRS, UMR 8523 – PhLAM – Physique des Lasers, Atomes et
Molécules, F-59000 Lille, France*

E-mail: j.v.pototschnig@vu.nl; diracsolutions@gmail.com; visscher@chem.vu.nl;
andre.gomes@univ-lille.fr

This is the supporting information for the manuscript entitled: "Electronic Spectra of Ytterbium Fluoride from Relativistic Electronic Structure Calculations" by J. V. Pototschnig, K. G. Dyall, L. Visscher and A. S. P. Gomes.

In section 1 a closer look is taken at the orbitals and their energies for the two different references, either with a closed or open f-shell. Orbital energies for different diatomic distances are depicted alongside orbitals for the Yb atom and the YbF diatomic (for two internuclear separations). Section 2 contains additional results obtained for Kramers restricted configuration interaction. Firstly, we compare results obtained with the X2C-AMFI code to full

4-component computations. Next, potential energy curves, including spectroscopic parameters, and dipole moments—both transition dipole moments (TDM) and permanent electric dipole moments (PEDM)—for different basis set sizes are presented. Subsequently, the problem of the relative position of the f^{13} and f^{14} states is addressed and its basis set dependence. Lastly, transition dipole moments are listed. Section 3 contains the potential energy curves and spectroscopic parameters for different basis set sizes applying the Fock space coupled cluster method and spectroscopic parameters for the states after adiabatic mixing as presented in the main text. An extended list of equation-of-motion coupled cluster transition energies for the Yb^+ is listed in section 4. This section also contains EOM-CCSD potential energy curves for different basis set sizes. Finally, in section 5 Franck-Condon factors for potentials stemming from the different methods are depicted and compared.

1 Orbitals

1.1 Orbital energies

In this part the orbital energies obtained by AOC-SCF for several internuclear separations are shown.

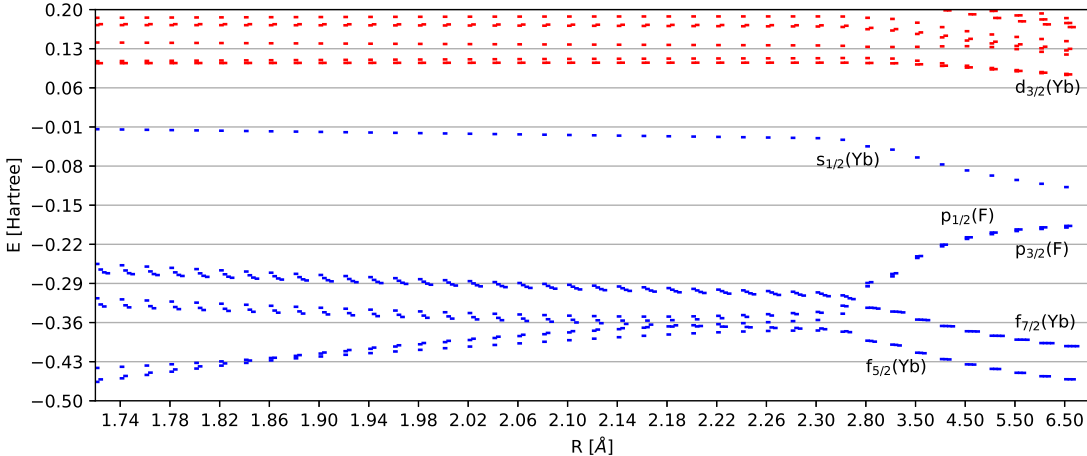


Figure 1: Orbital energies of YbF^- for different radii. Blue and red are occupied and virtual orbitals, respectively.

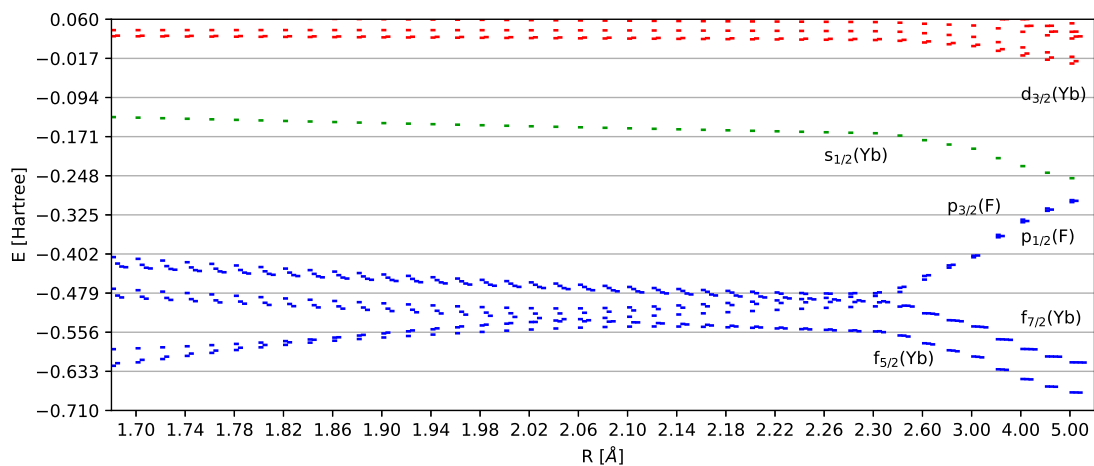


Figure 2: Orbital energies of YbF for different radii. Blue green, and red are occupied, partially filled and virtual orbitals, respectively.

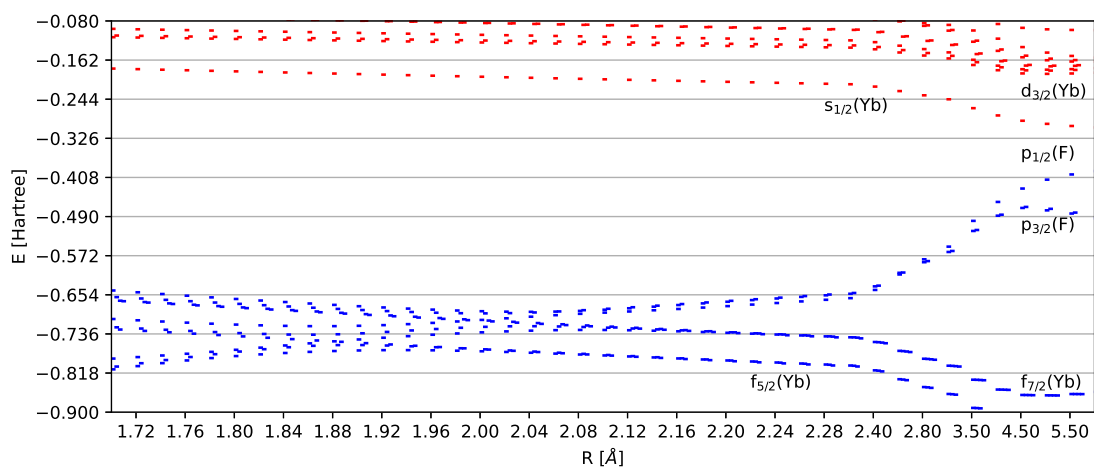
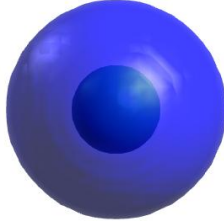
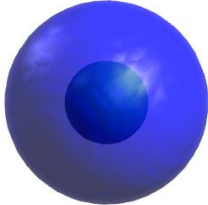
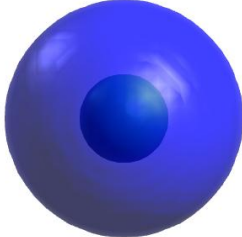
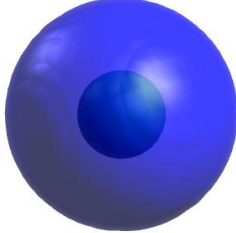


Figure 3: Orbital energies of YbF⁺ for different radii. Blue and red are occupied and virtual orbitals, respectively.

1.2 Atomic orbitals


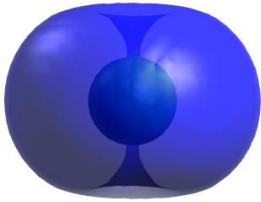
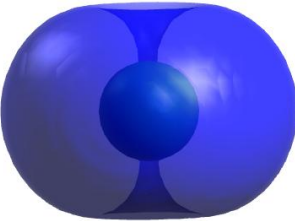
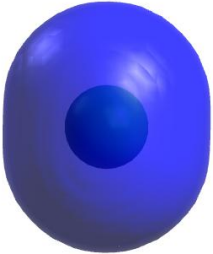


In this section we compare atomic orbitals that were either optimized for the f^{13} or f^{14} configurations.

Table 1: Orbitals obtained from an AOC-SCF computations for the Yb atom either with a fully occupied (f^{14}) or single hole (f^{13}) f-shell, the total energy in the first case is -14062.55463420 Hartree, for the second one it is -14062.50155764 Hartree. For each orbital we list the orbital energy according to a Koopmans definition.^{1,2}

| designation | f^{14} | f^{13} |
|-------------------------------|---|---|
| | -2.658500494 | -2.896356031 |
| 1/15 $5s_{1/2}(\text{Yb})$ |  |  |
| | -1.646207984 | -1.856152194 |
| 2/10 $5p_{1/2}(\text{Yb})$ |  |  |

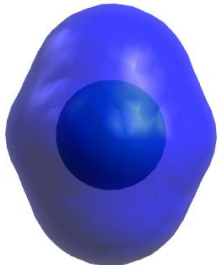
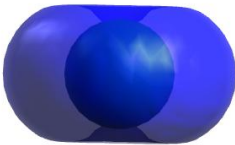
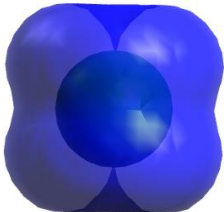


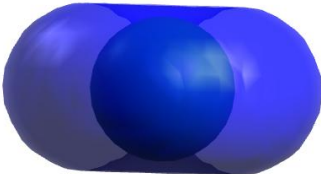
Continued on next page

Table 1 – *Continued from previous page*

| designation | f^{14} | f^{13} |
|-----------------------------------|---|---|
| | -1.410261382 | -1.604023002 |
| 2/11 $5p_{3/2}(\text{Yb})$ |  |  |
| | -1.410261382 | -1.604023002 |
| 2/12 $5p_{3/2}(\text{Yb})$ |  |  |
| | -0.767646169 | -1.068583089 |
| 2/13 $4f_{5/2,7/2}(\text{Yb})$ |  |  |

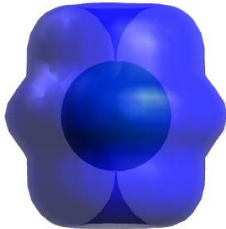
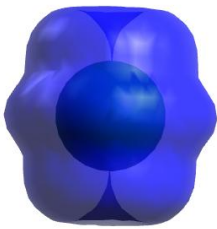
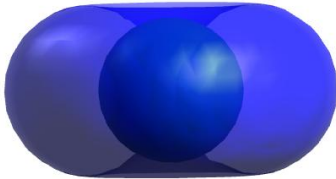


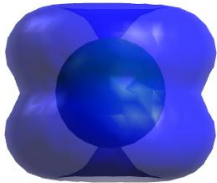
Continued on next page

Table 1 – *Continued from previous page*

| designation | f^{14} | f^{13} |
|-----------------------------------|---|--|
| | -0.767646168 | -1.068583087 |
| 2/14 $4f_{5/2,7/2}(\text{Yb})$ |  |  |
| | -0.767646168 | -1.068583087 |
| 2/15 $4f_{5/2,7/2}(\text{Yb})$ |  |  |
| | -0.708324589 | -1.010576973 |
| 2/16 $4f_{5/2,7/2}(\text{Yb})$ |  |  |

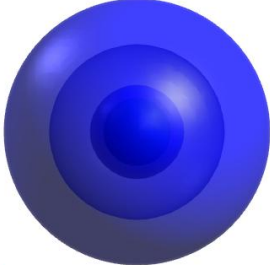
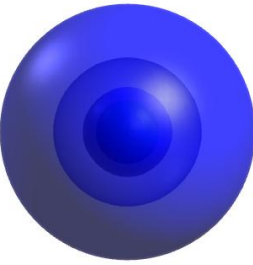
Continued on next page

Table 1 – *Continued from previous page*

| designation | f^{14} | f^{13} |
|-----------------------------------|---|---|
| | -0.708324585 | -1.010576972 |
| 2/17 $4f_{5/2,7/2}(\text{Yb})$ |  |  |
| | -0.708324585 | -1.010576972 |
| 2/18 $4f_{5/2,7/2}(\text{Yb})$ |  |  |
| | -0.708324583 | -1.010576968 |
| 2/18 $4f_{5/2,7/2}(\text{Yb})$ |  |  |

Continued on next page





Table 1 – *Continued from previous page*

| designation | f^{14} | f^{13} |
|-------------------------------|---|---|
| | -0.310402947 | -0.364220506 |
| 1/16 $5s_{1/2}(\text{Yb})$ |  |  |

1.3 Diatomic orbitals - equilibrium distance

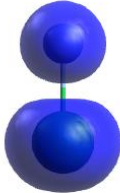
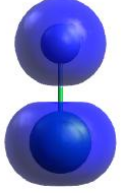


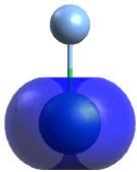
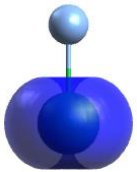


This section contains orbitals of the YbF diatomic for a internuclear distance close to the ground state equilibrium one.

Table 2: Orbitals obtained from an AOC-SCF computations either with a fully occupied (f^{14}) or single hole (f^{13}) f-shell for YbF with a distance of 2 Å. For each orbital we list the orbital energy according to a Koopman's definition.^{1,2} The contributing atomic orbitals contributing have been given in the first column.

| designation | f^{14} | f^{13} |
|---|---|---|
| | -2.475129022 | -2.606565796 |
| 25 $5s_{1/2}(\text{Yb})$ |  |  |
| | -1.511889433 | -1.611193447 |
| 26 $5p_{1/2}(\text{Yb})$ $2s_{1/2}(\text{F})$ |  |  |





Continued on next page

Table 2 – *Continued from previous page*

| designation | f^{14} | f^{13} |
|---|---|---|
| | -1.435750686 | -1.539604687 |
| 27 $5p_{1/2}(\text{Yb})$ $2s_{1/2}(\text{F})$ |  |  |
| |  |  |
| | -1.229656975 | -1.323836039 |
| 28 $5p_{3/2}(\text{Yb})$ |  |  |
| |  |  |

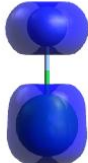
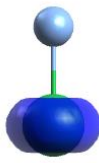
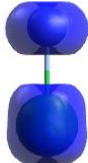
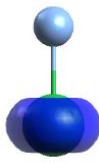



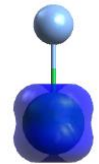

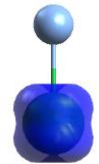


Continued on next page

Table 2 – *Continued from previous page*

| designation | f^{14} | f^{13} |
|---|---|---|
| | -1.210630046 | -1.311522305 |
| 29 $5p_{3/2}(\text{Yb})$ |  |  |
| | -0.594742161 | -0.774346397 |
| 30 $4f_{5/2,7/2}(\text{Yb})$ $2p_{1/2,3/2}(\text{F})$ |  |  |




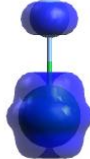
Continued on next page

Table 2 – *Continued from previous page*

| designation | f^{14} | f^{13} |
|---------------------------|---|---|
| | -0.584034308 | -0.773626615 |
| 31 | | |
| $4f_{5/2,7/2}(\text{Yb})$ |  |  |
| $2p_{1/2,3/2}(\text{F})$ |  |  |
| |  |  |
| | -0.582311174 | -0.772523010 |
| 32 | | |
| $4f_{5/2,7/2}(\text{Yb})$ |  |  |
| $2p_{1/2,3/2}(\text{F})$ |  |  |
| |  |  |

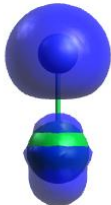
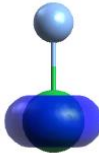
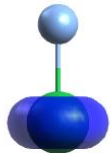
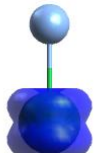
Continued on next page

Table 2 – *Continued from previous page*

| designation | f^{14} | f^{13} |
|---------------------------|---|---|
| | -0.574792083 | -0.719689709 |
| 33 |  |  |
| $4f_{5/2,7/2}(\text{Yb})$ | | |
| $2p_{1/2,3/2}(\text{F})$ | | |
| | -0.561976545 | -0.715455417 |
| 34 |  |  |
| $4f_{5/2,7/2}(\text{Yb})$ | | |
| $2p_{1/2,3/2}(\text{F})$ | | |

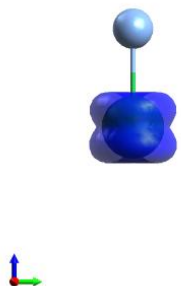
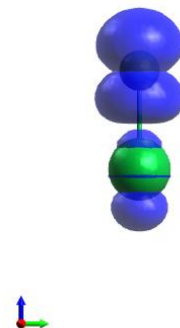
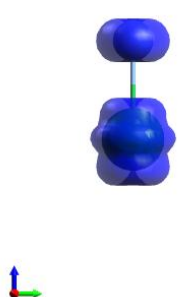
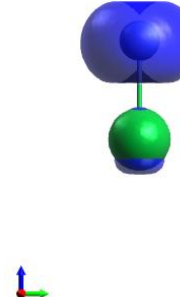
Continued on next page

Table 2 – *Continued from previous page*

| designation | f^{14} | f^{13} |
|---------------------------|---|---|
| | -0.55211333 | -0.715038003 |
| 35 |  |  |
| $4f_{5/2,7/2}(\text{Yb})$ | | |
| $2p_{1/2,3/2}(\text{F})$ | | |
| | -0.523207455 | -0.713718461 |
| 36 |  |  |
| $4f_{5/2,7/2}(\text{Yb})$ | | |
| $2p_{1/2,3/2}(\text{F})$ | | |

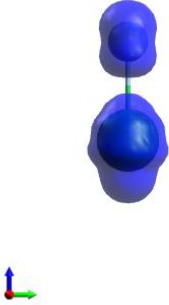
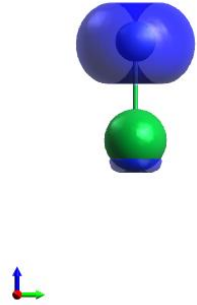
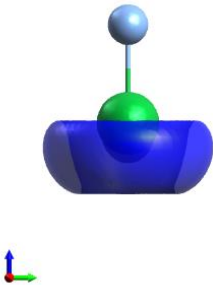
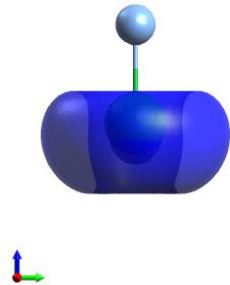
Continued on next page

Table 2 – *Continued from previous page*

| designation | f^{14} | f^{13} |
|---|---|--|
| | -0.521323830 | -0.653507491 |
| 37 $4f_{5/2,7/2}(\text{Yb})$ $2p_{1/2,3/2}(\text{F})$ |  |  |
| | -0.515413462 | -0.644769626 |
| 38 $4f_{5/2,7/2}(\text{Yb})$ $2p_{1/2,3/2}(\text{F})$ |  |  |

Continued on next page

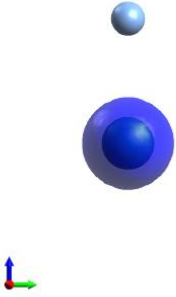



Table 2 – *Continued from previous page*

| designation | f^{14} | f^{13} |
|---|---|--|
| | -0.509924741 | -0.639112727 |
| 39 $4f_{5/2,7/2}(\text{Yb})$ $2p_{1/2,3/2}(\text{F})$ |  |  |
| | -0.129066590 | -0.241206568 |
| 40 $4f_{5/2,7/2}(\text{Yb})$ $2p_{1/2,3/2}(\text{F})$ |  |  |

1.4 Diatomic orbitals - long range

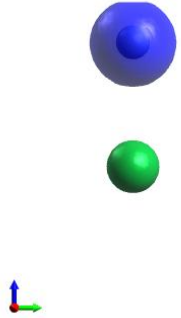

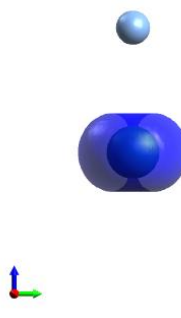
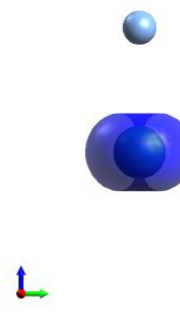
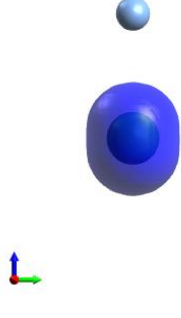

This section contains orbitals of the YbF diatomic for a internuclear distance significantly larger than the minima of most potential energy curves.

Table 3: Orbitals obtained from an AOC-SCF computations either with a fully occupied (f^{14}) or single hole (f^{13}) f-shell for YbF with a distance of 3 Å. The contributing atomic orbitals contributing have been given in the first column.

| designation | f^{14} | f^{13} |
|---|---|--|
| 25 $5s_{1/2}(\text{Yb})$ |  |  |
| 26 $5p_{1/2}(\text{Yb})$ $2s_{1/2}(\text{F})$ |  |  |

Continued on next page

Table 3 – *Continued from previous page*

| designation | f^{14} (3.0) | f^{13} (3.0) |
|---|---|--|
| 27 $5p_{1/2}(\text{Yb})$ $2s_{1/2}(\text{F})$ |  |  |
| 28 $5p_{3/2}(\text{Yb})$ |  |  |
| 29 $5p_{3/2}(\text{Yb})$ |  |  |

Continued on next page

Table 3 – *Continued from previous page*

| designation | f^{14} (3.0) | f^{13} (3.0) |
|---------------------------|----------------|----------------|
| 30 | | |
| $4f_{5/2,7/2}(\text{Yb})$ | | |
| $2p_{1/2,3/2}(\text{F})$ | | |
| | | |
| 31 | | |
| $4f_{5/2,7/2}(\text{Yb})$ | | |
| $2p_{1/2,3/2}(\text{F})$ | | |
| | | |
| 32 | | |
| $4f_{5/2,7/2}(\text{Yb})$ | | |
| $2p_{1/2,3/2}(\text{F})$ | | |
| | | |



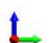








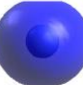


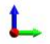

Continued on next page

Table 3 – *Continued from previous page*

| designation | f^{14} (3.0) | f^{13} (3.0) |
|---------------------------|----------------|----------------|
| 33 | | |
| $4f_{5/2,7/2}(\text{Yb})$ | | |
| $2p_{1/2,3/2}(\text{F})$ | | |
| | | |
| 34 | | |
| $4f_{5/2,7/2}(\text{Yb})$ | | |
| $2p_{1/2,3/2}(\text{F})$ | | |
| | | |
| 35 | | |
| $4f_{5/2,7/2}(\text{Yb})$ | | |
| $2p_{1/2,3/2}(\text{F})$ | | |
| | | |







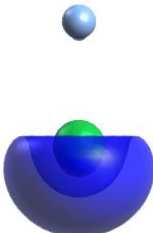

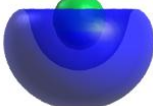



Continued on next page

Table 3 – *Continued from previous page*

| designation | f^{14} (3.0) | f^{13} (3.0) |
|---------------------|---|---|
| 36 |  |  |
| $4f_{5/2,7/2}$ (Yb) | | |
| $2p_{1/2,3/2}$ (F) | | |
| |  |  |
| 37 |  |  |
| $4f_{5/2,7/2}$ (Yb) | | |
| $2p_{1/2,3/2}$ (F) |  |  |
| |  |  |
| 38 |  |  |
| $4f_{5/2,7/2}$ (Yb) | | |
| $2p_{1/2,3/2}$ (F) |  |  |
| |  |  |

Continued on next page

Table 3 – *Continued from previous page*

| designation | f^{14} (3.0) | f^{13} (3.0) |
|---------------------------|---|---|
| 39 |  |  |
| $4f_{5/2,7/2}(\text{Yb})$ |  |  |
| $2p_{1/2,3/2}(\text{F})$ |  |  |
| 40 |  |  |
| $4f_{5/2,7/2}(\text{Yb})$ |  |  |
| $2p_{1/2,3/2}(\text{F})$ |  |  |

2 Kramers restricted configuration interaction (KRCI)

2.1 Hamiltonian

Due to limitations in the implementation it is not possible to run the more accurate ${}^2\text{DC}^M$ ³ in combination with Kramers-restricted configuration interaction. Therefore, we have run the computations with the X2C-AMFI^{4,5} Hamiltonian. In order to estimate the influence of this approximation we compare the results with the 4-component Dirac-Coulomb-Breit Hamiltonian (DCB) from the literature.⁶ in figure in tables 4 and 5 for the Yb cation. The

Table 4: Transition energies and transition dipole moments for the Yb cation. Reference values have been obtained from the NIST database,⁷ the computed values were obtained for different basis sets with Kramers-restricted configuration interaction.

| state | conf | NIST ⁸ | | 2z (x2c) | | 3z (x2c) | | 4z (x2c) | | 2z (DCB ⁶) | | 3z (DCB ⁶) | | 4z (DCB ⁶) | |
|------------------------------|-------------|-------------------|------|----------|------|----------|------|----------|------|------------------------|------|------------------------|------|------------------------|------|
| | | E | S | E | TDM | E | TDM | E | TDM | E | TDM | E | TDM | E | TDM |
| ${}^2\text{S}_{1/2}$ | $4f^{14}6s$ | 0 | | 0 | | 0 | | 0 | | 0 | | 0 | | 0 | |
| ${}^2\text{D}_{3/2}$ | $4f^{14}5d$ | 22961 | | 23322 | 0.0 | 22802 | 0.0 | 23606 | 0.0 | 23389 | 0.0 | 22871 | 0.0 | 23674 | 0.0 |
| ${}^2\text{D}_{5/2}$ | $4f^{14}5d$ | 24333 | | 23882 | 0.0 | 23321 | 0.0 | 24117 | 0.0 | 23945 | 0.0 | 23386 | 0.0 | 24182 | 0.0 |
| ${}^2\text{P}_{1/2}^{\circ}$ | $4f^{14}6p$ | 27062 | 6.1 | 25210 | 5.3 | 24533 | 5.5 | 25331 | 5.3 | 25241 | 5.3 | 24564 | 5.5 | 25362 | 5.3 |
| ${}^2\text{P}_{3/2}^{\circ}$ | $4f^{14}6p$ | 30392 | 11.4 | 28104 | 16.4 | 27385 | 17.3 | 28153 | 16.6 | 28139 | 16.4 | 27422 | 17.3 | 28189 | 16.6 |

Table 5: Transition energies between states with an open f-shell obtained with configuration interaction. Transition energies relative to the ${}^2\text{F}_{7/2}^{\circ}$ state are listed.

| state | conf | NIST ⁸ | x2c | | | DCB ⁶ | | |
|------------------------------|----------------|-------------------|------|------|------|------------------|------|------|
| | | | 2z | 3z | 4z | 2z | 3z | 4z |
| ${}^2\text{F}_{7/2}^{\circ}$ | $4f^{13}6s^2$ | 0 | 0 | 0 | 0 | 0 | 0 | 0 |
| ${}^3[3/2]_{5/2}^{\circ}$ | $4f^{13}5d 6s$ | 5340 | 4260 | 5538 | 4618 | 4349 | 5630 | 4711 |
| ${}^3[3/2]_{3/2}^{\circ}$ | $4f^{13}5d 6s$ | 7339 | 6387 | 7822 | 7123 | 6478 | 7917 | 7218 |
| ${}^3[11/2]_{9/2}^{\circ}$ | $4f^{13}5d 6s$ | 8806 | 8214 | 9325 | 8314 | 8304 | 9419 | 8408 |
| ${}^3[11/2]_{11/2}^{\circ}$ | $4f^{13}5d 6s$ | 9144 | 8320 | 9431 | 8447 | 8409 | 9524 | 8540 |

effect of the basis set is much larger and since no significant impact can be expected we used the X2C-AMFI Hamiltonian to obtain the data.

2.2 Closed f-shell - potential energy curves

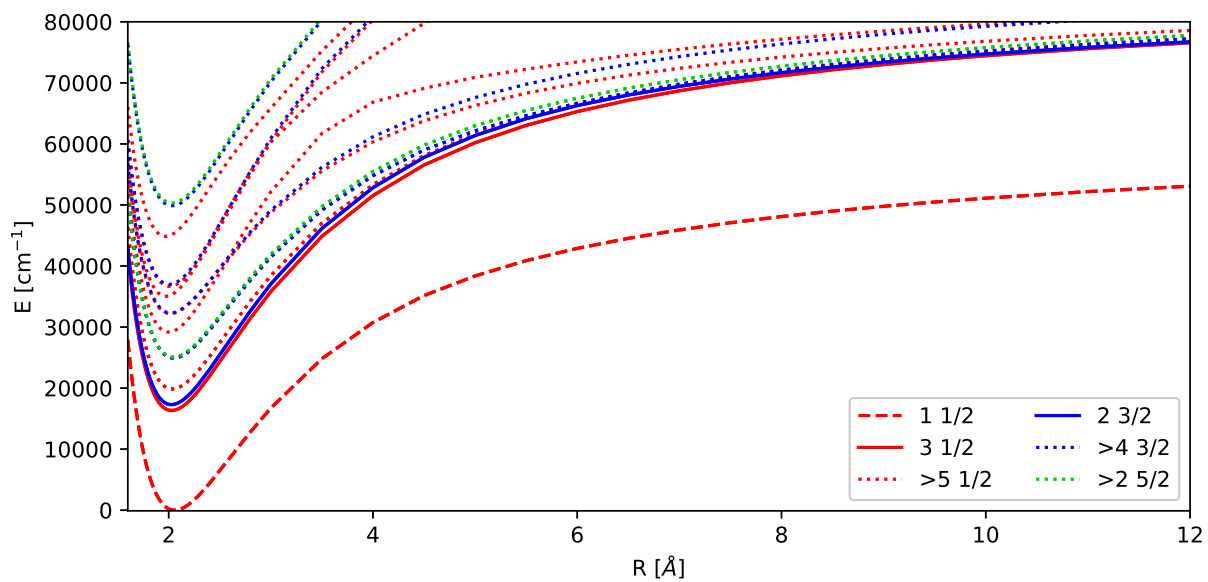


Figure 4: KRCI PECs for states with f^{14} for the quadruple zeta basis sets.

Table 6: Spectroscopic constants for the different electronic states ($\Omega = 1/2, 3/2, 5/2$) with f^{14} obtained by KRCI for the double and triple zeta basis sets. Vibrational constant (ω_e), anharmonicity constant ($\omega_e\chi_e$), and transition energy (T_e), are given in cm^{-1} , the equilibrium bond distance (r_e) in \AA .

| Ω | state | v2z | | | | v3z | | | |
|----------|-------|--------|------------|------------------|-------|--------|------------|------------------|-------|
| | | r_e | ω_e | $\omega_e\chi_e$ | T_e | r_e | ω_e | $\omega_e\chi_e$ | T_e |
| 1/2 | 1 | 2.0609 | 493 | 2.29 | 0 | 2.0594 | 493 | 2.27 | 0 |
| 1/2 | 2 | 2.0316 | 520 | 2.30 | 17319 | 2.0299 | 521 | 2.27 | 16663 |
| 1/2 | 3 | 2.0397 | 513 | 2.49 | 21252 | 2.0382 | 513 | 2.33 | 20270 |
| 1/2 | 4 | 2.1095 | 444 | 2.25 | 35868 | 2.0079 | 547 | 2.16 | 30993 |
| 1/2 | 5 | 2.0440 | 503 | 1.88 | 37977 | 2.0531 | 481 | 2.51 | 33700 |
| 1/2 | 6 | 2.0080 | 574 | 2.83 | 42795 | 1.9871 | 579 | 2.31 | 37776 |
| 1/2 | 7 | 2.0608 | 509 | 2.01 | 52474 | 2.0149 | 537 | 1.98 | 42915 |
| 3/2 | 1 | 2.0281 | 524 | 2.32 | 18425 | 2.0266 | 525 | 2.28 | 17667 |
| 3/2 | 2 | 2.0779 | 472 | 2.31 | 26817 | 2.0592 | 486 | 2.34 | 25450 |
| 3/2 | 3 | 2.1120 | 448 | 2.27 | 36017 | 2.0545 | 483 | 2.50 | 33792 |
| 3/2 | 4 | 2.0558 | 509 | 2.03 | 54498 | 2.0114 | 538 | 1.98 | 43720 |
| 5/2 | 1 | 2.0761 | 474 | 2.31 | 27016 | 2.0575 | 488 | 2.33 | 25572 |

Table 7: Spectroscopic constants for the different electronic states ($\Omega = 1/2, 3/2, 5/2$) with f^{14} obtained by KRCI for the quadruple zeta and extrapolation to the complete basis set. Vibrational constant (ω_e), anharmonicity constant ($\omega_e\chi_e$), and transition energy (T_e), are given in cm^{-1} , the equilibrium bond distance (r_e) in \AA .

| Ω | state | v4z | | | | CBS | | | |
|----------|-------|--------|------------|------------------|-------|--------|------------|------------------|-------|
| | | r_e | ω_e | $\omega_e\chi_e$ | T_e | r_e | ω_e | $\omega_e\chi_e$ | T_e |
| 1/2 | 1 | 2.0587 | 492 | 2.30 | 0 | 2.0829 | 465 | 2.40 | 0 |
| 1/2 | 2 | 2.0290 | 521 | 2.30 | 16338 | 2.0504 | 496 | 2.38 | 16189 |
| 1/2 | 3 | 2.0351 | 515 | 2.37 | 19857 | 2.0552 | 490 | 2.49 | 19631 |
| 1/2 | 4 | 2.0012 | 554 | 2.23 | 29183 | 2.0154 | 537 | 2.31 | 28043 |
| 1/2 | 5 | 2.0169 | 509 | 2.97 | 32206 | 2.0131 | 505 | 3.44 | 31208 |
| 1/2 | 6 | 1.9727 | 587 | 2.35 | 35042 | 1.9792 | 570 | 2.41 | 33312 |
| 1/2 | 7 | 2.0103 | 542 | 1.87 | 36658 | 2.0269 | 525 | 1.79 | 32245 |
| 3/2 | 1 | 2.0260 | 524 | 2.31 | 17296 | 2.0473 | 499 | 2.37 | 17123 |
| 3/2 | 2 | 2.0496 | 492 | 2.40 | 24927 | 2.0669 | 470 | 2.50 | 24583 |
| 3/2 | 3 | 2.0193 | 509 | 2.86 | 32297 | 2.0160 | 503 | 3.22 | 31295 |
| 3/2 | 4 | 2.0058 | 546 | 1.98 | 36990 | 2.0215 | 530 | 1.96 | 32245 |
| 5/2 | 1 | 2.0474 | 495 | 2.39 | 25067 | 2.0639 | 474 | 2.48 | 24744 |

2.3 Closed f-shell - dipole moments

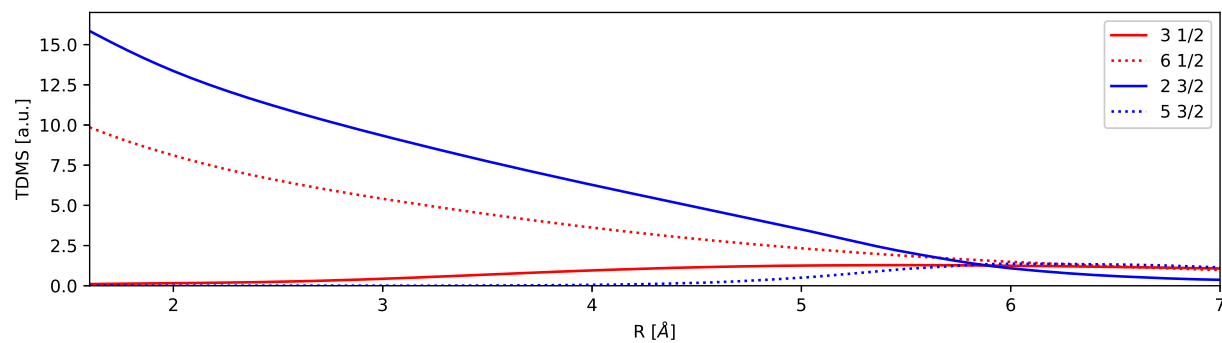


Figure 5: KRCI TDMs for states with f^{14} for the double zeta basis sets.

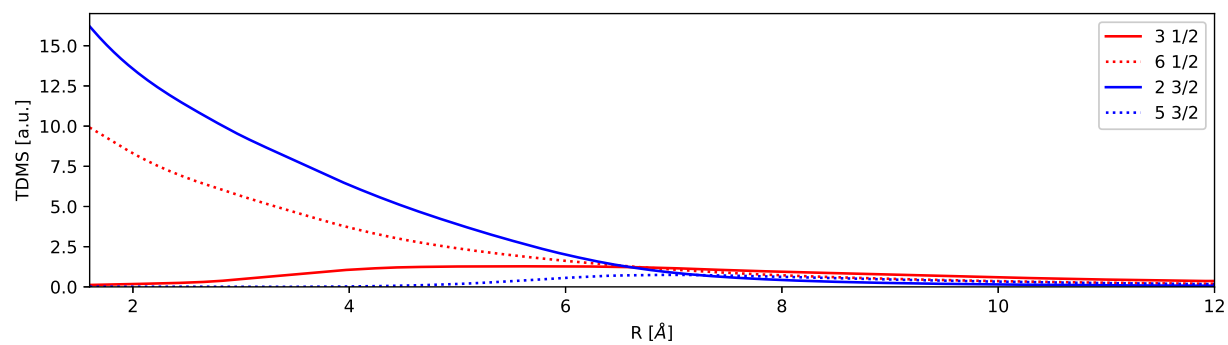


Figure 6: KRCI TDMs for states with f^{14} for the triple zeta basis sets.

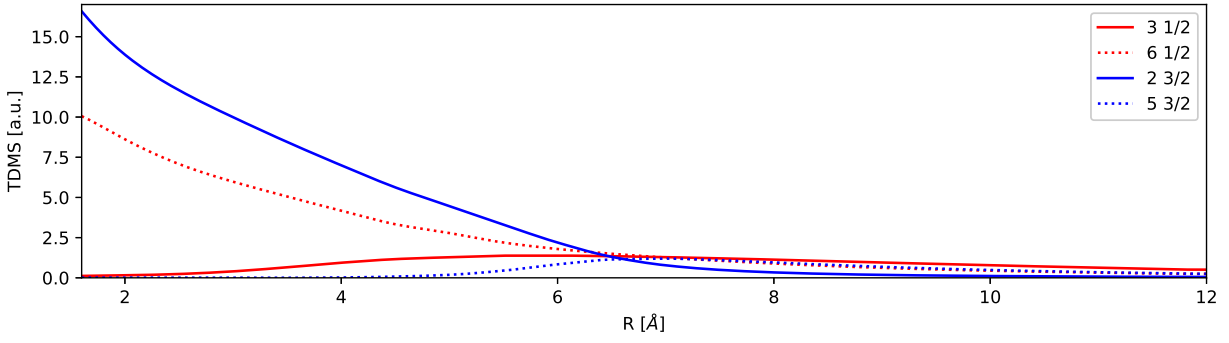


Figure 7: KRCI TDMs for states with f^{14} for the quadruple zeta basis sets.

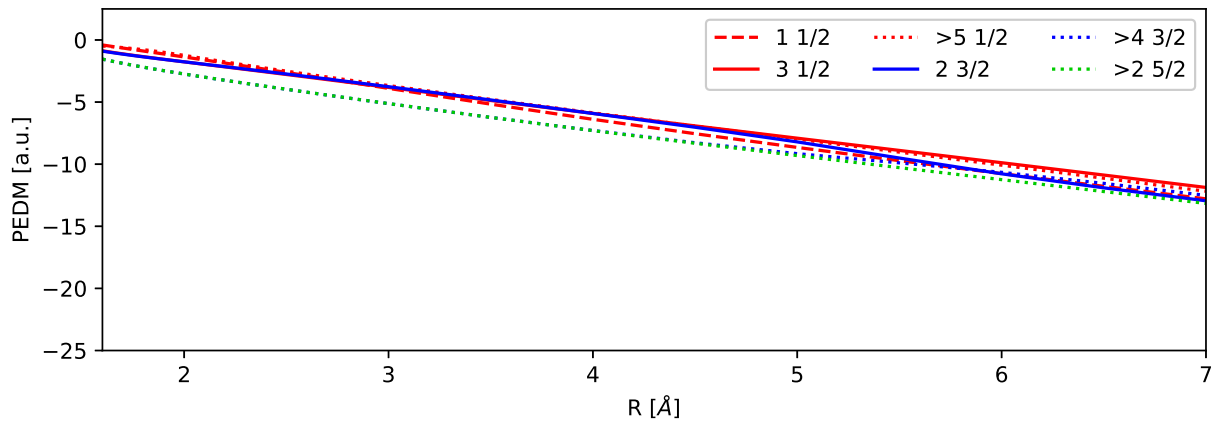


Figure 8: KRCI PEDMs for states with f^{14} for the double zeta basis sets.

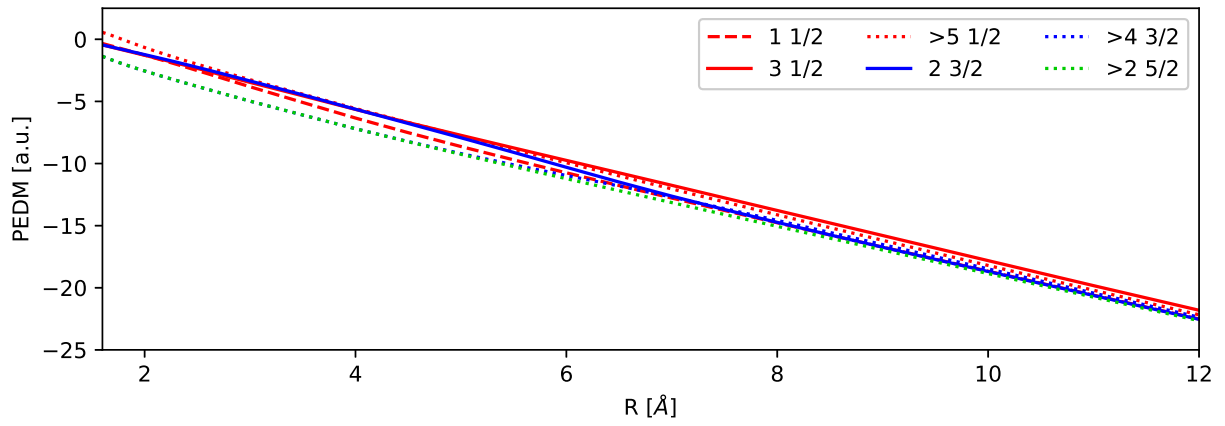


Figure 9: KRCI PEDMs for states with f^{14} for the triple zeta basis sets.

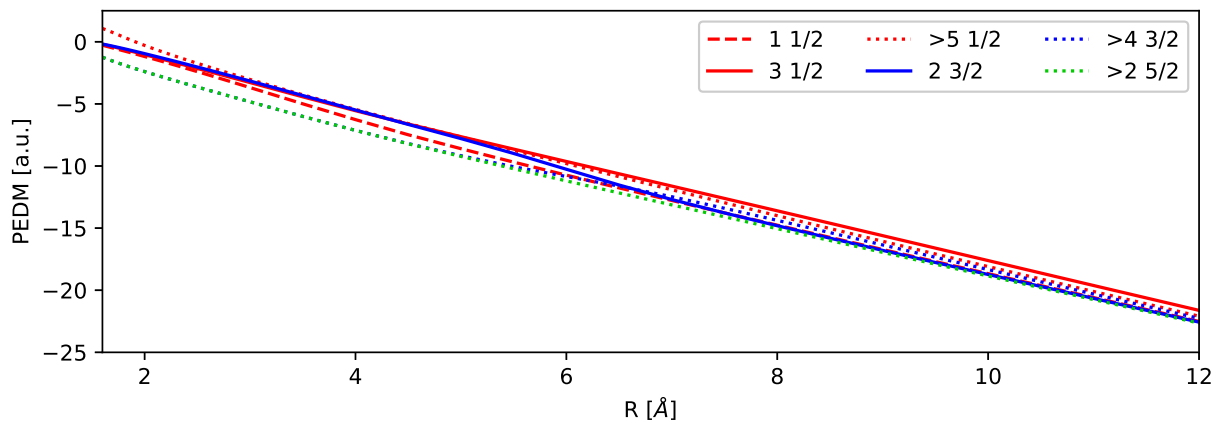


Figure 10: KRCI PEDMs for states with f^{14} for the quadruple zeta basis sets.

2.4 Open f-shell - potential energy curves

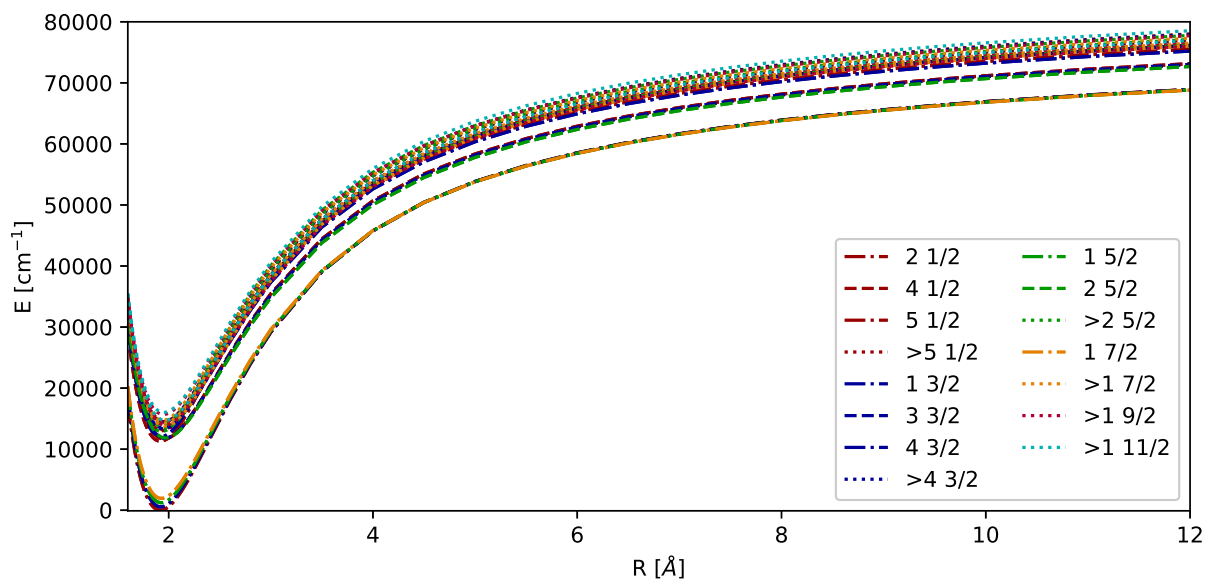


Figure 11: KRCI PECs for states with f^{13} for the triple zeta basis sets.

Table 8: Spectroscopic constants for the different electronic states ($\Omega = 1/2, 3/2, 5/2$) with f^{13} obtained by KRCI for the double and triple zeta basis sets. Vibrational constant (ω_e), anharmonicity constant ($\omega_e\chi_e$), and transition energy (T_e), are given in cm^{-1} , the equilibrium bond distance (r_e) in \AA .

| Ω | state | v2z | | | | v3z | | | |
|----------|-------|--------|------------|------------------|-------|--------|------------|------------------|-------|
| | | r_e | ω_e | $\omega_e\chi_e$ | T_e | r_e | ω_e | $\omega_e\chi_e$ | T_e |
| 1/2 | 1 | 1.9254 | 627 | 2.53 | 0 | 1.9188 | 631 | 2.73 | 0 |
| 1/2 | 2 | 1.9762 | 510 | 0.23 | 10834 | 1.9540 | 517 | 1.24 | 11083 |
| 1/2 | 3 | 1.9321 | 702 | 7.89 | 11243 | 1.9314 | 684 | 4.10 | 11352 |
| 1/2 | 4 | 1.9568 | 558 | 2.79 | 12833 | 1.9404 | 584 | 3.07 | 12811 |
| 1/2 | 5 | 1.9555 | 575 | 2.64 | 13071 | 1.9469 | 582 | 2.73 | 12946 |
| 1/2 | 6 | 1.9689 | 578 | 2.38 | 13663 | 1.9631 | 569 | 2.12 | 13947 |
| 1/2 | 7 | 1.9645 | 578 | 2.25 | 13884 | 1.9566 | 580 | 2.61 | 14069 |
| 3/2 | 1 | 1.9305 | 624 | 2.54 | 557 | 1.9239 | 628 | 2.76 | 545 |
| 3/2 | 2 | 1.9797 | 556 | 2.43 | 10849 | 1.9677 | 561 | 2.48 | 11212 |
| 3/2 | 3 | 1.9331 | 597 | 5.44 | 12028 | 1.9262 | 625 | 3.62 | 12045 |
| 3/2 | 4 | 1.9706 | 587 | 0.62 | 12938 | 1.9527 | 576 | 2.65 | 13073 |
| 3/2 | 5 | 1.9639 | 575 | 1.88 | 13087 | 1.9519 | 569 | 2.22 | 13194 |
| 3/2 | 6 | 1.9621 | 576 | 2.73 | 13632 | 1.9596 | 576 | 2.24 | 13797 |
| 3/2 | 7 | 1.9592 | 591 | 2.88 | 13966 | 1.9568 | 594 | 2.69 | 14083 |
| 5/2 | 1 | 1.9341 | 619 | 2.54 | 1272 | 1.9277 | 623 | 2.77 | 1227 |
| 5/2 | 2 | 1.9837 | 554 | 2.44 | 10843 | 1.9736 | 559 | 2.49 | 11295 |
| 5/2 | 3 | 1.9420 | 548 | 5.37 | 12945 | 1.9293 | 580 | 6.14 | 12923 |
| 5/2 | 4 | 1.9568 | 625 | 3.55 | 13211 | 1.9563 | 622 | 0.70 | 13264 |
| 5/2 | 5 | 1.9664 | 593 | 0.60 | 13543 | 1.9553 | 580 | 1.95 | 13670 |
| 5/2 | 6 | 1.9558 | 578 | 2.67 | 14218 | 1.9474 | 588 | 2.81 | 14225 |
| 7/2 | 1 | 1.9355 | 613 | 2.50 | 2017 | 1.9290 | 617 | 2.75 | 1931 |
| 7/2 | 2 | 1.9753 | 566 | 2.46 | 13192 | 1.9665 | 570 | 2.45 | 13424 |
| 7/2 | 3 | 1.9712 | 569 | 2.47 | 13565 | 1.9613 | 573 | 2.48 | 13819 |
| 7/2 | 4 | 1.9626 | 569 | 2.41 | 14333 | 1.9458 | 585 | 2.94 | 14475 |
| 9/2 | 1 | 1.9776 | 563 | 2.48 | 13226 | 1.9707 | 568 | 2.47 | 13576 |
| 9/2 | 2 | 1.9755 | 566 | 2.48 | 13544 | 1.9665 | 571 | 2.50 | 13933 |
| 9/2 | 3 | 1.9709 | 571 | 2.51 | 14319 | 1.9592 | 577 | 2.54 | 14880 |
| 11/2 | 1 | 1.9769 | 564 | 2.48 | 13466 | 1.9691 | 569 | 2.49 | 14001 |
| 11/2 | 2 | 1.9744 | 568 | 2.49 | 14177 | 1.9628 | 576 | 2.52 | 14904 |

Table 9: Spectroscopic constants for the different electronic states ($\Omega = 1/2, 3/2, 5/2$) with f^{13} obtained by KRCI for the quadruple zeta and extrapolation to the complete basis sets. Vibrational constant (ω_e), anharmonicity constant ($\omega_e\chi_e$), and transition energy (T_e), are given in cm^{-1} , the equilibrium bond distance (r_e) in \AA .

| Ω | state | v4z | | | | CBS | | | |
|----------|-------|--------|------------|------------------|-------|--------|------------|------------------|-------|
| | | r_e | ω_e | $\omega_e\chi_e$ | T_e | r_e | ω_e | $\omega_e\chi_e$ | T_e |
| 1/2 | 1 | 1.9183 | 632 | 2.60 | 0 | 1.9200 | 631 | 2.51 | 0 |
| 1/2 | 2 | 1.9191 | 583 | 8.23 | 11329 | 1.9038 | 655 | 13.57 | 11428 |
| 1/2 | 3 | 1.9497 | 641 | 0.17 | 11672 | 1.9603 | 620 | 0.08 | 11876 |
| 1/2 | 4 | 1.9366 | 593 | 2.73 | 13044 | 1.9360 | 598 | 2.50 | 13206 |
| 1/2 | 5 | 1.9426 | 588 | 2.65 | 13240 | 1.9417 | 592 | 2.56 | 13443 |
| 1/2 | 6 | 1.9566 | 576 | 2.40 | 14295 | 1.9539 | 582 | 2.71 | 14531 |
| 1/2 | 7 | 1.9503 | 580 | 2.75 | 14504 | 1.9479 | 578 | 2.71 | 14808 |
| 3/2 | 1 | 1.9236 | 628 | 2.61 | 543 | 1.9253 | 628 | 2.50 | 540 |
| 3/2 | 2 | 1.9589 | 530 | 0.82 | 11810 | 1.9505 | 516 | 0.80 | 12202 |
| 3/2 | 3 | 1.9306 | 667 | 4.87 | 12069 | 1.9331 | 711 | 8.45 | 12062 |
| 3/2 | 4 | 1.9483 | 582 | 2.55 | 13356 | 1.9473 | 585 | 2.47 | 13549 |
| 3/2 | 5 | 1.9440 | 578 | 2.90 | 13495 | 1.9408 | 584 | 3.30 | 13699 |
| 3/2 | 6 | 1.9545 | 575 | 2.67 | 14251 | 1.9528 | 574 | 2.97 | 14567 |
| 3/2 | 7 | 1.9575 | 591 | 1.96 | 14429 | 1.9601 | 589 | 1.50 | 14667 |
| 5/2 | 1 | 1.9276 | 623 | 2.61 | 1227 | 1.9296 | 622 | 2.46 | 1223 |
| 5/2 | 2 | 1.9690 | 563 | 2.45 | 11828 | 1.9677 | 564 | 2.42 | 12196 |
| 5/2 | 3 | 1.9282 | 614 | 3.10 | 12923 | 1.9302 | 635 | 1.41 | 12919 |
| 5/2 | 4 | 1.9579 | 592 | 1.08 | 13556 | 1.9627 | 571 | 0.93 | 13747 |
| 5/2 | 5 | 1.9482 | 582 | 2.57 | 14030 | 1.9451 | 584 | 3.07 | 14278 |
| 5/2 | 6 | 1.9449 | 593 | 2.66 | 14442 | 1.9453 | 596 | 2.53 | 14590 |
| 7/2 | 1 | 1.9293 | 617 | 2.59 | 1935 | 1.9315 | 616 | 2.43 | 1933 |
| 7/2 | 2 | 1.9627 | 573 | 2.43 | 13764 | 1.9620 | 574 | 2.42 | 13994 |
| 7/2 | 3 | 1.9552 | 576 | 2.39 | 14284 | 1.9528 | 577 | 2.31 | 14607 |
| 7/2 | 4 | 1.9424 | 595 | 2.81 | 14729 | 1.9422 | 601 | 2.69 | 14905 |
| 9/2 | 1 | 1.9669 | 570 | 2.49 | 13962 | 1.9663 | 571 | 2.49 | 14224 |
| 9/2 | 2 | 1.9613 | 575 | 2.48 | 14516 | 1.9596 | 576 | 2.45 | 14923 |
| 9/2 | 3 | 1.9494 | 584 | 2.59 | 15691 | 1.9444 | 588 | 2.62 | 16262 |
| 11/2 | 1 | 1.9645 | 572 | 2.49 | 14706 | 1.9633 | 574 | 2.48 | 15202 |
| 11/2 | 2 | 1.9525 | 584 | 2.52 | 16023 | 1.9472 | 588 | 2.51 | 16817 |

2.5 Open f-shell - dipole moments

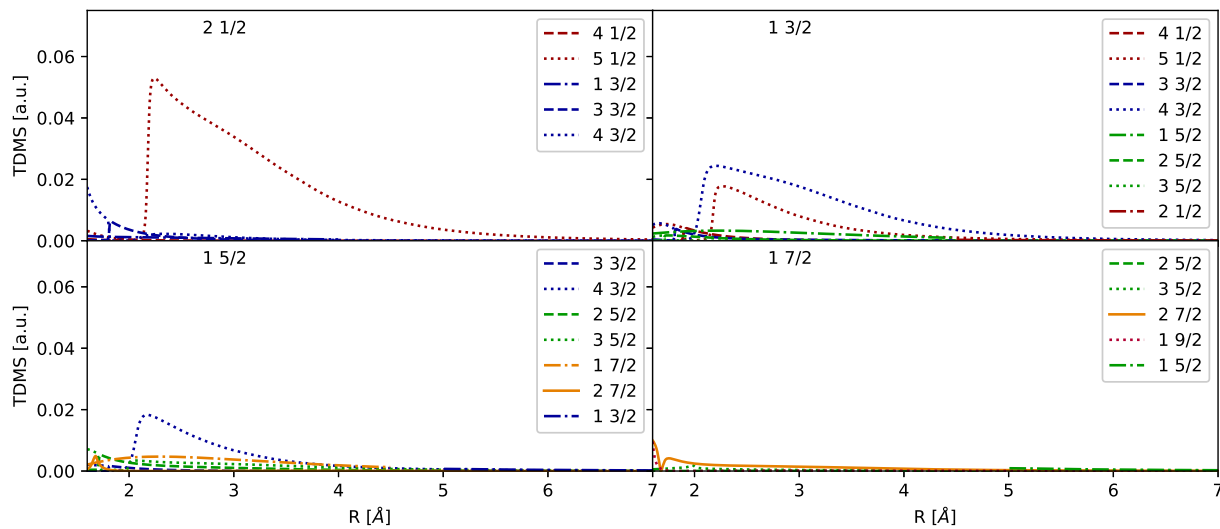


Figure 12: KRCI TDMs for states with f^{14} for the double zeta basis sets.

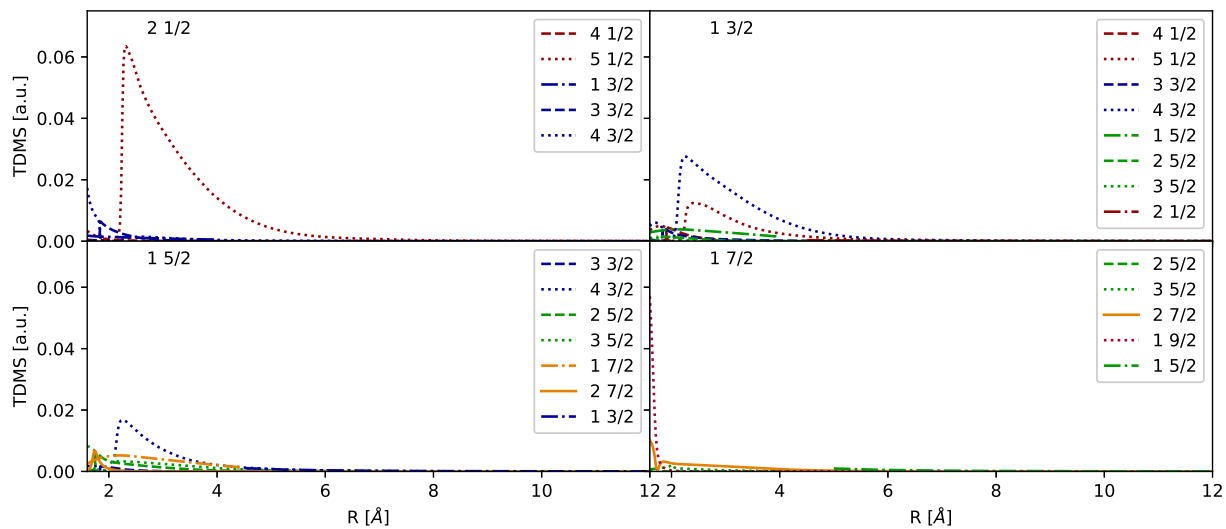


Figure 13: KRCI TDMs for states with f^{14} for the triple zeta basis sets.

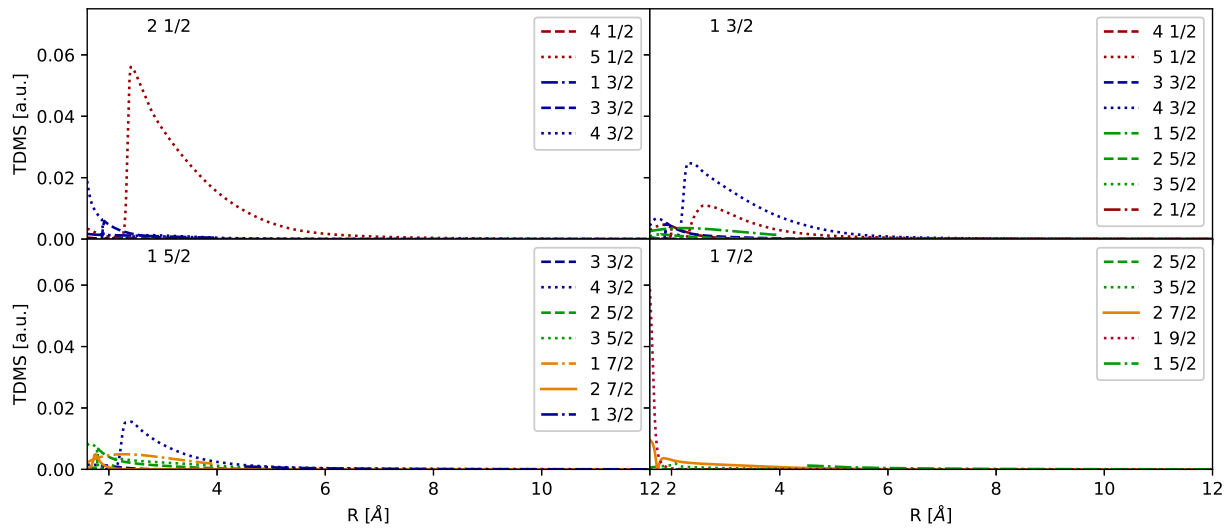


Figure 14: KRCI TDMS for states with f^{14} for the quadruple zeta basis sets.

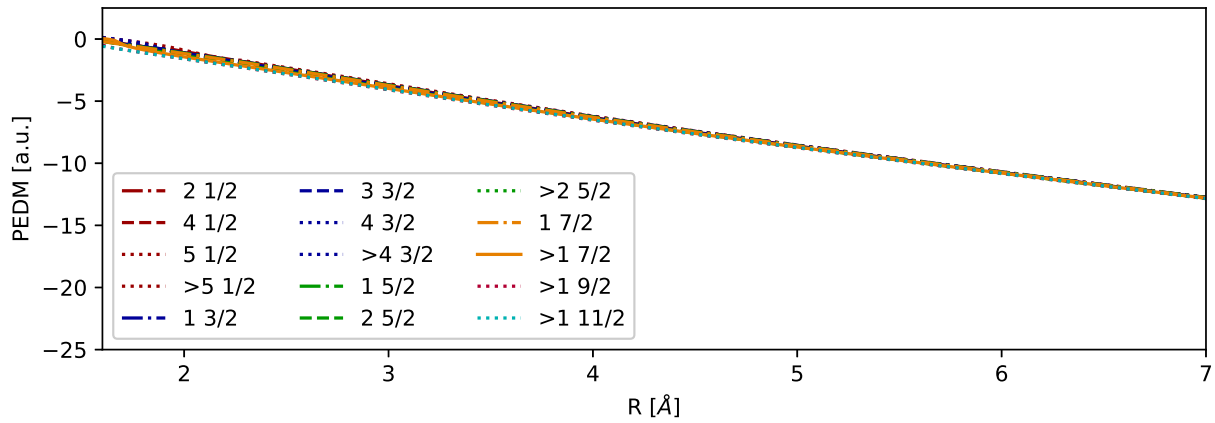


Figure 15: KRCI PEDMs for states with f^{13} for the double zeta basis sets.

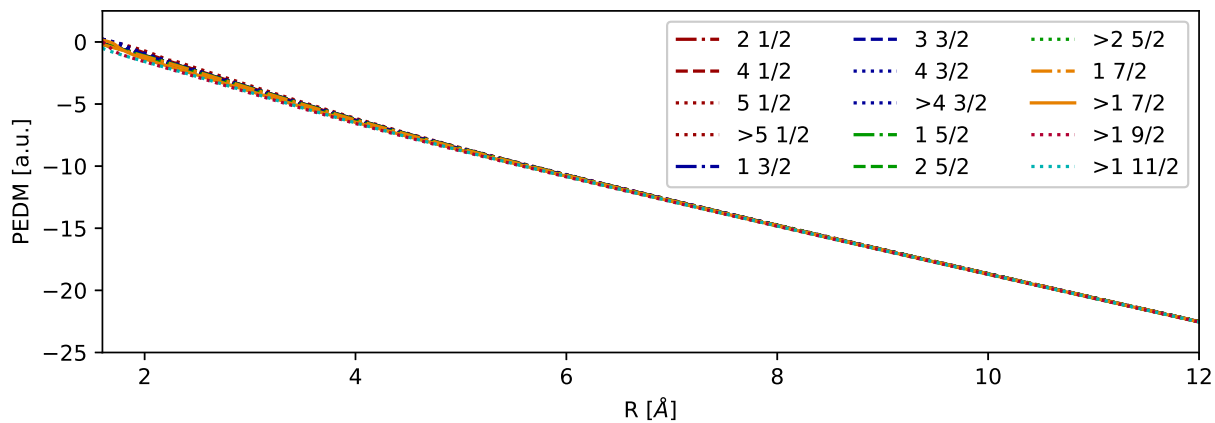


Figure 16: KRCI PEDMs for states with f^{13} for the triple zeta basis sets.

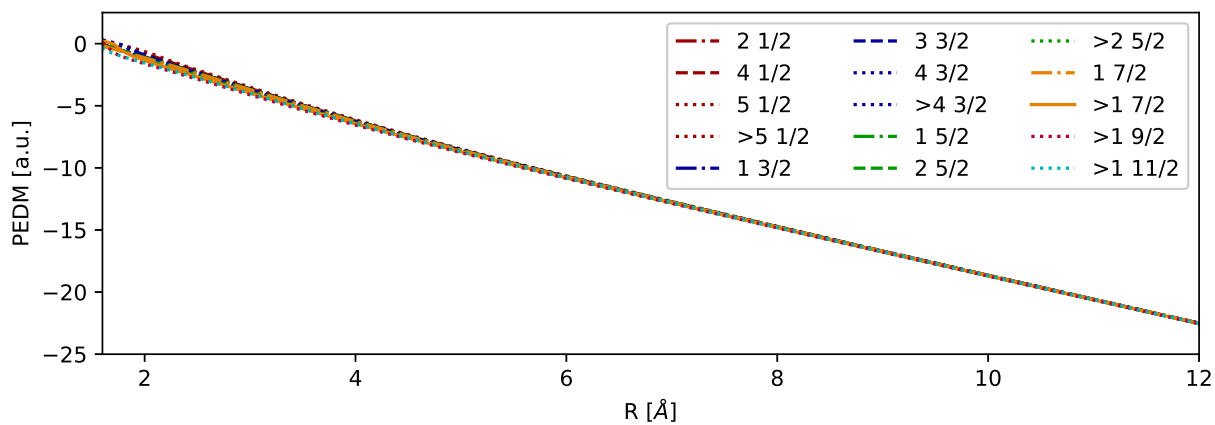


Figure 17: KRCI PEDMs for states with f^{13} for the triple zeta basis sets.

2.6 Combined potentials, shifting

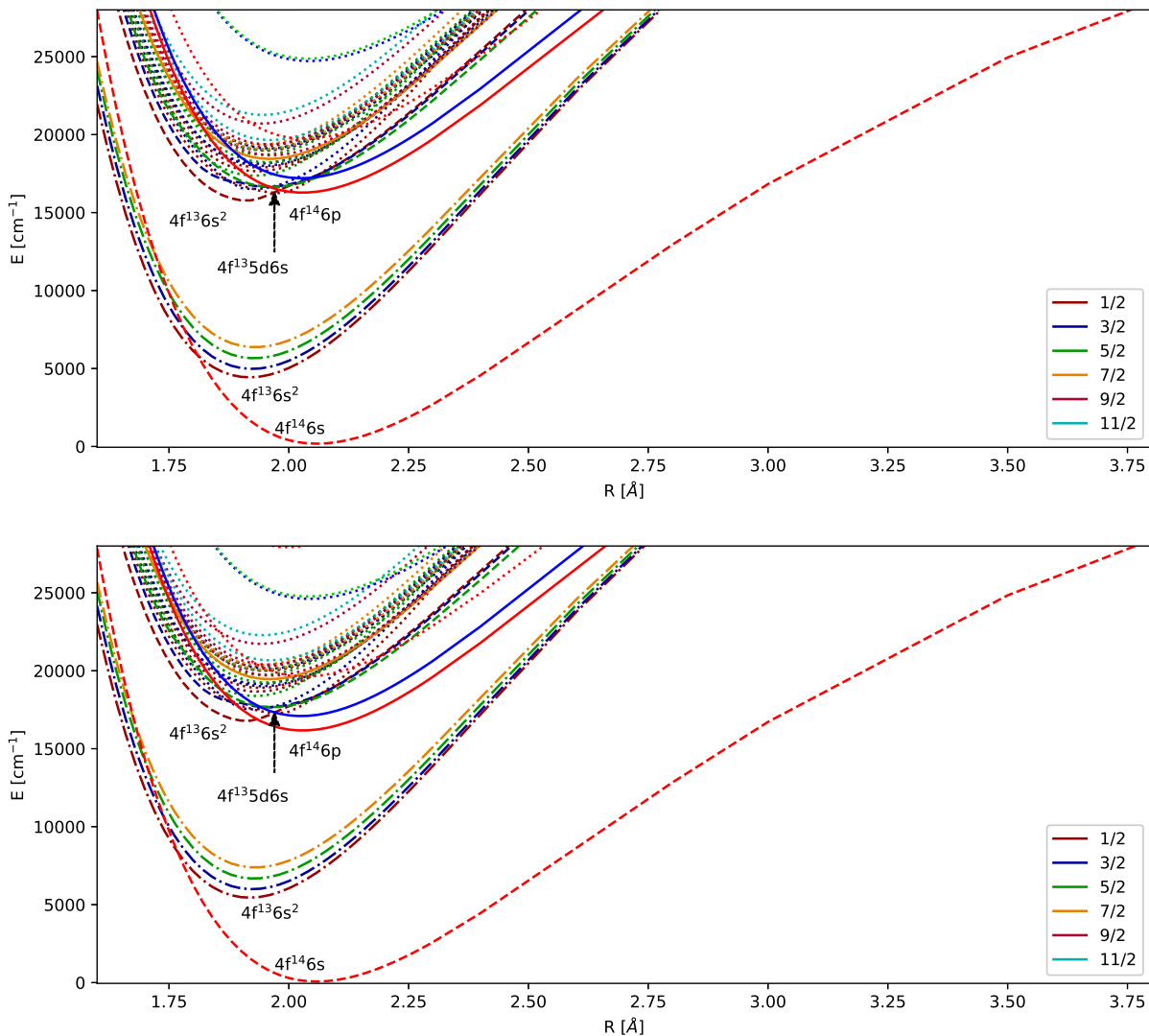


Figure 18: Combination of the sets of KRCI potentials. The lowest $\Omega = 1/2$ are denoted by the assigned dominant configuration. For the upper the shift was applied at 15\AA for the lower picture at 10\AA .

The combination of the potential energy by shifting according to the outermost point is shown in figure 18. While the minimum of the potential changes from about 45000 to 53000 cm^{-1} , there are only small changes in the relative position of the minima of different electronic states.

Figures 19 to 21 show the combined potentials energy curves for different basis set sizes.

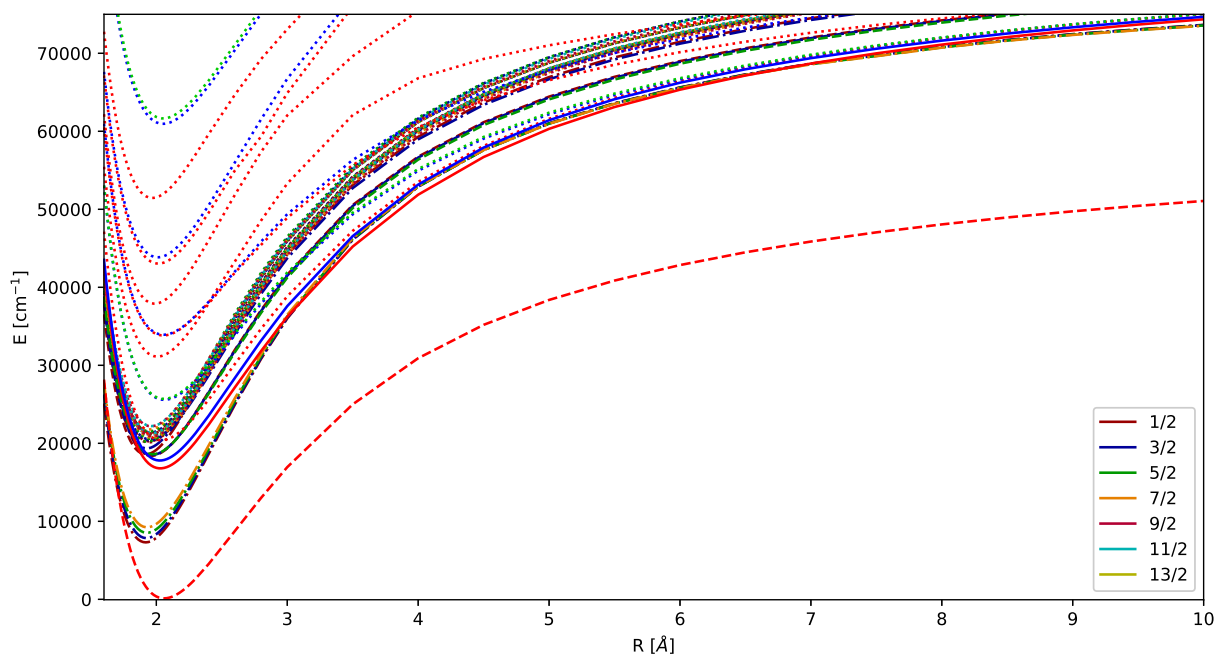


Figure 19: KRCI PECs for states with open and closed f-shell for the triple zeta basis sets.

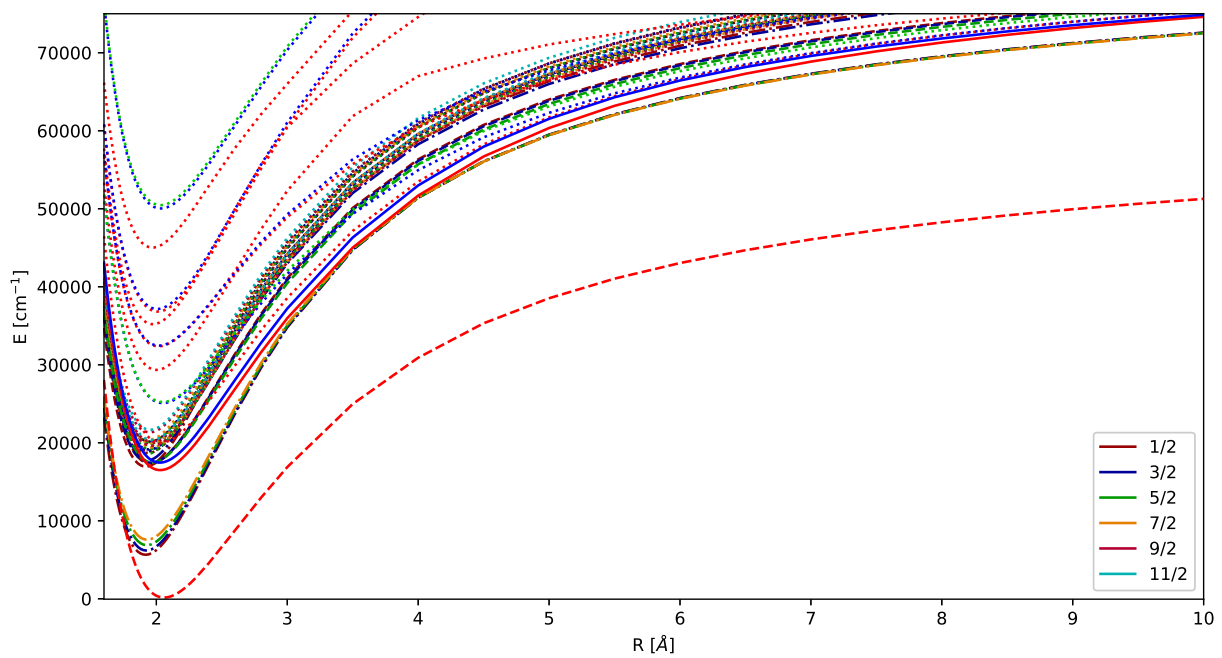


Figure 20: KRCI PECs for states with open and closed f-shell for the quadruple zeta basis sets.

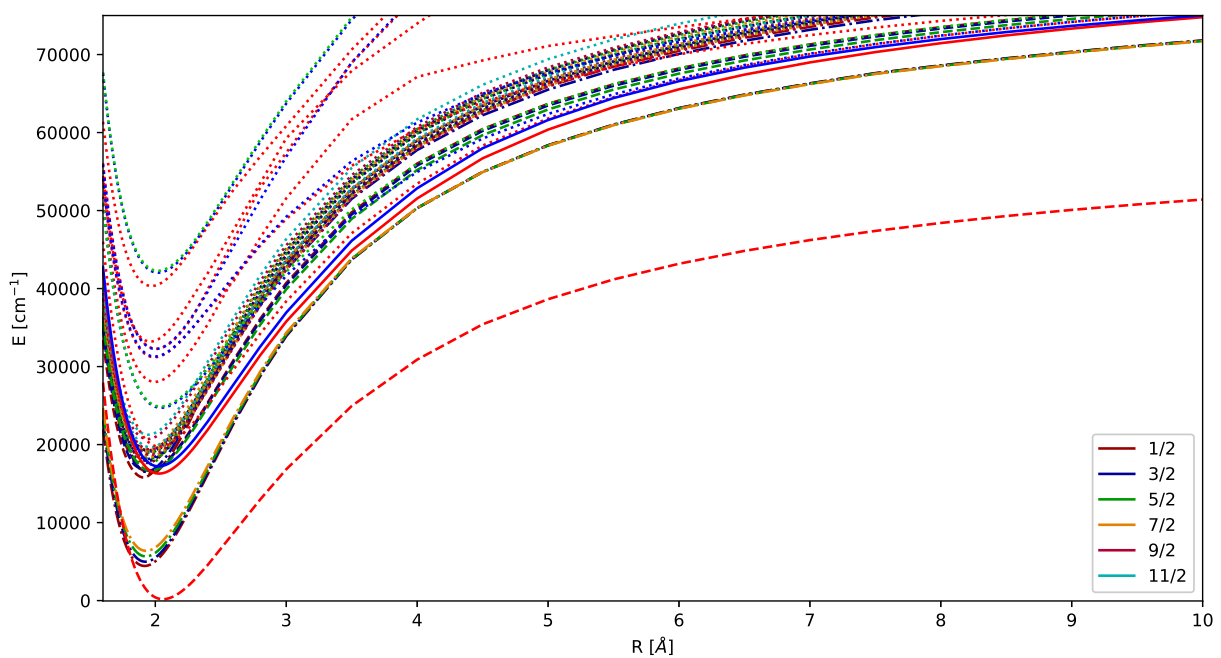


Figure 21: KRCI PECs for states with open and closed f-shell for extrapolation to the basis set limit.

2.7 Collection - transition dipole moments

Table 10: KRCI transition dipole moment table for the equilibrium distances of ground state.

| Ω_1 | state ₁ | Ω_2 | state ₂ | TDMs [a.u.] |
|------------|--------------------|------------|--------------------|-------------|
| 1 | 1 | 1 | 3 | 0.163 |
| 2 | 1 | 2 | 6 | 8.410 |
| 3 | 1 | 3 | 2 | 13.571 |
| 4 | 1 | 4 | 5 | 0.012 |
| 5 | 2 | 5 | 4 | 0.000 |
| 6 | 2 | 6 | 5 | 0.001 |
| 7 | 2 | 7 | 1 | 0.001 |
| 8 | 2 | 8 | 3 | 0.006 |
| 9 | 1 | 9 | 4 | 0.000 |
| 10 | 1 | 10 | 5 | 0.004 |
| 11 | 1 | 11 | 3 | 0.005 |
| 12 | 1 | 12 | 4 | 0.000 |
| 13 | 1 | 13 | 1 | 0.003 |
| 14 | 1 | 14 | 2 | 0.001 |
| 15 | 1 | 15 | 3 | 0.001 |
| 16 | 1 | 16 | 4 | 0.000 |
| 17 | 1 | 17 | 2 | 0.005 |
| 18 | 1 | 18 | 3 | 0.000 |
| 19 | 1 | 19 | 1 | 0.004 |
| 20 | 1 | 20 | 2 | 0.001 |
| 21 | 1 | 21 | 2 | 0.000 |
| 22 | 1 | 22 | 3 | 0.001 |
| 23 | 1 | 23 | 1 | 0.003 |
| 24 | 1 | 24 | 2 | 0.001 |
| 25 | 2 | 25 | 2 | 0.000 |

3 Intermediate Hamiltonian Fock Space Coupled Cluster (IHFS-CCSD)

3.1 Closed f-shell - potential energy curves

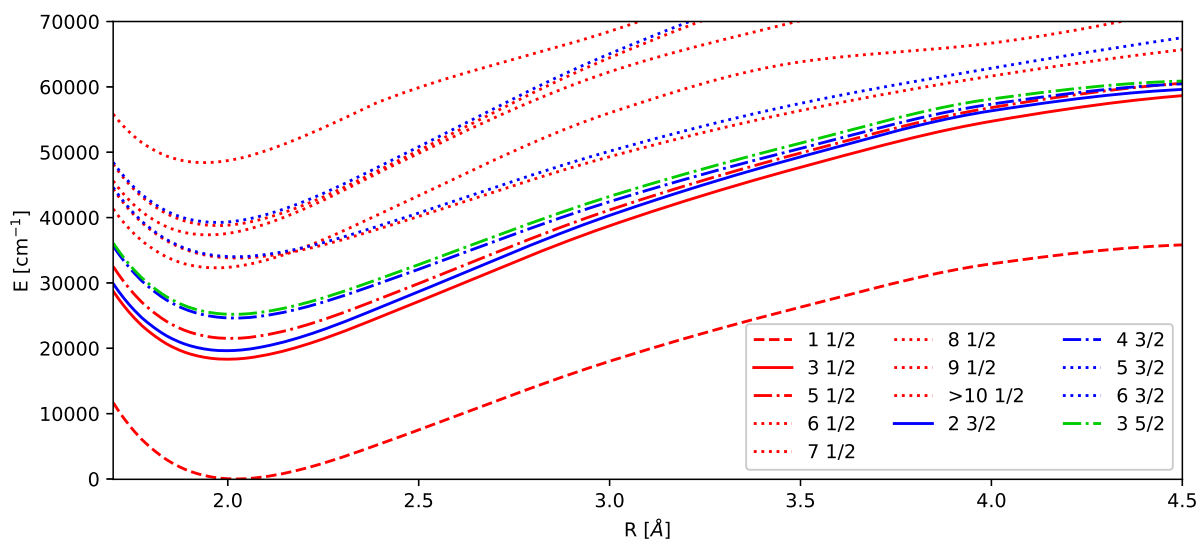


Figure 22: IHFS-CCSD PECs for states from the (0h,1p) sector with a cation reference for the quadruple zeta basis sets.

Table 11: Spectroscopic constants for the different electronic states ($\Omega = 1/2, 3/2, 5/2$) obtained by IHFS-CCSD for the (0h,1p) sector using double and triple zeta basis sets. Vibrational constant (ω_e), anharmonicity constant ($\omega_e\chi_e$), and transition energy (T_e), are given in cm^{-1} , the equilibrium bond distance (r_e) in \AA .

| Ω | state | v2z | | | | v3z | | | |
|----------|-------|--------|------------|------------------|-------|--------|------------|------------------|-------|
| | | r_e | ω_e | $\omega_e\chi_e$ | T_e | r_e | ω_e | $\omega_e\chi_e$ | T_e |
| 1/2 | 1 | 2.0315 | 502 | 2.33 | 0 | 2.0281 | 504 | 2.32 | 0 |
| 1/2 | 2 | 2.0045 | 524 | 2.19 | 18610 | 2.0037 | 526 | 2.22 | 18425 |
| 1/2 | 3 | 2.0133 | 518 | 2.31 | 22113 | 2.0127 | 521 | 2.28 | 21687 |
| 1/2 | 4 | 2.0905 | 443 | 2.21 | 36083 | 1.9680 | 543 | 6.91 | 33550 |
| 1/2 | 5 | 1.9873 | 518 | 3.00 | 38956 | 2.0481 | 524 | 0.02 | 34724 |
| 1/2 | 6 | 1.9994 | 569 | 2.17 | 42974 | 1.9648 | 582 | 2.30 | 39207 |
| 1/2 | 7 | 2.0383 | 508 | 1.98 | 56216 | 1.9964 | 532 | 1.92 | 46115 |
| 1/2 | 8 | 1.8438 | 813 | 3.41 | 66635 | 1.9414 | 591 | 2.37 | 54196 |
| 3/2 | 1 | 2.0010 | 527 | 2.20 | 19980 | 2.0004 | 530 | 2.24 | 19747 |
| 3/2 | 2 | 2.0394 | 484 | 2.17 | 25904 | 2.0268 | 496 | 2.24 | 24977 |
| 3/2 | 3 | 2.0892 | 450 | 2.19 | 36389 | 2.0448 | 470 | 2.39 | 34962 |
| 3/2 | 4 | 2.0319 | 510 | 2.01 | 58253 | 1.9909 | 535 | 1.99 | 46891 |
| 5/2 | 1 | 2.0372 | 486 | 2.18 | 26612 | 2.0243 | 499 | 2.26 | 25563 |
| ION | | 1.9506 | 594 | 2.08 | 48113 | 1.9483 | 597 | 2.15 | 48352 |

Table 12: Spectroscopic constants for the different electronic states ($\Omega = 1/2, 3/2, 5/2$) obtained by IHFS-CCSD for the (0h,1p) sector using double and triple zeta and extrapolation to the complete basis sets. Vibrational constant (ω_e), anharmonicity constant ($\omega_e\chi_e$), and transition energy (T_e), are given in cm^{-1} , the equilibrium bond distance (r_e) in \AA .

| Ω | state | v4z | | | | CBS | | | |
|----------|-------|--------|------------|------------------|-------|--------|------------|------------------|-------|
| | | r_e | ω_e | $\omega_e\chi_e$ | T_e | r_e | ω_e | $\omega_e\chi_e$ | T_e |
| 1/2 | 1 | 2.0220 | 510 | 2.60 | 0 | 2.0176 | 515 | 2.82 | 0 |
| 1/2 | 2 | 1.9988 | 533 | 2.46 | 18323 | 1.9953 | 539 | 2.63 | 18249 |
| 1/2 | 3 | 2.0072 | 527 | 2.54 | 21506 | 2.0032 | 533 | 2.73 | 21375 |
| 1/2 | 4 | 1.9649 | 574 | 4.13 | 32306 | 1.9644 | 581 | 1.82 | 31416 |
| 1/2 | 5 | 2.0298 | 506 | 0.35 | 33748 | 2.0155 | 494 | 0.68 | 33018 |
| 1/2 | 6 | 1.9477 | 599 | 2.29 | 37343 | 1.9359 | 610 | 2.08 | 35954 |
| 1/2 | 7 | 1.9732 | 577 | 2.08 | 38770 | 1.9597 | 608 | 1.95 | 33366 |
| 1/2 | 8 | 1.9384 | 592 | 2.46 | 48402 | 1.9363 | 592 | 2.39 | 44179 |
| 3/2 | 1 | 1.9955 | 537 | 2.46 | 19629 | 1.9920 | 542 | 2.63 | 19543 |
| 3/2 | 2 | 2.0182 | 505 | 2.53 | 24624 | 2.0120 | 512 | 2.73 | 24363 |
| 3/2 | 3 | 2.0208 | 482 | 2.69 | 34007 | 2.0031 | 493 | 2.96 | 33271 |
| 3/2 | 4 | 1.9703 | 576 | 2.10 | 39254 | 1.9582 | 605 | 1.96 | 33646 |
| 5/2 | 1 | 2.0154 | 508 | 2.53 | 25193 | 2.0089 | 515 | 2.77 | 24919 |
| ION | | 1.9450 | 604 | 1.98 | 48426 | 1.9437 | 609 | 1.86 | 49901 |

3.2 Open f-shell - potential energy curves

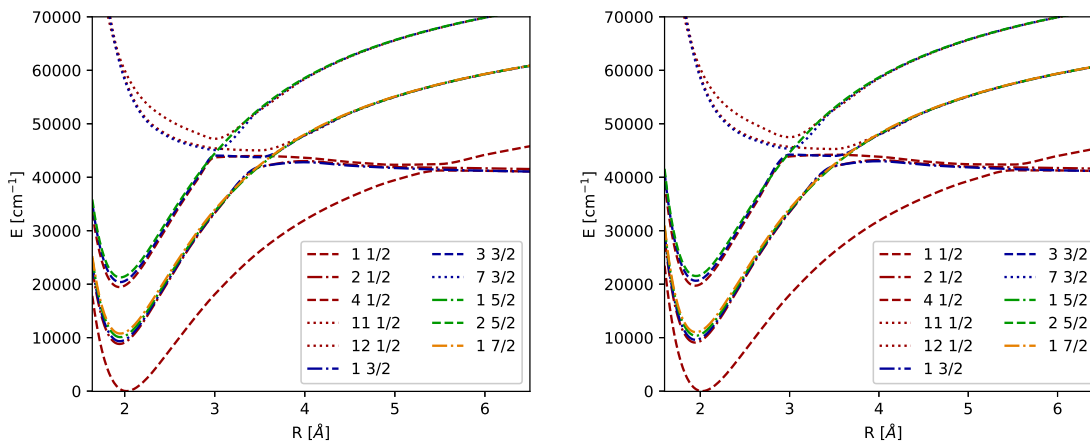


Figure 23: IHFS-CCSD PECs for (1h,0p) sector starting from the anion reference for the quadruple zeta basis sets and a shift of 0.2 and 0.1 Hartree.

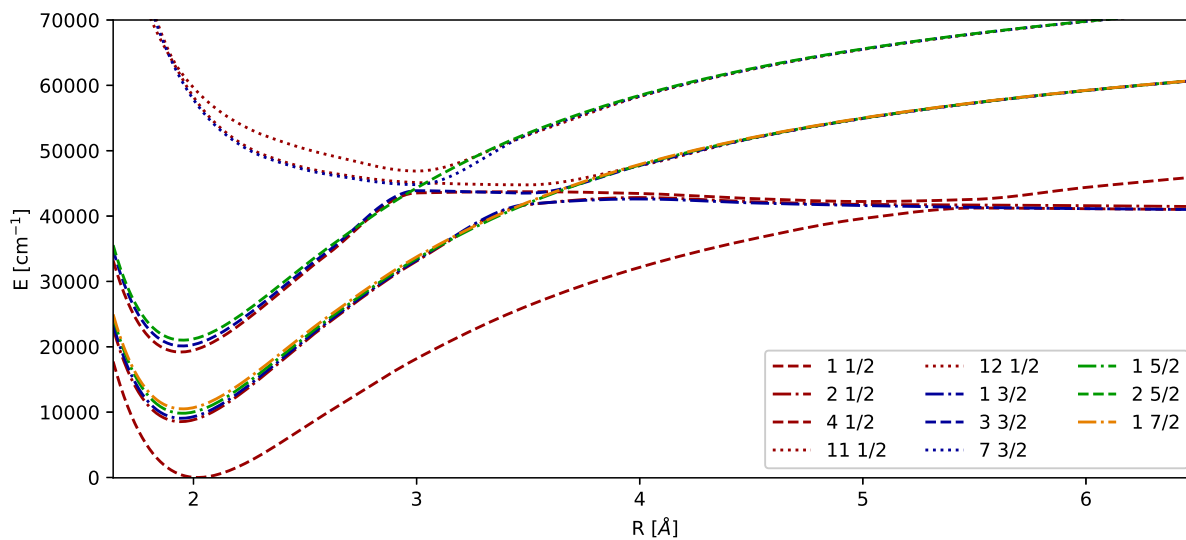


Figure 24: XIHFS-CCSD PECs for (1h,0p) sector starting from the anion reference for the quadruple zeta basis sets, extrapolation using the results in figure 23

Table 13: Spectroscopic constants for the different electronic states ($\Omega = 1/2, 3/2, 5/2$) obtained by XIHFS-CCSD for the (1h,0p) sector using double and triple zeta basis sets. Vibrational constant (ω_e), anharmonicity constant ($\omega_e\chi_e$), and transition energy (T_e), are given in cm^{-1} , the equilibrium bond distance (r_e) in \AA .

| Ω | state | v2z | | | | v3z | | | |
|----------|-------|--------|------------|------------------|-------|--------|------------|------------------|-------|
| | | r_e | ω_e | $\omega_e\chi_e$ | T_e | r_e | ω_e | $\omega_e\chi_e$ | T_e |
| 1/2 | 1 | 2.0239 | 497 | 2.06 | 0 | 2.0244 | 504 | 2.26 | 0 |
| 1/2 | 2 | 1.9481 | 619 | 3.17 | 4282 | 1.9463 | 598 | 2.81 | 7059 |
| 1/2 | 3 | 1.9410 | 605 | 2.73 | 14808 | 1.9444 | 594 | 2.72 | 17729 |
| 3/2 | 1 | 1.9440 | 602 | 2.73 | 4630 | 1.9479 | 591 | 2.73 | 7521 |
| 3/2 | 2 | 1.9478 | 599 | 2.75 | 15710 | 1.9518 | 588 | 2.72 | 18616 |
| 5/2 | 1 | 1.9488 | 597 | 2.74 | 5407 | 1.9530 | 586 | 2.72 | 8263 |
| 5/2 | 2 | 1.9491 | 592 | 2.73 | 16625 | 1.9533 | 581 | 2.71 | 19483 |
| 7/2 | 1 | 1.9487 | 591 | 2.73 | 6102 | 1.9529 | 581 | 2.71 | 8918 |
| ION | | 2.1018 | 425 | 2.71 | -8767 | 2.0935 | 430 | 2.66 | -9418 |

Table 14: Spectroscopic constants for the different electronic states ($\Omega = 1/2, 3/2, 5/2$) obtained by XIHFS-CCSD for the (1h,0p) sector using quadruple zeta and extrapolation to the complete basis sets. Vibrational constant (ω_e), anharmonicity constant ($\omega_e\chi_e$), and transition energy (T_e), are given in cm^{-1} , the equilibrium bond distance (r_e) in \AA .

| Ω | state | v4z | | | | CBS | | | |
|----------|-------|--------|------------|------------------|-------|--------|------------|------------------|-------|
| | | r_e | ω_e | $\omega_e\chi_e$ | T_e | r_e | ω_e | $\omega_e\chi_e$ | T_e |
| 1/2 | 1 | 2.0195 | 509 | 2.35 | 0 | 2.0159 | 513 | 2.42 | 0 |
| 1/2 | 2 | 1.9425 | 599 | 2.80 | 8543 | 1.9396 | 599 | 2.79 | 9627 |
| 1/2 | 3 | 1.9417 | 596 | 2.75 | 19195 | 1.9397 | 597 | 2.78 | 20267 |
| 3/2 | 1 | 1.9455 | 593 | 2.76 | 9057 | 1.9438 | 595 | 2.79 | 10180 |
| 3/2 | 2 | 1.9496 | 590 | 2.76 | 20121 | 1.9480 | 591 | 2.80 | 21222 |
| 5/2 | 1 | 1.9508 | 588 | 2.76 | 9825 | 1.9493 | 589 | 2.78 | 10968 |
| 5/2 | 2 | 1.9513 | 583 | 2.75 | 21011 | 1.9499 | 584 | 2.77 | 22127 |
| 7/2 | 1 | 1.9510 | 582 | 2.74 | 10494 | 1.9496 | 583 | 2.77 | 11645 |
| ION | | 2.0851 | 435 | 2.74 | -9579 | 2.0823 | 437 | 2.79 | -8197 |

3.3 Combined potentials

In this section we combine the potentials from the previous two sections for different basis sets sizes.

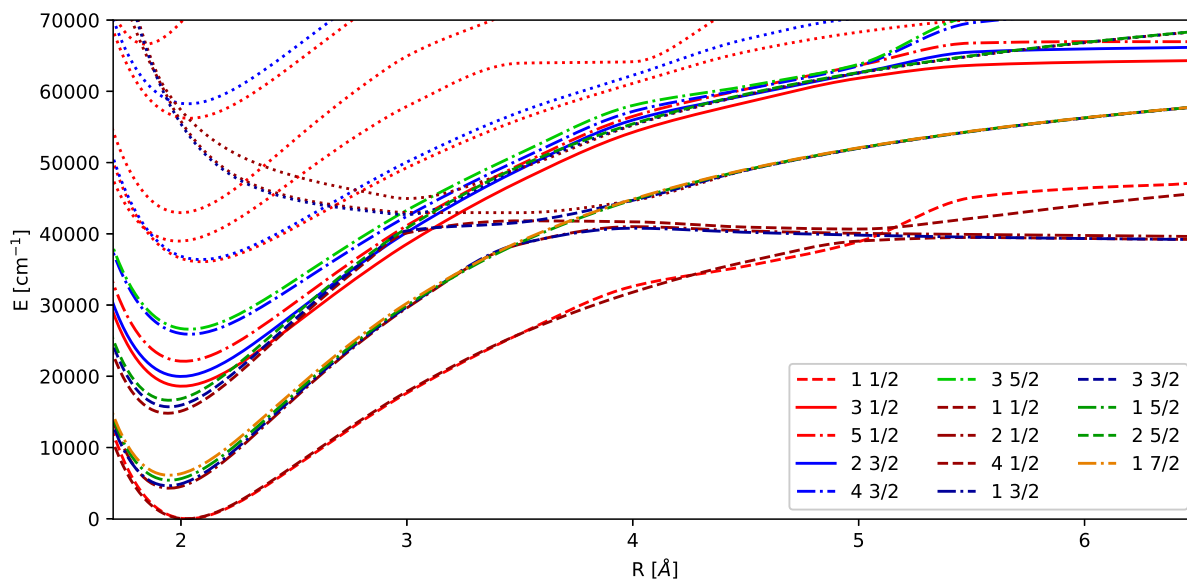


Figure 25: IHFS-CCSD PECs generated by the use of two different sectors and reference systems for the double zeta basis sets.

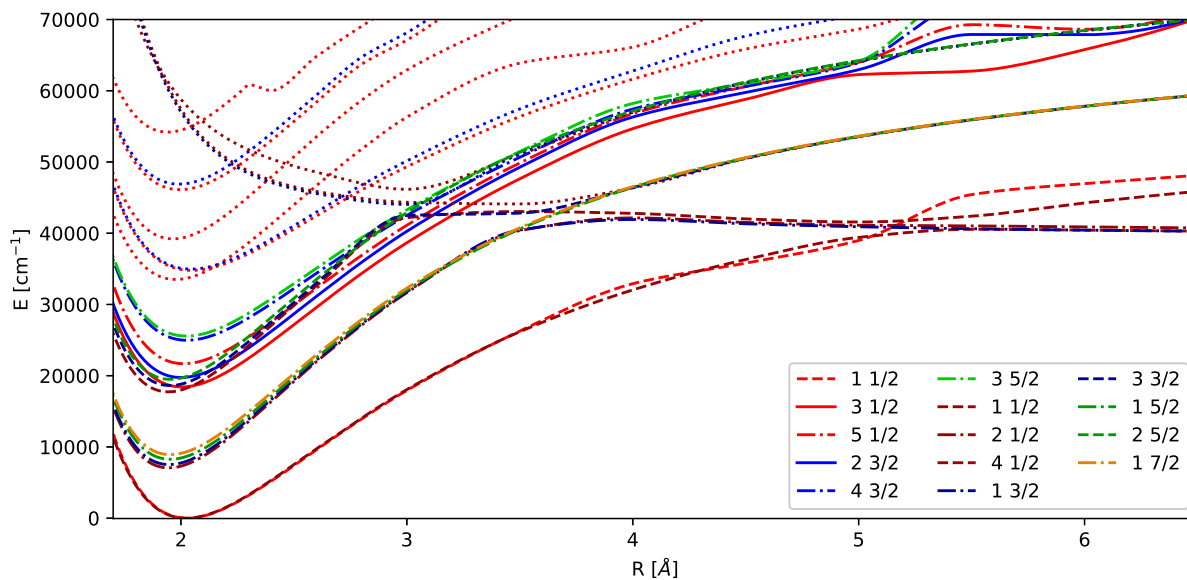


Figure 26: IHFS-CCSD PECs generated by the use of two different sectors and reference systems for the triple zeta basis sets.

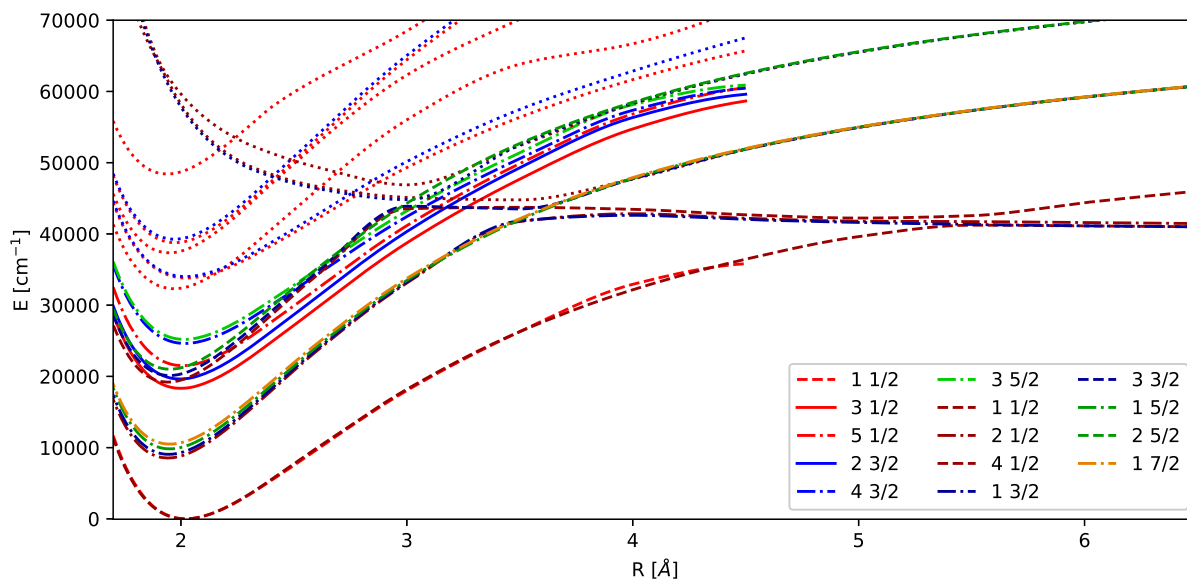


Figure 27: IHFS-CCSD PECs generated by the use of two different sectors and reference systems for the quadruple zeta basis sets.

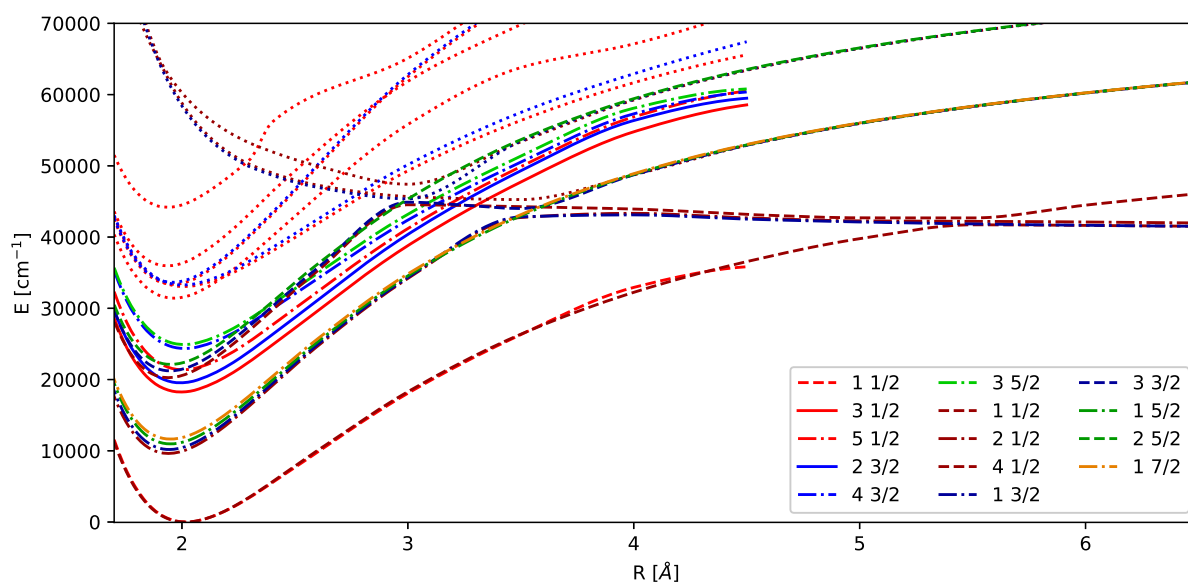


Figure 28: IHFS-CCSD PECs generated by the use of two different sectors and reference systems for extrapolation to the basis sets limit.

3.4 Spectroscopic quantities after mixing

We extracted the spectroscopic quantities for the adiabaticized potentials shown in the main text and listed them here.

Table 15: Spectroscopic constants for the different electronic states ($\Omega = 1/2, 3/2, 5/2$) obtained by IHFS-CCSD after basis set extrapolation, results from two sectors are combined using adiabaticization with different coupling constants (C). Vibrational constant (ω_e), anharmonicity constant ($\omega_e\chi_e$), and transition energy (T_e), are given in cm^{-1} , the equilibrium bond distance (r_e) in Å.

| Ω | state | C = 10 cm^{-1} | | | | C = 100 cm^{-1} | | | | C = 1000 cm^{-1} | | | |
|----------|-------|-------------------------|------------|------------------|-------|--------------------------|------------|------------------|-------|---------------------------|------------------|-------|-------|
| | | r_e | ω_e | $\omega_e\chi_e$ | T_e | r_e | ω_e | $\omega_e\chi_e$ | T_e | ω_e | $\omega_e\chi_e$ | T_e | |
| 1/2 | 1 | 2.0177 | 515 | 2.80 | 0 | 2.0177 | 515 | 2.80 | 0 | 2.0167 | 515 | 2.80 | 0 |
| 1/2 | 2 | 1.9397 | 599 | 2.77 | 9618 | 1.9397 | 599 | 2.77 | 9617 | 1.9418 | 596 | 2.76 | 9522 |
| 1/2 | 3 | 1.9953 | 539 | 2.61 | 18249 | 1.9952 | 538 | 2.60 | 18247 | 1.9843 | 533 | 2.35 | 18066 |
| 1/2 | 4 | 1.9337 | 609 | 8.95 | 20260 | 1.9349 | 603 | 8.61 | 20258 | 1.9654 | 561 | 3.65 | 20160 |
| 1/2 | 5 | 2.0035 | 586 | 0.25 | 21336 | 2.0019 | 586 | 0.38 | 21359 | 1.9860 | 577 | 2.10 | 22209 |
| 1/2 | 6 | 1.9644 | 581 | 1.83 | 31417 | 1.9644 | 581 | 1.83 | 31419 | 1.9645 | 580 | 1.96 | 31667 |
| 1/2 | 7 | 2.0149 | 470 | 0.14 | 33029 | 2.0149 | 470 | 0.14 | 33031 | 2.0132 | 472 | 0.24 | 33255 |
| 1/2 | 8 | 1.9647 | 633 | 2.62 | 33384 | 1.9647 | 633 | 2.62 | 33386 | 1.9656 | 628 | 2.61 | 33633 |
| 3/2 | 1 | 1.9438 | 594 | 2.76 | 10171 | 1.9438 | 594 | 2.76 | 10170 | 1.9447 | 593 | 2.76 | 10097 |
| 3/2 | 2 | 1.9921 | 542 | 2.61 | 19543 | 1.9919 | 542 | 2.60 | 19540 | 1.9820 | 541 | 2.50 | 19316 |
| 3/2 | 3 | 1.9480 | 591 | 2.77 | 21213 | 1.9482 | 591 | 2.80 | 21217 | 1.9621 | 580 | 3.13 | 21524 |
| 3/2 | 4 | 2.0121 | 512 | 2.72 | 24363 | 2.0121 | 512 | 2.69 | 24369 | 2.0059 | 528 | 2.33 | 24897 |
| 3/2 | 5 | 2.0023 | 473 | 1.95 | 33287 | 2.0023 | 473 | 1.95 | 33290 | 1.9998 | 476 | 2.25 | 33537 |
| 3/2 | 6 | 1.9608 | 632 | 3.13 | 33644 | 1.9608 | 632 | 3.13 | 33647 | 1.9630 | 623 | 2.67 | 33954 |
| 5/2 | 1 | 1.9493 | 589 | 2.75 | 10959 | 1.9493 | 589 | 2.75 | 10960 | 1.9496 | 588 | 2.76 | 11075 |
| 5/2 | 2 | 1.9500 | 584 | 2.75 | 22118 | 1.9500 | 583 | 2.76 | 22117 | 1.9542 | 572 | 3.01 | 22014 |
| 5/2 | 3 | 2.0090 | 515 | 2.75 | 24920 | 2.0089 | 516 | 2.72 | 24926 | 2.0024 | 532 | 2.38 | 25513 |

4 Equation-of-motion coupled cluster (EOM-CCSD)

4.1 Yb cation transition energies

Table 16: Transition energies for the Yb cation. Reference values have been obtained from the Nist database, the computed values were obtained for different basis sets with IP-EOM-CCSD or EA-EOM-CCSD coupled cluster.

| state | conf | NIST ⁸ | EA | | | IP | | |
|----------------------------|----------------|-------------------|-------|-------|-------|-------|-------|-------|
| | | E | 2z | 3z | 4z | 2z | 3z | 4z |
| $^2S_{1/2}$ | $4f^{14}6s$ | 0 | 0 | 0 | 0 | 0 | 0 | 0 |
| $^2F_{7/2}^{\circ}$ | $4f^{13}6s^2$ | 21419 | | | | 12054 | 13524 | 16092 |
| $^2F_{5/2}^{\circ}$ | $4f^{13}6s^2$ | 31568 | | | | 22629 | 24139 | 26655 |
| $^2D_{3/2}$ | $4f^{14}5d$ | 22961 | 24209 | 24073 | 24060 | 32956 | 33306 | 33712 |
| $^2D_{5/2}$ | $4f^{14}5d$ | 24333 | 25457 | 25351 | 25341 | 33589 | 33865 | 34263 |
| $^2P_{1/2}^{\circ}$ | $4f^{14}6p$ | 27062 | 27780 | 27539 | 27857 | 31553 | 31938 | 32112 |
| $^2P_{3/2}^{\circ}$ | $4f^{14}6p$ | 30392 | 31246 | 30954 | 31323 | 34621 | 34975 | 35147 |
| $^3 [3/2]_{5/2}^{\circ}$ | $4f^{13}5d 6s$ | 26759 | | | | | | |
| $^3 [3/2]_{3/2}^{\circ}$ | $4f^{13}5d 6s$ | 28758 | | | | | | |
| $^3 [11/2]_{9/2}^{\circ}$ | $4f^{13}5d 6s$ | 30224 | | | | | | |
| $^3 [11/2]_{11/2}^{\circ}$ | $4f^{13}5d 6s$ | 30563 | | | | | | |

4.2 Closed f-shell - potential energy curves

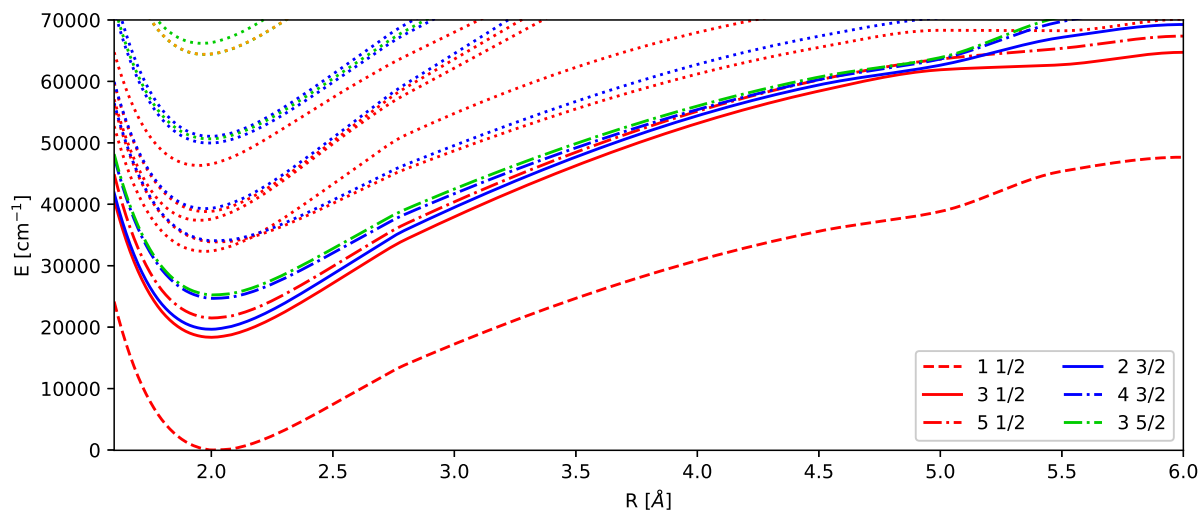


Figure 29: EOM-CCSD PECs for states from the (0h,1p) sector with a cation reference for the quadruple zeta basis sets.

Table 17: Spectroscopic constants for the different electronic states ($\Omega = 1/2, 3/2, 5/2$) obtained by EOM-CCSD for the (0h,1p) sector using different basis set sizes. Vibrational constant (ω_e), anharmonicity constant ($\omega_e\chi_e$), and transition energy (T_e), are given in cm^{-1} , the equilibrium bond distance (r_e) in Å.

| Ω | state | v3z | | | | v4z | | | | CBS | | | |
|----------|-------|--------|------------|------------------|-------|--------|------------|------------------|-------|--------|------------|------------------|-------|
| | | r_e | ω_e | $\omega_e\chi_e$ | T_e | r_e | ω_e | $\omega_e\chi_e$ | T_e | r_e | ω_e | $\omega_e\chi_e$ | T_e |
| 1/2 | 1 | 2.0287 | 503 | 2.30 | 0 | 2.0248 | 508 | 2.57 | 0 | 2.0230 | 511 | 2.80 | 0 |
| 1/2 | 2 | 2.0040 | 525 | 2.22 | 18407 | 2.0012 | 532 | 2.52 | 18384 | 2.0004 | 536 | 2.72 | 18373 |
| 1/2 | 3 | 2.0128 | 521 | 2.27 | 21631 | 2.0093 | 527 | 2.58 | 21524 | 2.0079 | 532 | 2.78 | 21448 |
| 1/2 | 4 | 1.9718 | 513 | 8.14 | 33599 | 1.9646 | 567 | 4.96 | 32407 | 1.9726 | 593 | 0.60 | 31497 |
| 1/2 | 5 | 2.0408 | 552 | 0.10 | 34419 | 2.0334 | 510 | 0.28 | 33772 | 2.0294 | 479 | 0.29 | 33299 |
| 1/2 | 6 | 1.9652 | 580 | 2.32 | 39226 | 1.9499 | 596 | 2.33 | 37425 | 1.9405 | 607 | 2.20 | 36100 |
| 1/2 | 7 | 1.9899 | 550 | 1.95 | 43303 | 1.9753 | 575 | 2.10 | 38850 | 1.9667 | 593 | 2.19 | 35591 |
| 1/2 | 8 | 1.9482 | 577 | 2.53 | 51348 | 1.9460 | 582 | 2.56 | 46354 | 1.9456 | 584 | 2.58 | 42725 |
| 3/2 | 1 | 2.0006 | 529 | 2.23 | 19738 | 1.9979 | 535 | 2.52 | 19696 | 1.9971 | 540 | 2.72 | 19672 |
| 3/2 | 2 | 2.0273 | 496 | 2.25 | 24996 | 2.0210 | 503 | 2.56 | 24691 | 2.0177 | 509 | 2.78 | 24468 |
| 3/2 | 3 | 2.0481 | 470 | 2.30 | 34695 | 2.0237 | 480 | 2.71 | 34062 | 2.0068 | 489 | 3.03 | 33563 |
| 3/2 | 4 | 1.9862 | 549 | 1.97 | 44290 | 1.9724 | 575 | 2.13 | 39335 | 1.9646 | 593 | 2.14 | 35711 |
| 3/2 | 5 | 2.0073 | 525 | 2.10 | 60165 | 1.9900 | 550 | 2.33 | 50005 | 1.9797 | 569 | 2.45 | 42573 |
| 3/2 | 6 | 2.0096 | 539 | 2.15 | 62569 | 1.9961 | 563 | 2.39 | 51099 | 1.9881 | 581 | 2.54 | 42720 |
| 5/2 | 1 | 2.0248 | 498 | 2.25 | 25584 | 2.0181 | 507 | 2.56 | 25259 | 2.0146 | 513 | 2.80 | 25023 |
| 5/2 | 2 | 2.0085 | 523 | 2.10 | 61177 | 1.9905 | 548 | 2.34 | 50686 | 1.9796 | 567 | 2.48 | 43011 |
| 5/2 | 3 | 1.9834 | 549 | 2.24 | 75514 | 1.9711 | 569 | 2.39 | 64418 | 1.9642 | 581 | 2.34 | 56321 |
| 5/2 | 4 | 1.9526 | 583 | 2.56 | 77193 | 1.9601 | 582 | 2.24 | 66234 | 1.9659 | 583 | 2.18 | 58242 |
| 7/2 | 1 | 1.9834 | 549 | 2.24 | 75566 | 1.9712 | 569 | 2.39 | 64446 | 1.9643 | 581 | 2.34 | 56331 |
| 7/2 | 2 | 1.9499 | 582 | 2.45 | 77694 | 1.9463 | 590 | 2.48 | 80882 | 1.9006 | 708 | 45.10 | 83343 |
| ION | 0 | 1.9485 | 596 | 2.16 | 48387 | 1.9471 | 604 | 2.02 | 48471 | 1.9471 | 609 | 1.91 | 48578 |

4.3 Open f-shell - potential energy curves

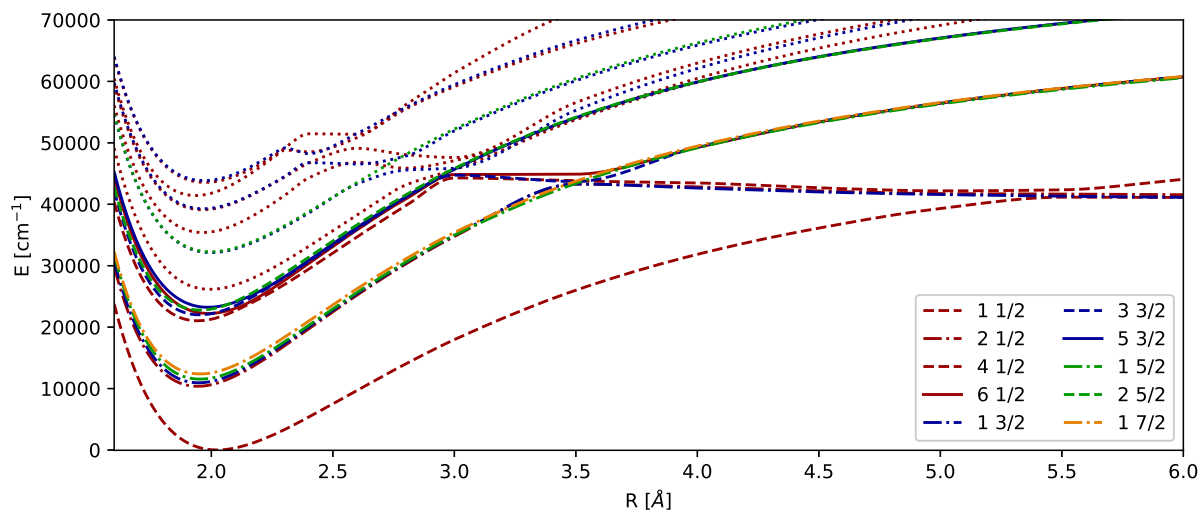


Figure 30: EOM-CCSD PECs for states from the (1h, 0p) sector with an anion reference for the quadruple zeta basis sets.

Table 18: Spectroscopic constants for the different electronic states ($\Omega = 1/2, 3/2, 5/2$) obtained by EOM-CCSD for the (1h,0p) sector using different basis set sizes. Vibrational constant (ω_e), anharmonicity constant ($\omega_e\chi_e$), and transition energy (T_e), are given in cm^{-1} , the equilibrium bond distance (r_e) in \AA .

| Ω | state | v3z | | | | v4z | | | | CBS | | | |
|----------|-------|--------|------------|------------------|-------|--------|------------|------------------|-------|--------|------------|------------------|-------|
| | | r_e | ω_e | $\omega_e\chi_e$ | T_e | r_e | ω_e | $\omega_e\chi_e$ | T_e | r_e | ω_e | $\omega_e\chi_e$ | T_e |
| 1/2 | 1 | 2.0247 | 503 | 2.27 | 0 | 2.0233 | 507 | 2.41 | 0 | 2.0250 | 508 | 2.53 | 0 |
| 1/2 | 2 | 1.9462 | 597 | 2.78 | 7380 | 1.9431 | 595 | 2.67 | 10361 | 1.9432 | 591 | 2.59 | 12568 |
| 1/2 | 3 | 1.9445 | 593 | 2.70 | 18046 | 1.9428 | 588 | 3.23 | 21029 | 1.9432 | 582 | 4.06 | 23241 |
| 1/2 | 4 | 1.9922 | 548 | 2.31 | 22306 | 1.9889 | 564 | 1.51 | 22205 | 1.9886 | 573 | 1.18 | 22147 |
| 1/2 | 5 | 1.9991 | 543 | 2.36 | 26384 | 1.9941 | 549 | 2.39 | 26151 | 1.9931 | 551 | 2.40 | 25991 |
| 1/2 | 6 | 1.9735 | 571 | 2.21 | 36936 | 1.9645 | 584 | 2.21 | 35391 | 1.9606 | 591 | 2.18 | 34280 |
| 1/2 | 7 | 1.9973 | 524 | 2.77 | 40983 | 1.9634 | 567 | 2.82 | 39091 | 1.9441 | 595 | 2.76 | 37639 |
| 1/2 | 8 | 1.9506 | 609 | 2.41 | 43943 | 1.9346 | 620 | 2.33 | 41412 | 1.9252 | 625 | 2.24 | 39575 |
| 3/2 | 1 | 1.9482 | 590 | 2.71 | 7848 | 1.9475 | 590 | 2.66 | 10931 | 1.9494 | 588 | 2.61 | 13211 |
| 3/2 | 2 | 1.9521 | 587 | 2.72 | 18941 | 1.9516 | 586 | 2.68 | 21994 | 1.9537 | 584 | 2.64 | 24251 |
| 3/2 | 3 | 1.9889 | 551 | 2.31 | 23370 | 1.9855 | 556 | 2.30 | 23227 | 1.9857 | 557 | 2.28 | 23137 |
| 3/2 | 4 | 2.0100 | 522 | 2.37 | 32680 | 1.9987 | 533 | 2.47 | 32132 | 1.9936 | 539 | 2.45 | 31734 |
| 3/2 | 5 | 2.0017 | 523 | 2.70 | 41181 | 1.9659 | 564 | 2.79 | 39262 | 1.9451 | 591 | 2.75 | 37778 |
| 5/2 | 1 | 1.9532 | 585 | 2.72 | 8588 | 1.9530 | 584 | 2.66 | 11529 | 1.9553 | 582 | 2.61 | 13703 |
| 5/2 | 2 | 1.9536 | 580 | 2.71 | 19807 | 1.9535 | 579 | 2.65 | 22768 | 1.9559 | 577 | 2.62 | 24957 |
| 5/2 | 3 | 2.0085 | 524 | 2.39 | 32839 | 1.9974 | 534 | 2.46 | 32257 | 1.9923 | 540 | 2.45 | 31834 |
| 7/2 | 1 | 1.9532 | 580 | 2.71 | 9245 | 1.9532 | 579 | 2.64 | 12373 | 1.9556 | 577 | 2.62 | 14685 |
| ION | 0 | 2.0941 | 429 | 2.64 | -9522 | 2.0889 | 431 | 2.99 | -9713 | 2.0883 | 432 | 3.25 | -9876 |

4.4 Combined potentials

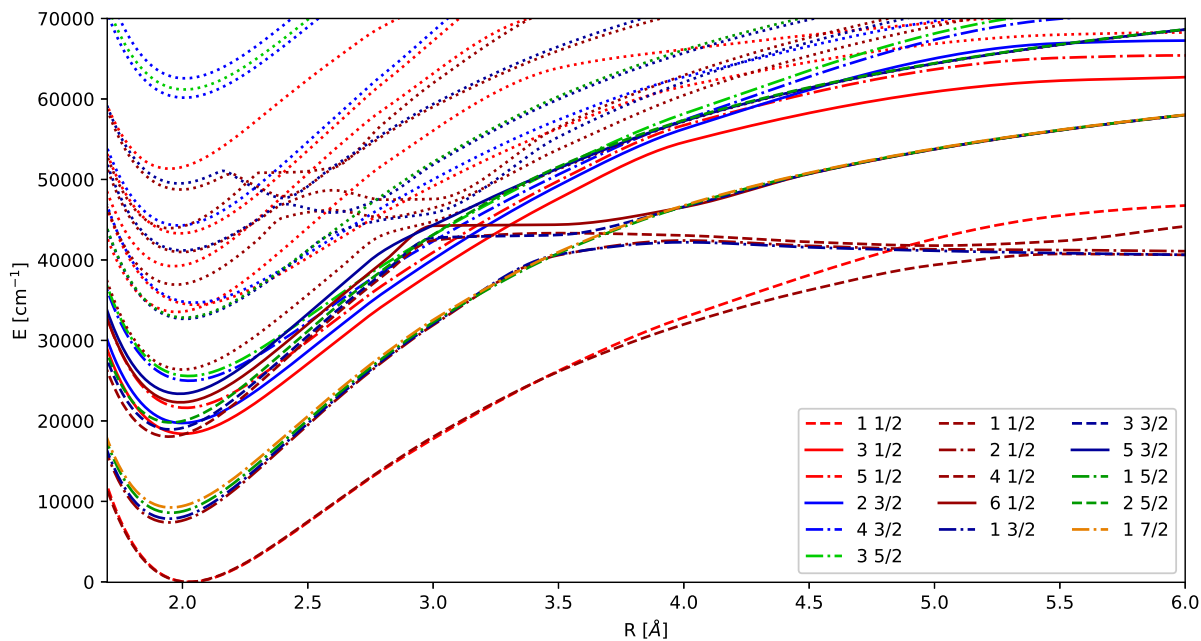


Figure 31: EOM-CCSD PECs generated by the use of two different sectors and reference systems for the triple zeta basis sets.

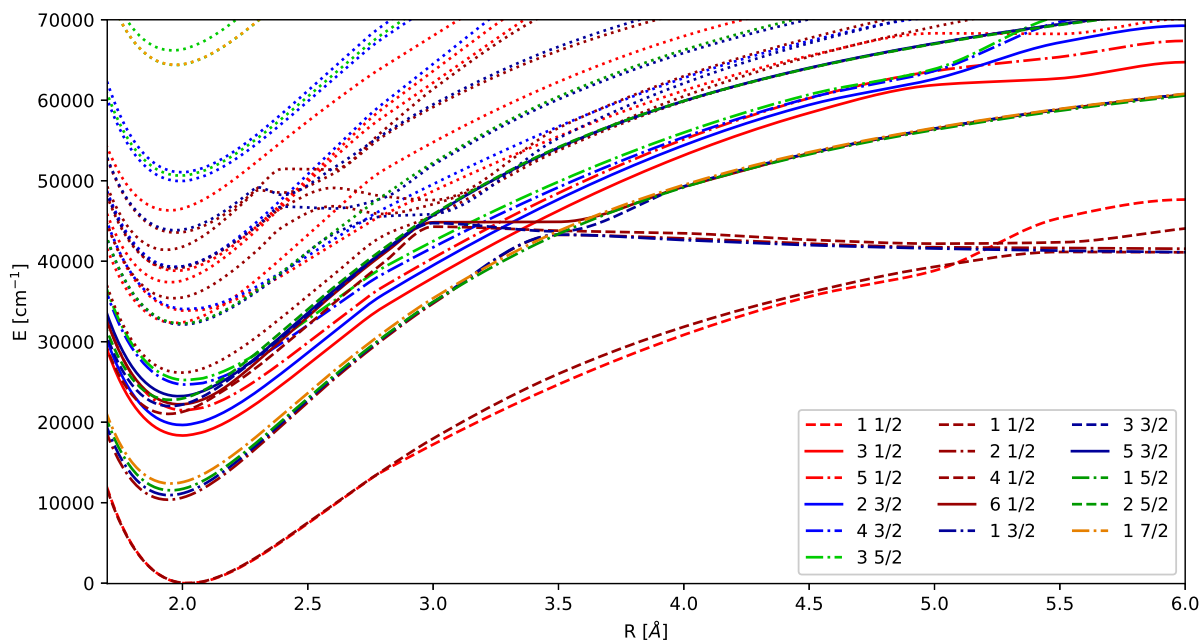


Figure 32: EOM-CCSD PECs generated by the use of two different sectors and reference systems for the quadruple zeta basis sets.

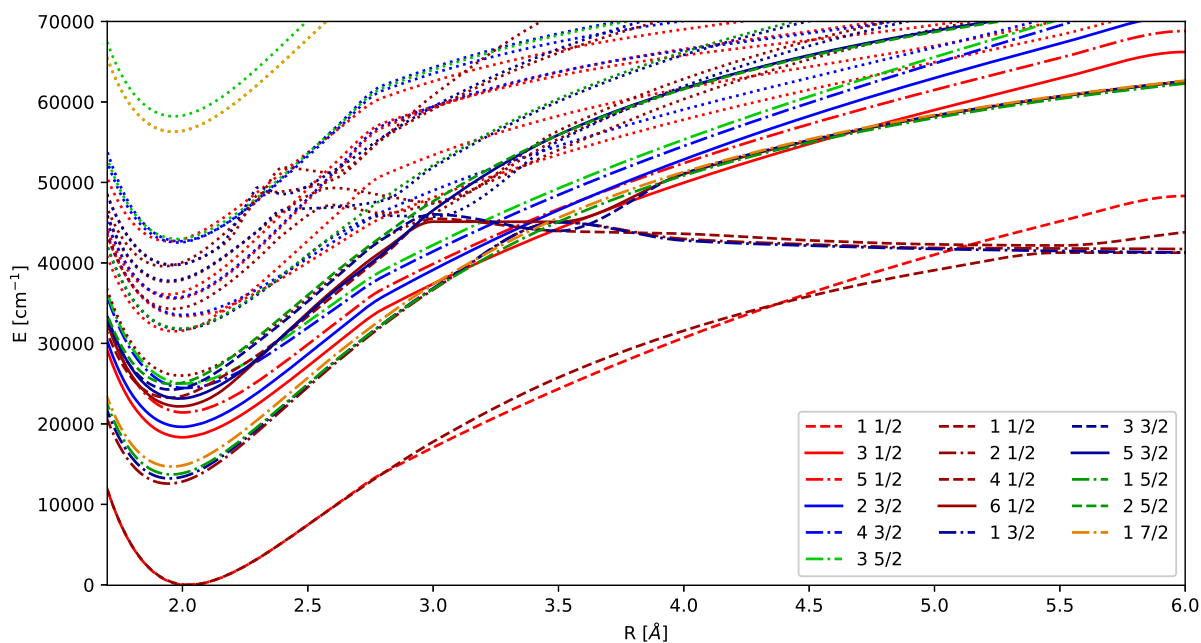


Figure 33: EOM-CCSD PECs generated by the use of two different sectors and reference systems for extrapolation to the basis set limit.

5 Frank-Condon factors (FCFs) for different methods

Frank-Condon factors are shown in figure 34 for MRCI, EOM-CCSD and IHFS-CCSD. From it, we observe a marked difference between the configuration interaction and coupled cluster results: first, the equilibrium distance and curvature are quite different, something that, in turn, change the overlap and resulting Frank-Condon factors as well as the progression of the vibrational levels.

Additionally, there is more uncertainty with regards to the position of the potential energy curves, as configuration interaction is not size consistent and we observe transition in the range from 14000 to 19000 cm^{-1} for these states. The states are more dense in this case, which is expected as states of the $\text{Yb}(4f^{13}[F_{7/2}^{\circ}]5d\sigma_{6s})F$ configuration are included, which are missing in the coupled cluster descriptions.

The EOM-CCSD and IHFS-CCSD Frank-Condon factors are quite similar to each other, with the exception of the additional $6_{1/2}$ state in EOM-CCSD, probably stemming from the contributions by (2h,1p)/(1h,2p) to the final states. The results for the $3_{1/2}$ and $2_{3/2}$ state are close to the experimentally observed positions, only about 500 cm^{-1} too high, and show the same splitting. The transition of the $5_{1/2}$ states are also similar in both coupled cluster treatments.

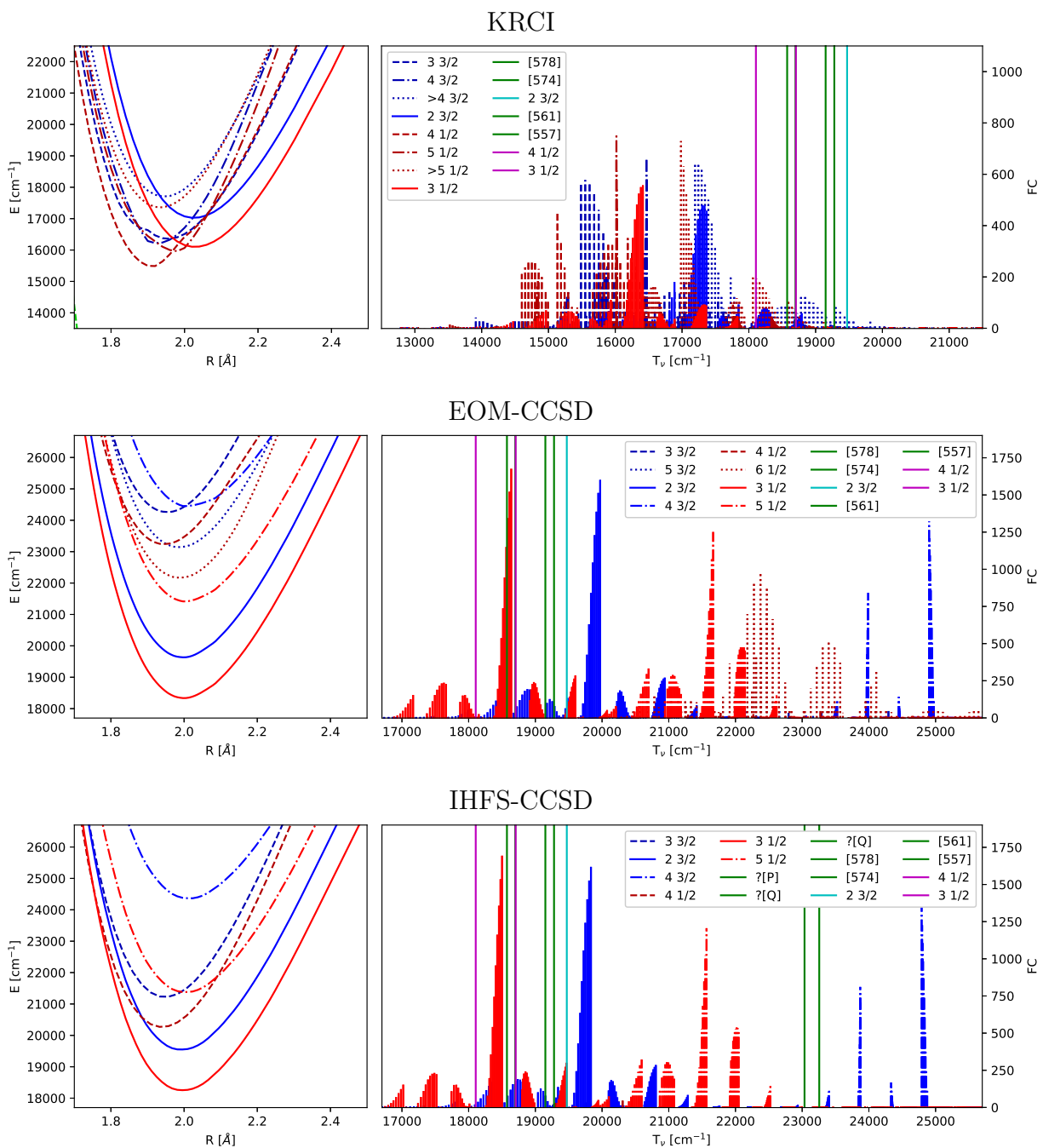


Figure 34: Frank-Condon factors obtained by using the potential energy curves on the left, which have been obtained by different ab-initio methods. The lowest 10 vibrational levels of the ground state were used as well as the lowest 60 vibrational levels of the excited state. The experimental values have been added as straight lines.⁹⁻¹¹

References

- (1) Thyssen, J. Development and Applications of Methods for Correlated Relativistic Calculations of Molecular Properties. Ph.D. thesis, University of Southern Denmark, 2001.
- (2) Cox, P. A. Ionization energies of open-shell molecules in the frozen orbital approximation. *null* **1975**, *30*, 389–403.
- (3) Sikkema, J.; Visscher, L.; Saue, T.; Iliáš, M. The molecular mean-field approach for correlated relativistic calculations. *J. Chem. Phys.* **2009**, *131*, 124116.
- (4) Ilias, M.; Saue, T. An infinite-order two-component relativistic Hamiltonian by a simple one-step transformation. *J. Chem. Phys.* **2007**, *126*, 064102.
- (5) Schimmelpfennig, B. *AMFI, an atomic mean-field spin-orbit integral program*. University of Stockholm, Stockholm, Sweden; 1999.
- (6) Eliav, E.; Kaldor, U.; Ishikawa, Y. Transition energies of ytterbium, lutetium, and lawrencium by the relativistic coupled-cluster method. *PRA* **1995**, *52*, 291–296.
- (7) Kramida, A.; Yu. Ralchenko,; Reader, J.; and NIST ASD Team, NIST Atomic Spectra Database (ver. 5.8), [Online]. Available: <https://physics.nist.gov/asd> [2017, April 9]. National Institute of Standards and Technology, Gaithersburg, MD., 2020.
- (8) Huber, K.; Herzberg, G. Constants of Diatomic Molecules. National Institute of Standards and Technology, Gaithersburg MD, 20899, 2005; (data prepared by J.W. Gallagher and R.D. Johnson, III) in NIST Chemistry WebBook, NIST Standard Reference Database Number 69, Eds. P.J. Linstrom and W.G. Mallard.
- (9) Dunfield, K. L.; Linton, C.; Clarke, T. E.; McBride, J.; Adam, A. G.; Peers, J. R. D. Laser spectroscopy of the lanthanide monofluorides: Analysis of the A(2)Pi-X(2)Sigma(+) transition of ytterbium monofluoride. *Journal of Molecular Spectroscopy* **1995**, *174*, 433–445.

- (10) Lim, J.; Almond, J. R.; Tarbutt, M. R.; Nguyen, D. T.; Steimle, T. C. The [557]-X-2 Sigma(+) and [561]-X-2 Sigma(+) bands of ytterbium fluoride, (YbF)-Yb-174. *Journal of Molecular Spectroscopy* **2017**, *338*, 81–90.
- (11) Smallman, I. J.; Wang, F.; Steimle, T. C.; Tarbutt, M. R.; Hinds, E. A. Radiative branching ratios for excited states of 174YbF: Application to laser cooling. *Spectroscopic Tests of Fundamental Physics* **2014**, *300*, 3–6.